A Magneto-rheological Actuator for Assistive Knee Braces

by

CHEN, Jinzhou

A Thesis Submitted in Partial Fulfillment

of the Requirements for the Degree of

Doctor of Philosophy

in

Automation & Computer-Aided Engineering

June 2009

ProQuest LLC.
789 East Eisenhower Parkway
P.O. Box 1346
Ann Arbor, MI 48106 - 1346

ABSTRACT

It has been found that magneto-rheological (MR) devices can produce large controllable force/torque while consuming little power. In this research, an MR actuator that can function as a clutch or a brake is developed, in order to be applied to an assistive knee brace. The torque capability and dynamic characteristics of the MR actuator are evaluated. The relationship between the torque output and the applied coil current is given. The response time is also measured. Experimental results show that the MR actuator can provide enough torque for normal activities with sufficiently fast response. IP control and adaptive control are proposed to control the MR actuator. Experiments under these controls are carried out. With anti-windup strategies, both controls achieve good performances. However, adaptive control would be more promising since it can adapt to parameter variations and maintain good performance. An assistive knee brace that contains this MR actuator and a DC motor is developed. In order to study the performances of the knee brace before applied to human body, experiments are conducted for evaluation under a custom-built testing structure. IP-based state control and adaptive control are used to control both the MR actuator and DC motor. Experimental results demonstrate that the MR actuator and DC motor work well together to provide assistance as expected. Compared with that without MR actuator, the evaluation results show that the knee brace with MR actuator is more energy efficient during normal walking, while having better force controllability and safety.

摘要

磁流變器件能夠在消耗很少能量的情況下產生很大的力或者力矩，並且它本身具有良好的控制性能，這使得磁流變近年來得到廣泛的應用。在本研究中，作者開發了一種應用於助力膝架的磁流變驅動器，這種磁流變器件根據需要既可以作為離合器也可以作為制動器使用。磁流變驅動器的性能通過實驗進行了評估。實驗結果表明開發的磁流變驅動器能夠在足夠快的時間內提供適當的助力。IP控制和適應控制都被用來對磁流變驅動器的輸出進行控制。實驗結果表明，磁流變驅動器在兩種不同控制方法下都可以取得很好的力矩輸出跟蹤性能。但是適應控制因為可以在參數發生改變的情況下依然保持良好的控制性能，因而更具前景。作者設計並製作了採用本磁流變驅動器與直流馬達的助力膝架。並在自行設計的測試裝置上進行了測試與評估。測試結果顯示，本助力膝架能夠跟預期一樣提供適當的主動和被動的助力。作者開發了兩種膝架運動控制器：基於IP的狀態控制器以及適應狀態控制器。在不同的控制器下，助力膝架都能夠推動負載按照指定的軌跡運動。作爲評估參照，作者製作了沒有使用磁流變驅動器的助力膝架並對兩種膝架從不同方面進行了評估和比較。評估結果顯示，採用了磁流變執行器的助力膝架與單純使用馬達的助力膝架相比在正常走路時具有更高的能量效率、更好的控制性能以及更好的安全性。

ACKNOWLEDGEMENTS

I give my sincere gratitude to my supervisor, Professor Liao Wei-Hsin （廖維新教授）, who supports and encourages me all through this research. I am also very grateful to Professor Huang Jie （黃捷教授）, Professor Liu Yunhui （劉雲輝教授）, Professor Li Wen Jung （李文榮教授）, and Professor Ma Shugen （馬書根教授） for serving as my committee members and providing comments on this research.

I would like to express my appreciation to my parents （李盛莊女士，陳顯求先生）, my wife Ms. Xu Qichun （徐琪春女士） and my sisters and brothers for their love and support over the years; to SMS Lab members — Dr. Chan Kwong Wah （陳光華博士）, Dr. Guan Mingjie （關明杰博士）, Dr. Dai Ruoli （戴若犁博士）, Mr. Cheung Wai Ming （張偉明先生）, Mr. Guo Hongtao (郭洪濤先生), Mr. Liang Junrui (梁俊睿先生), Miss Jia Jiangying (賈江瑩小姐), Mr. Chen Chao （陳超先生）, Miss Liu Lu (劉璐小姐) and Miss Du Xiaona (杜曉娜小姐)— for the discussions and their help in experiments; to my roommate Dr. Guo Yuming （郭玉明博士）— for his friendship.

*This research is supported by the Shun Hing Institute of Advanced Engineering (BME 8/07)

TABLE OF CONTENTS

LIST OF FIGURES

LIST OF TABLES

CHAPTER ONE

INTRODUCTION

This chapter presents background knowledge and related literature reviews on assistive devices for mobility and magneto-rheological devices. The background and history of mobility assistive devices are provided. Actuators for these devices are described. The basic knowledge and general information about MR fluids and MR devices are introduced. Recent researches on MR devices that used in mobility assistive devices are reviewed. At the end of this Chapter, the research objectives and organization of this thesis are introduced.

1.1 Background

1.1.1 Mobility impaired problems

The percentage of aged persons in society is increasing, and their physical deterioration has become a social problem in many countries, such as China, Japan, etc. In late 2004, the population of aged persons (older than 60 years) in China has reached 143 million. In this new century, the aged tendency of population will become more serious. It is estimated that the percentage of aged population would reach 30% in China between 2030 and 2050. Elderly people with weak muscle strength may not be able to walk or lose their stability during walk, if these people don't walk, their muscle would be further deteriorated and they may become bedridden. The most effective method to avoid people from becoming bedridden is to provide a way for them to be able to continue walking.

Knee osteoarthritis (OA) is very prevalent in old people; it is about 60% in men and 70% in women after the age of 65 years [Piercarlo et al., 2005]. Studies show that exercise can do positive effects to OA patients [Fischer et al, 1993, Piercarlo et al., 2005]. Some kinds of devices were developed to provide exercises; however, these devices are usually for hospital or home use and can not provide assistance for people with mobility problems.

Stroke is the leading cause of long-term adult disability in US [Johnson et al., 2005]. Researches found that exercise training can increase strength and may improve motor activity in people with cerebral palsy (CP) without adverse effects [Damiano et al., 2000, Dodd et al., 2002]; also it was demonstrated to increase the strength of affected

major muscle groups of stroke survivors [Teixeira-Salmela et al., 1999, Andrews et al., 2003].

1.1.2 Powered mobility assistive device

Conventional mobility assistive devices including crutches or wheeled walkers, however, these devices may either cause ugly gait or can not provide assistance in areas with bumps or steps.

Knee braces are widely used to prevent people from injury or further injury. According to the American Academy of Orthopedic Surgeons, there are four categories of knee braces [Paluska et al., 2000]: (1) Prophylactic knee brace – prevent or reduce the severity of knee injury in sports; (2) Patellofemoral knee brace – improve patellar tracking and relieve anterior knee pain; (3) Rehabilitative knee brace – allow protected and controlled motion during the rehabilitation of injured knees; (4) Functional knee brace – provide stability for unstable knees. These knee braces were proven to be effective to provide stabilization and protect knee joint. But they have disadvantages such as constraint of motion capability.

An exoskeleton is an external structural mechanism whose joints correspond to those of the human body. It is worn by the wearer and the physical contact between the operator and the exoskeleton allows direct transfer of mechanical power and signals.

Exoskeleton can be used for three different applications: (1) Power amplifier, where the wearer provides control signals and the exoskeleton provides assisting power for

performing tasks; (2) Master device of a master/slave teleoperating system, where the exoskeleton (master) is attached to an operator to control a robot arm (slave); (3) Haptic device, which is applied to virtual reality to simulate human interaction with virtual objects.

As power amplifier, exoskeletons have two main target users: as performance-enhancing devices for healthy people, such as soldiers, firemen, etc; as rehabilitation devices or permanent assisting devices for motor impaired patients.

Leg exoskeletons that assisting for lower limbs were widely researched in recent years. Johnson et al. proposed an exoskeleton system that used pneumatic muscles as actuators to aid in the mobilization of walking-impaired patients [Johnson et al., 1996]. The system uses the fingers to control the motion of the leg joints, i.e. the function of each leg joint is primarily directed through the output of a finger joint sensor. However, this research was not successful since it was manually controlled and the motions of fingers were constrained, and the errors of mapping the finger joints to leg joints limited the mobility of the legs.

Pratt et al. developed a one degree of freedom exoskeleton called RoboKnee [Pratt. et al., 2004]. This exoskeleton system could provide assistance for wearer to climb stairs and perform deep knee bends while carrying a significant load in a backpack. Low impedance was achieved by using series elastic actuators. However, this device can only work 30-60 minutes of heavy use with 4kg of nickel-metal-hydride batteries.

The most successful exoskeleton nowadays is the HAL (Hybrid Assistive Limb) developed by Sankai et al. [Kawamoto et al., 2002, 2003, Lee et al., 2002, 2003, Hayashi et al., 2005]. HAL-3 used DC servo motors and gears as actuators, and used EMG sensors, angle sensors and force sensors to detect human intent and motion information. HAL-3 aimed to provide the self-walking aid for gait disorder persons or aged persons. However, it also has the problem of short lifetime of batteries between two charges. Moreover, it has large impedance, people wearing the exoskeleton feel as if they were driving it. So it is not suitable for disabled people due to the safety concern. In the latest version, the aim of the HAL is to enhance the physical capabilities of healthy persons.

1.1.3 Actuators for powered mobile assistive devices

DC motors are widely used in powered mobile assistive devices. It could be precisely controlled and easily applied to mobile devices. With gearbox having high gear ratio, DC motor has benefit of high power-to-weight ratio. However, to perform discontinuous or nonrepetitive task reduces the efficiency of motor; the large gear ratio also lowers the efficiency. The gears also bring friction, backlash, torque ripple, noise, and large reflected inertia. The large reflected inertia makes the system fragile to shock loads [Pratt et al., 1995].

Pratt et al. incorporated series elasticity within a stiff actuator (motor plus gearbox) and this series elastic actuator (SEA) has benefits of shock tolerance, lower reflected inertia, more accurate and stable force control, less damage to the environment, and energy storage [Pratt et al., 1995]. These advantages make SEA suitable for

applications of humanoid robots and human assistive devices. Lots of researches have been conducted in this area [Robinson et al., 1999, Pratt et al., 2004, Sensinger et al., 2005, 2006, Vallery et al., 2007, Wyeth, 2008, Kyoungchul et al., 2009]. However, the introduction of elastic component increases the order of the system and thus reduces the bandwidth of force output. Chew et al. fabricated series damper actuator, where a magnetorheological damper is used to replace the elastic component of SEA [Chew et al., 2004]. This series damper actuator has good output force/torque fidelity, low output impedance, and large force/torque range. However, it is not energy efficient. Lauria et al. developed differential elastic actuator (DEA), which has similar performance to SEA while in a more compact and simple design [Lauria et al., 2008].

Artificial muscle technologies are widely researched in recent years and different types of artificial muscle materials and actuators are developed, such as dielectric elastomer artificial muscle [Pelrine et al., 2002, Jung et al., 2004], electrostrictive polymer artificial muscle [Kornbluh et al., 1998], ionic polymer metal composite (IPMC) based artificial muscle [Bhat and Kim, 2004, Lee et al., 2006], conducting polymer artificial muscle [Otero and Sansinena, 1995, Bay et al., 2003]. These artificial muscles demonstrate some advantages like natural muscle such as compliance, quiet operation, high power-mass ratio etc., at the same time they have some significant limitations for practical applications such as high field requirement, difficult to scale to large size etc. [Madden et al., 2004, Herr and Kornbluh, 2004] McKibben artificial muscle, which is operated by pressured gas, is the most promising artificial muscle for robots that shares its working space with its environment. Its characters are similar to human skeletal muscle and has surprisingly high force-to-weight ratio [Tondu and Lopez, 2000]. The McKibben muscles are commercialized in

robots [Inoue K., 1988] and also successful applied to an ankle-foot orthosis [Ferris et al., 2005]. However, a separate pump is needed to provide pressured gas for McKibben muscle, which limits the application of this muscle in mobile assistive devices.

1.1.4 Magnetorheological (MR) fluids and their applications

MR fluids are dispersions that comprise microscale (typically 1-10 μm) ferromagnetic or ferrimagnetic (high purity iron particles are most commonly used) particulates dispersed in an organic or aqueous carrier liquid. When a magnetic field is applied to this fluid, the dispersed magnetic particles become magnetized and behave like tiny magnets. The magnetic interactions between these particles line up the magnetic particles along the direction of the magnetic field (shown in Figure 1.1-1). A shear stress or a pressure drop is needed to disrupt this structure. And the apparent yield stress increases as the magnetic field increases. These smart materials were first studied and reported by Rabinow in 1948 [Rabinow, 1948a, 1948b]. However, there are few published information on MR fluids after their initial discovery. Only since 1990s has a resurgence in interest in MR fluids been seen [Shtarkman 1991, 1992, Calson and Chrzan, 1994].

Electro-rhelogical (ER) fluids are another kind of smart fluids. They are colloidal suspensions whose properties depend strongly and reversibly on the electric field [Halsey, 1992]. ER phenomena was first reported by Winslow in 1949 [Winslow, 1949], and ER fluids have been extensively studied in recent years [Parthasarathy et al., 1996, Choi et al., 2001, Wen et al., 2003, Hiamtup et al., 2006, Ivlev et al., 2008].

MR fluids have the following advantages: (1) High yield stress - normally, MR fluid has a highest shear stress of nearly 100 kPa, and that of ER fluid is one order lower; (2) Temperature stability - MR fluids is relative stable between -40 and +150 ℃; (3) Low voltage supply - the required working field for ER fluids is about 3kV/mm, but the voltage for MR fluids may be only several volts. The power supply for MR devices is easier to be derived and safer.

These advantages of MR fluids make them more attractive than ER fluids. However, it is noticeable that an ER fluid which has giant electrorheological effect has been developed in recent years, which has maximum yield strength of 130 kPa [Wen et al., 2003].

Basically, there are three operation modes for MR fluids in applications: flow mode (valve mode), shear mode (clutch mode) and squeeze mode (compression mode), as shown in Figure 1.1-2 [Carlson and Jolly, 2000].

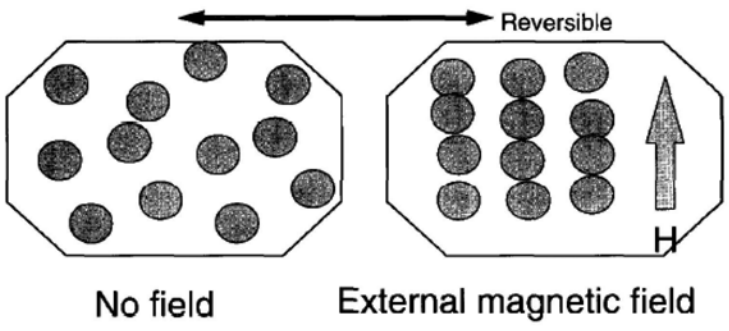

Figure 1.1-1 Schematic of the MR effect

[Phule, 2001]

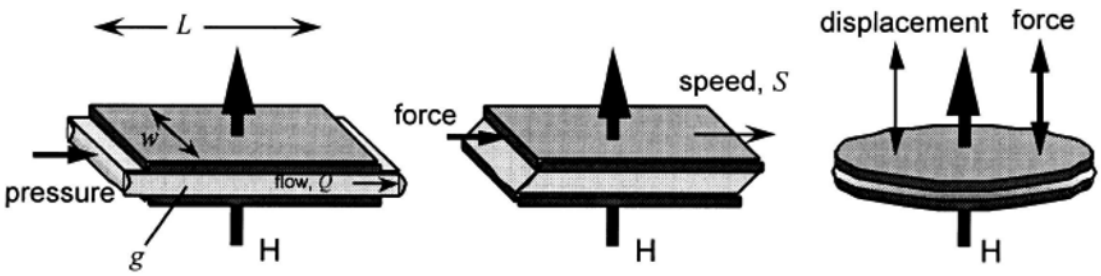

Figure 1.1-2 Basic operation modes for MR fluids

[Carlson and Jolly, 2000]

Application examples for flow mode include servo-valves, dampers, shock absorbers, etc; examples of shear mode include clutches, brakes, chucking and locking devices, etc; the squeeze mode has been used in small amplitude vibration and impact dampers.

Vibration control and torque transfer are important applications utilizing MR fluids. The Lord Corporation has manufactured commercial MR fluid devices for applications including passenger protection of vehicles, knob & detent of automobiles, clutches of vehicles, vehicle seat suspensions, seismic protection, cable-stayed bridges, noise and vibration suppression of washing machines, smart prosthetic joints [http://www.lord.com, 2008]. Delphi and Cadillac developed commercial MR fluid based MagneRide^{TM} semi-active suspension systems [http://www.delphi.com, 2008].

Other applications of MR fluids include train suspensions [Liao and Wang, 2003, Lau and Liao, 2005], dissipative passive haptic displays [Swanson and Book, 2003, An and Kwon, 2009], hydraulic power actuation systems [Yoo and Wereley, 2002, 2004], MR fluid isolators [Oh, 2004], high precision finishing [Kordonski and Golini, 1999, Shimada et al., 2002] etc.

1.1.5 Soft magnetic materials

Soft magnetic material is one that loses its memory of previous magnetization. It has the properties of low coercivity and high permeability. Soft magnetic materials are used as core materials in MR devices to enhance the magnetic field of the electric coil. Some important properties of soft magnetic materials are as follows:

Coercivity - the coercivity, also called the coercive field, of a ferromagnetic material is the intensity of the applied magnetic field required to reduce the magnetization of that material to zero after the magnetization of the sample has been driven to saturation [http://www.wikipedia.org]. The coercivity is a measure of the degree of magnetic hysteresis and therefore characterizes the lossiness of soft magnetic materials for their common applications. So low coercivity is desirable for core materials, especially for high frequency applications.

Permeability – in electromagnetism, permeability is the degree of magnetization of a material that responds linearly to an applied magnetic field [http://www.wikipedia.org]. A good magnetic core material must have high permeability. Permeability varies with magnetic field and frequency.

Magnetic saturation - saturation is the state reached when an increase in applied external magnetizing field H cannot increase the magnetization of the material further, so the total magnetic flux density B levels off [http://www.wikipedia.org]. With high magnetic saturation, the magnetic circuit can be made compact in size while keeping the same magnetic flux, so soft magnetic materials with high saturation is desirable.

Resistivity – resistivity is a very important property for core materials in high frequency applications. According to electromagnetic theory, when the magnetic field varies in the core of electric coil, electric field is developed and eddy current appears. The eddy current dissipates energy and creats a magnetic field that tends to oppose the change in the field. If the resistivity is small, the eddy current will be large, so low resistivity is desirable for core materials.

Some other properties should also be considered while choosing core materials, such as mechanical strength, machinability, cost, etc. Table 1.4-1 shows the properties of common soft magnetic materials.

Table 1.4-1 Soft magnetic materials
[http://baike.baidu.com, http://www.wikipedia.org, http://www.thecdi.com]

(B_s: Saturation magnetic flux density, μ : Permeability, H_c : Coercivity, ρ : Resistivity)

Soft magnetic materials	Composition	Properties
Pure electric iron	Fe, C (<0.04%), Few Mn, Si, P, S	High B_s, high μ , low H_c , low ρ
low carbon steel	Fe, C ($\approx$ 0.05~0.15%), Mn (=0.1~0.5%) Few Si, P, S	High B_s, high μ , low H_c , low ρ
Silicon steel	Fe, C ($\leq$ 0.05%), Si (= 0.5 ~ 4.8%), Mn (= 0.1 ~ 0.3%), Few S, P, O	High B_s, high μ , low H_c , high ρ
Fe-Ni alloy	Fe, Ni (= 30 ~ 90%), Mo (<5%)	High μ at low H, low H_c
Fe-Al alloy	Fe, Al (= 6 ~ 16%)	High ρ , relatively low μ
Fe-Co alloy	Fe, Co (= 27 ~ 50%)	Very high B_s, high μ , low ρ
Soft ferrites	Fe, O	Very high ρ , relatively low B_s

For Fe-Ni alloys, increases the Ni content will increase the initial permeability but at the same time the saturation induction is decreased. For Fe-Co alloys, increase the Co content will slightly decrease the saturation flux density but the resistivity is increased.

1.1.6 Application of MR fluids in medical devices

Carlson designed a portable controllable MR fluid device for rehabilitation of injured limbs appendages and joints [Carlson, 1998]. It includes two fix brackets and a controllable MR fluid brake between the two brackets. The resistance force can be adjusted through a panel. The patent provided the detail description of the mechanical structure, but did not show the performance of this device.

Carlson et al. developed a smart prosthetics utilizing a controllable MR damper, where the MR damper is used to provide controllable damping to the knee joint and

thus make the prosthesis adaptable to the person while interacting with environment [Carlson et al., 2001]. This smart prosthetic knee system was introduced to the orthopedics and prosthetics market in 2000. Powered by a li-ion battery, the system is able to operate for 2 days when fully charged.

Herr and his associates [Herr. et al., 2003, Deffenbaugh et al., 2004] developed a prosthetic knee with an MR brake. Using local sensing information of force, torque and position, the MR knee prosthetic can automatically adapt knee damping to the gait of the amputee. With multiple disks structure, the MR brakes can produce a torque of 0.5~50 Nm [Deffenbaugh et al., 2004]. However, since only an MR brake is used, which can only control the damping of the knee joint, the prosthetic can not provide active assistance for human mobility.

Dong et al. developed a versatile rehabilitation device [2006 a, 2006 b] with an MR damper. This device is in the form of rotating joint arm mounted on an adjustable seat that provides passive resistance during strength training for muscles. The MR damper is controlled based on the prescription of the therapist such that it can provide both isometric and isokinetic strength training for several human joints.

Li et al. [2006] developed a prosthetic ankle joint to make user walk more naturally and smoothly. The ankle joint is intelligently controlled by a specially designed linear MR brake. The prosthetic ankle joint has been evaluated with walking experiments and it was proved that this device can help people walk easier. However, more work needs to be done before putting this device into real applications.

Zite and his associates developed passive knee brace [Zite et al., 2006] and active knee brace [Ahmadkhanlou et al., 2007] using MR fluid based joint to overcome the disadvantages of high customization costs and reduction of natural mobility of current rehabilitative knee braces. For the passive knee brace, several magnets are used to provide the magnetic field. However, the produced resistant torque is only 1.8 Nm for the MR brake when two magnets are used. For the active knee brace, electric coil are used to provide the magnetic field thus the produced torque can be controlled. The maximum torque produced by the knee brace is 6 Nm when 4 A current is applied.

Besides MR fluids, ER fluids were also used for active knee braces [Nikitczuk et al., 2005, 2006, Weinberg et al., 2007]. With multiple concentric cylindrical electrodes, the ER brake is capable of producing a torque of 12.6 Nm at 3kV [Weinberg et al., 2007]. However, this knee brace can only produce passive torque. And compact high voltage power source is not easy to be implemented for mobile devices.

1.2 Research Objective

This research is aimed to develop MR actuators for hybrid assistive knee braces. The principle of the MR actuator is proposed. The MR actuator can function as an MR brake or MR clutch as needed. The magnetic circuit is analyzed with FEM to improve the design of the magnetic circuit. A set of MR actuator testing structure is designed and constructed. The fabricated MR actuator is evaluated under different coil currents and rotating speeds. The relationship between torque and applied coil current, as well as the step response of the MR actuator are studied.

IP control and adaptive control are proposed for the torque output control of MR actuator. Sinusoidal signal and pulse signal are used as target reference torques and experiments are carried out to study the torque tracking ability of the MR actuator. The control performances of different control algorithms will be compared and further improved based on experimental results.

An assistive knee brace that utilizing the MR actuator together with a DC motor will be developed. When active torque is desired, the DC motor works and the MR actuator functions as a clutch to transfer the torque generated by the motor to the leg; when passive torque is desired, the DC motor is turned off and the MR actuator functions as a brake to provide controllable passive torque. Potentiometer and strain gauges are used to detect the position and force information of the knee brace. The knee brace can provide active or passive assistive torque based on the working condition of the knee brace. A testing structure is developed and experiments are carried out for testing the knee brace.

The motion of the knee brace under the testing structure is analyzed. IP-based state control and adaptive state control are proposed for the control of the knee brace motion under the testing structure. The knee brace with MR actuator is evaluated in three aspects as compared to that without MR actuator: power consumptions, performance and safety. The evaluation results demonstrated that the knee brace with MR actuator can be more energy efficient, safer while having better performance.

1.3 Thesis Organization

This thesis consists of six chapters. In Chapter One, background and literature review on related research are introduced. In Chapter Two, the principle of the MR actuator is proposed. The magnetic circuit is analyzed with Finite Element Method (FEM). The MR actuator is fabricated and a custom-built testing structure is used for testing the MR actuator. The relationship between the applied coil current and torque output, and the step response of the MR actuator are evaluated. In Chapter Three, IP control and adaptive control are proposed to control the MR actuator. Experiments on torque tracking under control are carried out. The experimental results are compared and the control algorithms are further improved based on the experimental data. In Chapter Four, the assistive knee brace with the MR actuator and DC motor is developed. Strain gauges and potentiometer are used to detect force and position information. A testing structure that mimics the motion of human body is designed and fabricated. The knee brace is tested on the testing structure. The motion of the knee brace in the testing structure is analyzed. IP-based state control and adaptive control are proposed for the control of knee brace. Experiments of the knee brace under control are carried out. In Chapter Five, the knee brace with MR actuator is evaluated. For comparison, a knee brace without MR actuator is also developed. The power consumption of the knee brace with MR actuator during bending, extending and normal walking is studied and compared to that of knee brace without MR actuator. The performances including impedance, force controllability of both knee braces are studied and compared. The safety of the knee braces under some extreme conditions is also discussed. Finally, conclusion and future work are summarized in Chapter Six.

CHAPTER TWO

DESIGN AND TESTING OF MR ACTUATOR

In this chapter, the MR fluid that is to be used is introduced first; the working condition of MR actuator is analyzed; an MR actuator is designed; for the proposed MR actuator, the torque of the MR actuator is analyzed.

The performance of the MR actuator is greatly affected by the performance of the magnetic circuit. In order to develop an MR actuator that meets the requirements of applying to assistive knee braces, the magnetic circuit of the MR actuator is analyzed and designed with FEM.

The MR actuator is fabricated based on analysis and tested in a custom-built testing structure. The torque output properties such as torque-current relationship and dynamic torque response are measured. The experimental results are discussed and compared to the theoretical results.

2.1 MR Fluids and Coil Core Materials

MR fluids are commercially available. Among the suppliers of MR fluids, Lord Corp. holds the world's most extensive patent portfolio on MR fluid formulations, devices and systems. They have compiled a body of scientific data through aggressive life cycle testing and installed commercial applications that demonstrate the effectiveness, durability and performances of MR fluids. Three types of MR fluids are available in Lord Corp. They are MRF-122EG, MRF-132DG and MRF-140CG. All of them are hydrocarbon-based MR fluids. In this research, MRF-132DG is chosen as the working fluid. Compared to the other two kinds of MR fluids, MRF-132DG presents relative large yield stress under magnetic field while shows relative low yield stress without magnetic field. MRF-132DG has the benefits of fast response time, broad dynamic yield strength, wide operating temperature, low hard settling and non-abrasive [see Appendix A]. Figure 2.1-1 to Figure 2.1-3 show the properties of MRF-132DG.

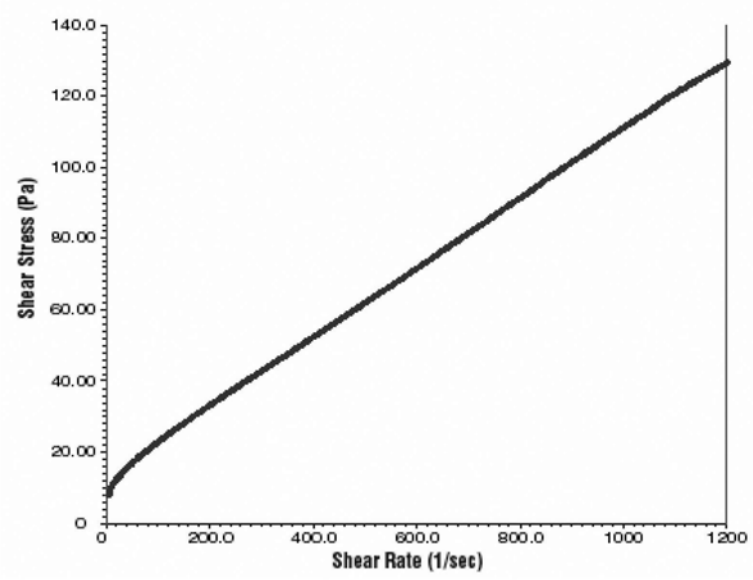

Figure 2.1-1 Shear stress as a function of shear rate with no magnetic field applied at 40 °C [Lord Corp., 2008]

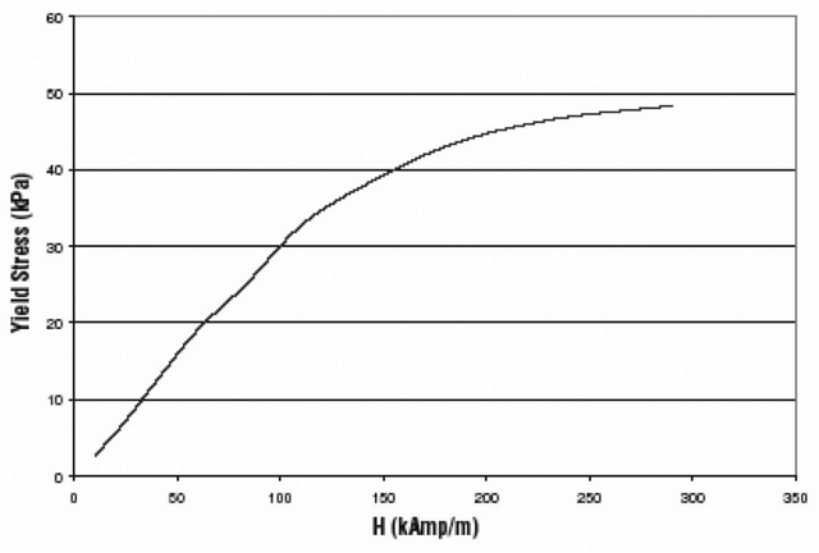

Figure 2.1-2 Yield stress vs. magnetic field strength

[Lord Corp., 2008]

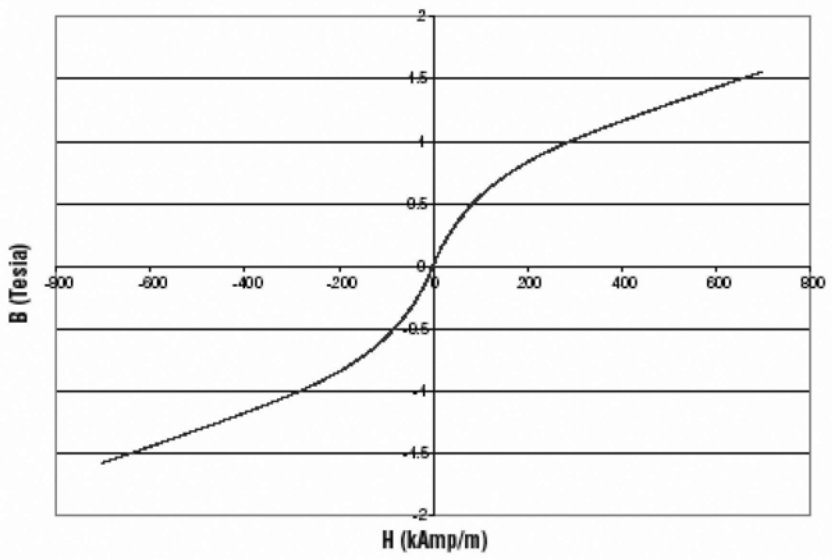

Figure 2.1-3 Typical magnetic properties

[Lord Corp., 2008]

As introduced in Chapter One, Fe-Co alloys have the highest saturation flux density, so Fe-Co alloy with high Co content (increase the resistivity so as to reduce eddy current loss) is desirable for coil core materials. However, Fe-Co alloys are very

expensive and hard to be machined. The saturation flux density of electric pure iron is high as compared to other soft magnetic materials. At the same time, electric pure iron is very cheap and easy to be machined, so electric pure iron is chosen as the coil core material for the first prototype of the MR actuator. The resistivity of iron is low but it will be fine as the MR actuator only works at low frequency. The electric pure iron used here is DT4C bought from Advanced Technology & Materials Co. Ltd. Figure 2.1-4 shows the magnetic properties of DT4C.

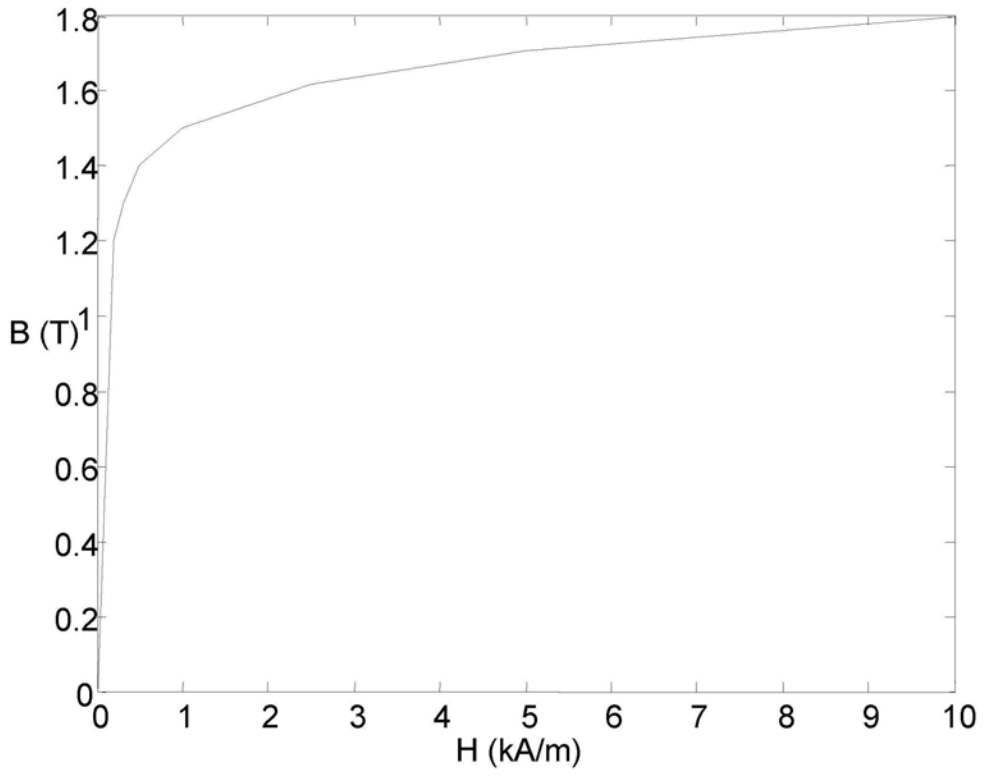

Figure 2.1-4 Typical magnetic properties of electric pure iron

[Data from http://www.atmcn.com]

2.2 Principle of MR Actuator

The MR actuator is supposed to function as a brake or a clutch as required. So the working conditions of the MR actuator are:

1) When passive assistive torque is required, the MR device acts as a brake, which can provide controllable passive torque.
2) When no torque is needed for the knee joint, the MR device does not work and the knee joint can rotate freely.
3) When active assistive torque is required, a motor works and the MR device acts as a clutch to transfer the torque from the motor to the leg.

With multiple disks structure, rotary MR actuator can produce larger torque as compared to single disk MR actuator with the same size. For example, the MR brake developed by Deffenbaugh et al. (2004), can produce a maximum torque of 50 Nm; the MR clutch developed by Kavlicoglu et al. (2006), can produce a torque of 244 Nm at 3.0 A coil current. But for single disk structure, the produced torque is relatively small, such as the MR brake developed by Ahmadkhanlou et al. [2007] can only provide a torque less than 6 Nm. To produce large torque and keep the MR actuator compact in size, the MR actuator utilizes a plurality of interspersed and alternating rotors (inner disks) and stators (outer disks). The principle of the MR actuator is shown in Figure 2.2-1. It consists of three modules:

1) Fork module, which contains two outer forks, is connected to the lower knee brace;
2) Core module, which consists of core, coil, inner cylinder, and inner disks, is connected to the output shaft of a DC motor;
3) Outer cylinder module, which contains outer disks and outer cylinder, is

connected to the upper knee brace.

The inner disks are engaged in the inner cylinder and the outer disks are engaged in outer cylinder. MR fluids are filled between the outer and inner disks. MR fluids are used in shear mode to produce or transfer torque. The motor is mounted on the outer forks. A lock/unlock mechanism is used between the core and outer forks.

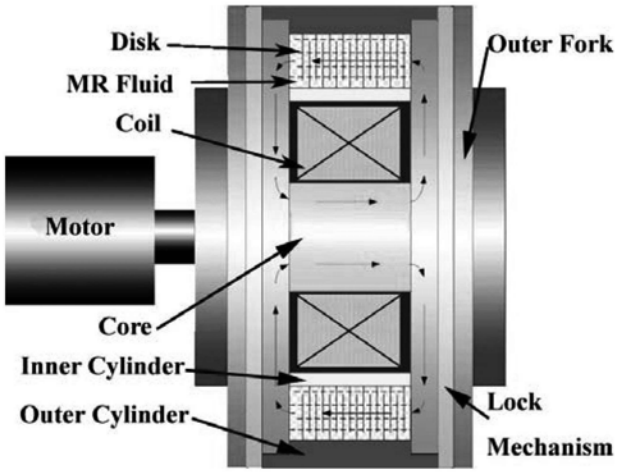

Figure 2.2-1 Schematic of MR actuator

The three modules can rotate relatively. The motion relationship of these three modules is shown in Figure 2.2-2. When the core and the fork is unlocked or no magnetic field is applied to MR fluid, the outer forks can rotate freely with respect to the outer cylinder, i.e. the knee joint can rotate freely; when the core and the outer forks are locked and a magnetic field is applied to MR fluid, a resistive torque is developed if the outer cylinder is forced to rotate with respect to the outer forks, and the amplitude of the torque is controlled by the magnetic field, i.e. the MR actuator functions as a controllable brake; when the core and the outer forks are unlocked and a magnetic field is applied to MR fluid and the motor is rotating, the torque produced by the motor is transferred to the outer cylinder and thus can drive the outer cylinder to rotate relatively to the outer forks, i.e. the MR actuator functions as a clutch.

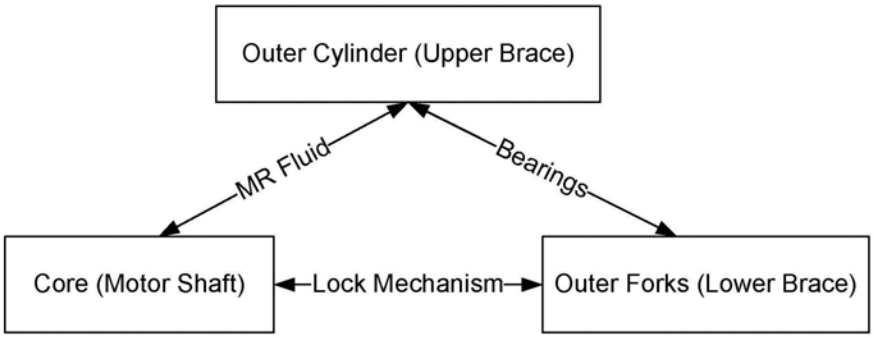

Figure 2.2-2 Motion relationship of modules of MR actuator

According to Bingham plastic model for the MR fluid, the shear stress τ can be calculated as follows [Weiss et al., 1994]:

$$\tau = \begin{cases} \tau_y + \mu\dot{\gamma} & \tau > \tau_y \\ G\gamma & \tau \le \tau_y \end{cases} \tag{2.1}$$

where τ_y is yield stress, μ is viscosity of MR fluid, $\dot{\gamma}$ is the shear rate, γ is the shear strain, G is field dependent material modulus. The configuration of the disks in the actuator is shown in Figure 2.2-3.

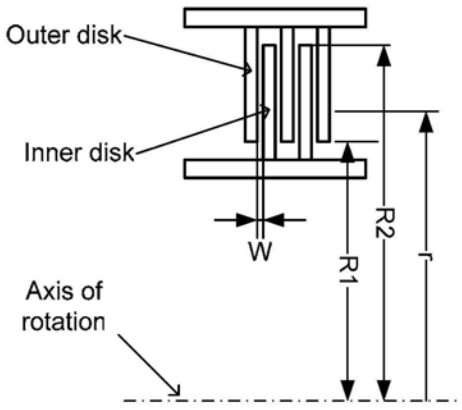

Figure 2.2-3 Disks in the MR actuator

In this system,

$$\dot{\gamma} = \frac{\omega r}{w} \tag{2.2}$$

where ω is the angular velocity of the inner disk, r is the radius, w is the width of the gap between the adjacent outer disk and inner disk. The torque generated by the actuator under post-yield state can be calculated as follows

$$T = 2N \int_{R_1}^{R_2} 2\tau\pi r^2 dr = 4N\pi \left[\frac{\tau_y (R_2^3 - R_1^3)}{3} + \frac{\mu\omega(R_2^4 - R_1^4)}{4w} \right] \tag{2.3}$$

where N is the number of the inner disks, R_1 and R_2 are the inner and outer radius of overlapping areas of disks from the axis of rotation. The first term of equation (2.3) is produced by the yield stress, and the second term is generated by the viscosity of the MR fluid.

It has been shown that, the average peak torque during extension in isometric exercises is 172 Nm for healthy men and 112 Nm for healthy women [Neder et al., 1999]. In fact, for normal activities, the knee torque is much smaller than these peak values; for example, the maximum torque of MR brake used in the knee prosthetic developed by Deffenbaugh et al. (2004) is 50 Nm. A design goal of 20% of healthy knee's torque ability of men is set for the assistive knee brace. It makes the required torque for the MR actuator be 34.4 Nm.

2.3 Magnetic Circuit Design

For the MR actuator, the magnetic field applied to MR fluids determines the on-state torque. Therefore it is important to design an appropriate magnetic circuit. As shown in Figure 2.2-1, the magnetic circuit is formed by the shaft core, side plates, the air gaps between the shaft core and side plates, disks, and MR fluids. The equivalent magnetic circuit is shown in Figure 2.3-1.

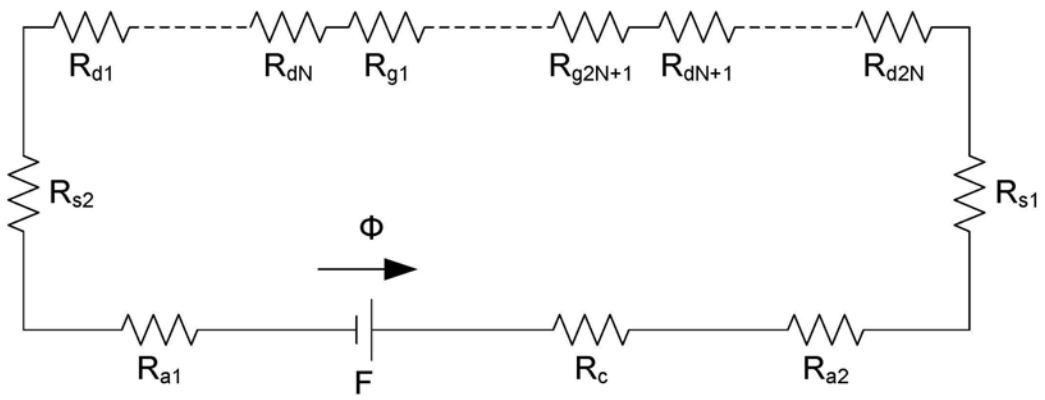

Figure 2.3-1 The equivalent magnetic circuit of MR actuator

If the magnetic circuit is not saturated, the equation of the magnetic circuit is as follows:

$$nI = \sum_{i=1}^{m} R_i \Phi_i \tag{2.4}$$

where I is the coil current, n is number of the coils, R_i is the magnetic reluctance, Φ_i is the magnetic flux, and

$$R_i = \frac{l_i}{\mu_i S_i} \tag{2.5}$$

where l_i is the length of magnetic circuit component, S_i is the area of the cross section, μ_i is magnetic permeability. Since the magnetic circuit components are connected in series, the magnetic induction is the same in the circuit, let $\Phi = \Phi_i$. Therefore, we can obtain

$$\Phi = \frac{nI}{\sum_{i=1}^{m} R_i} = \frac{nI}{R_c + 2R_s + 2R_a + 2NR_d + (2N+1)R_g} \tag{2.6}$$

where R_c, R_s, R_a, R_d, R_g are the magnetic reluctance of shaft core, side plate, air gap between the shaft core and side plate, disk, and the gap between disks (filled with MR fluids), respectively.

The magnetic flux will not always increase with the coil current. When one component is saturated, the magnetic flux will not be increased further. Therefore,

$$\Phi_{\max} = \min(B_{cs}S_c, B_{ss}S_s, B_aS_a, B_{ds}S_d, B_{gs}S_g) \tag{2.7}$$

where B_{cs}, S_c, B_{ss}, S_s, B_a, S_a, B_{ds}, S_d, B_{gs}, S_g are the saturation magnetic flux density and area of shaft core, side plate, air gap, disk, MR fluid gap, respectively.

To improve the performance of the MR actuator, FEM is used to analyze the magnetic circuit. From equation (2.6), we know that the magnetic flux will remain the same if we change the sequence of the magnetic circuit components. Therefore, we can simplify finite element analysis by putting the MR fluid gaps together.

Finite element analysis is first carried out to an existing rotary MR brake developed by Deffenbaugh et al. (2004). The magnetic circuit of the MR brake includes an core, two side plates, forty outer disks, forty one inner disks and MR fluid filled between disks. Commercial FEM software ANSYS is used for analysis. The MR brake is approximately axi-symmetric, so the model is chosen as a 2D axi-symmetric model. The element "PLANE13" is chosen to model all the components in the simulation. PLANE13 has a 2-D magnetic, thermal, electrical, piezoelectric, and structural field capability with limited coupling between the fields. PLANE13 is defined by four nodes with up to four degrees of freedom per node. The element has nonlinear magnetic capability for modeling B-H curves or permanent magnet demagnetization curves. PLANE13 has large deflection and stress stiffening capabilities. When used in pure structural analyses, PLANE13 also has large strain capabilities. Figure 2.3-2 shows the FEM model of the MR brake. A1 is air, A2 is the core, A3 and A4 are side plates, A5 and A6 are disks, A7 is MR fluid, A8 is the coil and A9 is inner cylinder. A2, A3 and A4 are made by Fe-Co alloys; A5 and A6 are made by steel; A9 is made by Ti alloys. The core mates the two side plates via interference fits, so it is assumed that no air exists between the core and side plates.

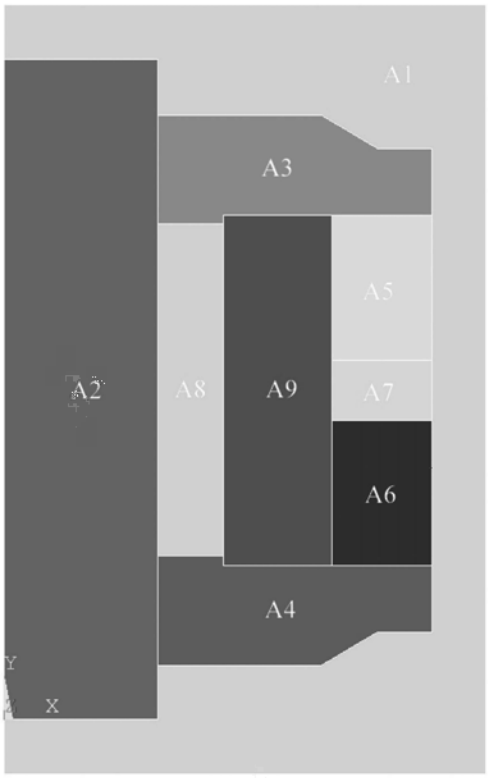

Figure 2.3-2 FEM model of MR brake

The relative permeability of coil and Ti alloys are treated as constant 1. The permeability of soft magnetic material is given as a *B*-*H* curve. Figure 2.3-3 and Figure 2.3-4 show the magnetic properties of Fe-Co alloy (Type Hiperco® alloy 50, which contains 49% Fe, 49% Co, 2% V) and low carbon steel (Type 1010).

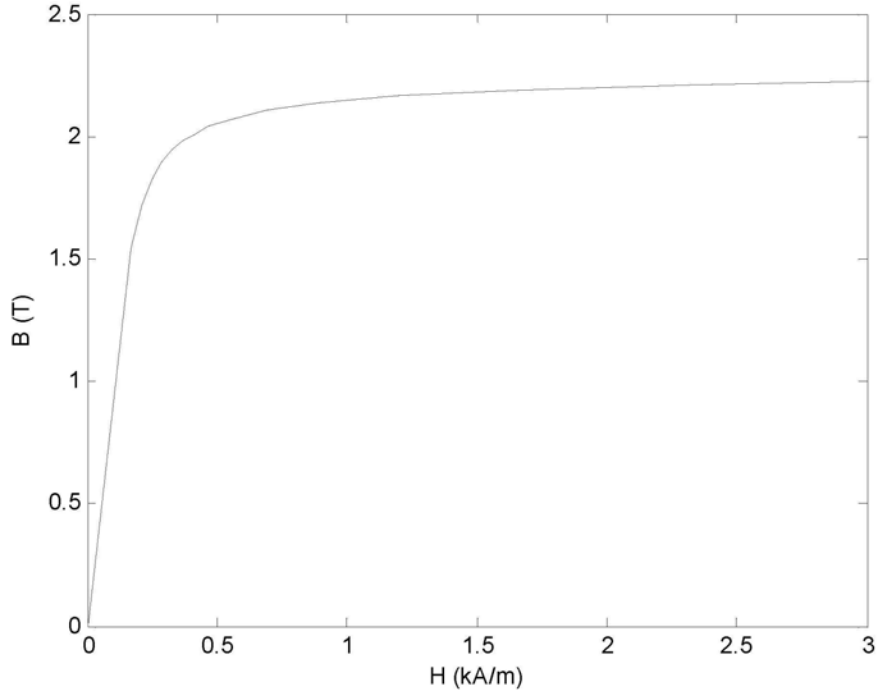

Figure 2.3-3 Magnetic properties of Fe-Co alloy

[Data from http://www.matweb.com]

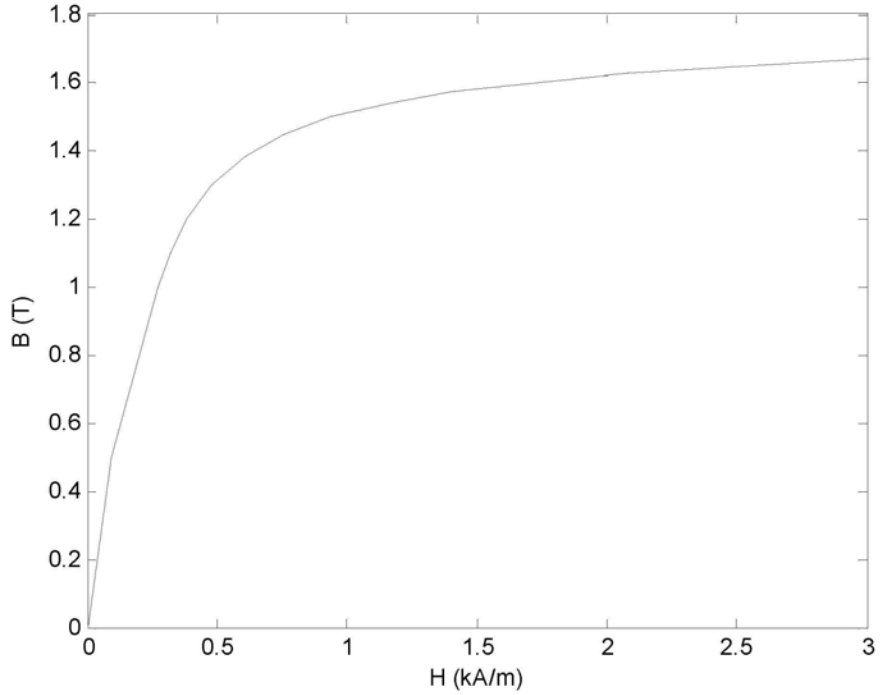

Figure 2.3-4 Magnetic properties of low carbon steel

[Data from ANSYS material library]

The size of the core is $r_c = 8.65\,\text{mm}$, $l_c = 36.9\,\text{mm}$; the size of the overlapping area between inner disk and outer disk is $R_1 = 18.4\,\text{mm}$ $R_2 = 24\,\text{mm}$; the thickness of the disk is 0.2 mm; the gap between inner disk and outer disk is 0.04 mm. The average mesh size is chosen to be 0.25 mm. The number of the turns of the coil is 340.

Figure 2.3-5 and 2.3-6 show the simulation results with an applied current of 1.0A and 1.5 A, respectively. It can be seen that when the applied coil current is 1.5 A, a maximum value of 2.314 T is reached at the core, which is the saturation magnetic flux density of Fe-Co alloy (see Figure 2.3-3). It means that the magnetic flux density of the MR brake can not be further increased with higher coil current value. In fact, it can be found that the magnetic flux density of MR fluid only increases slightly when the coil current increases from 1.0 A to 1.5 A.

The average magnetic flux density of the MR fluid under 1.5 A coil current is about 0.64 T. From Figure 2.1-3, it can be found that the corresponding magnetic field in MR fluid is about 130 kA/m. The yield stress is about 36 kPa as seen from Figure 2.1-2. With Equation (2-3), the maximum torque of the MR brake can be calculated as 47 Nm, which is very close to the actual maximum torque of 50 Nm.

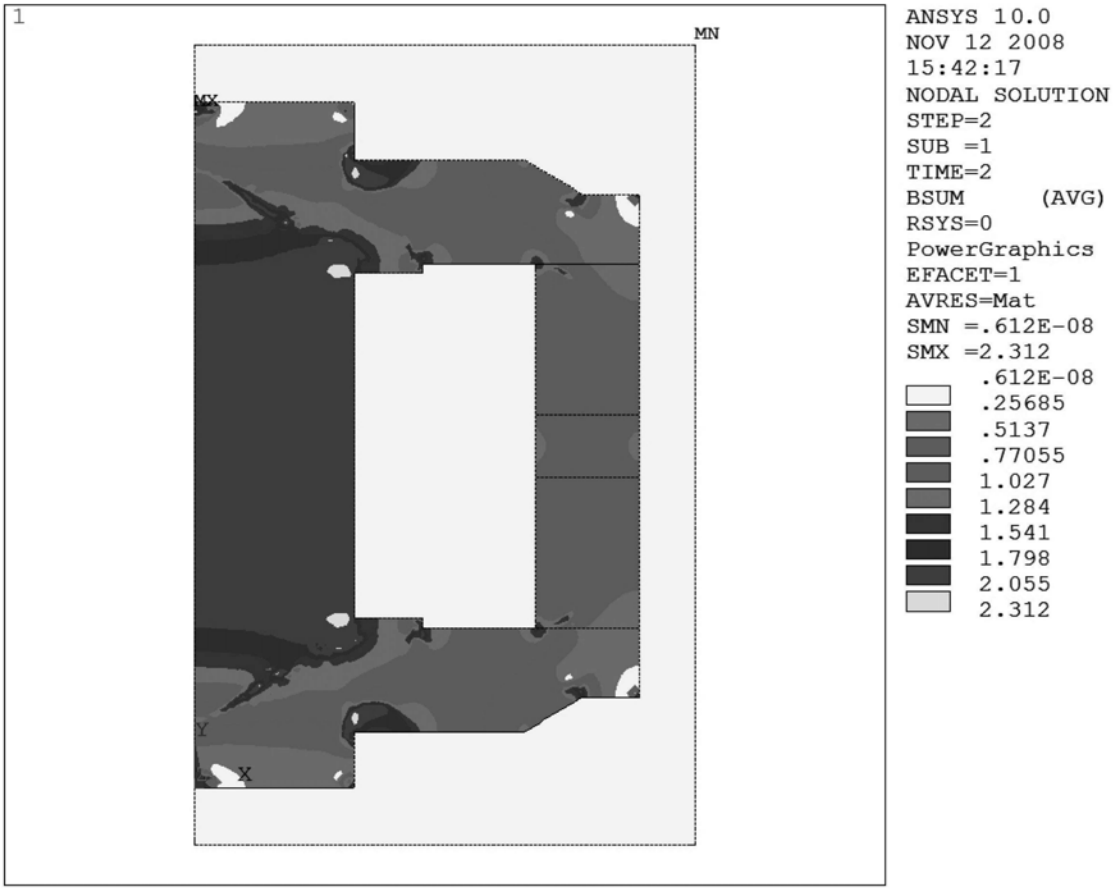

(a)

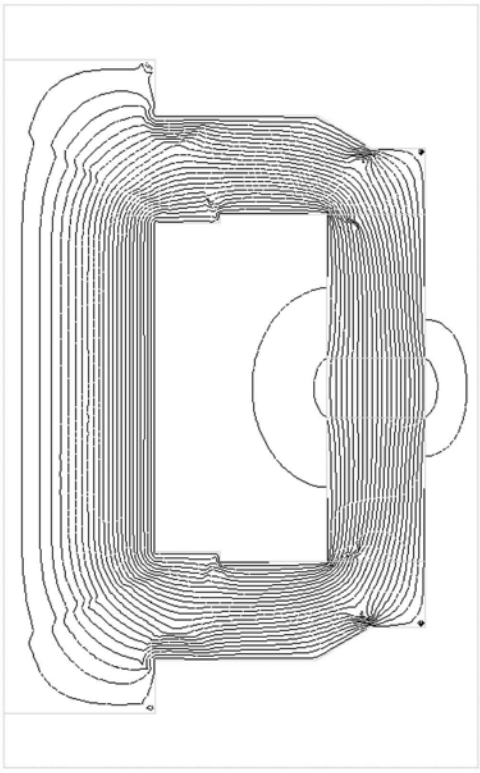

(b)

Figure 2.3-5 Magnetic flux density (a) and magnetic flux (b) of MR brake under 1.0 A coil current

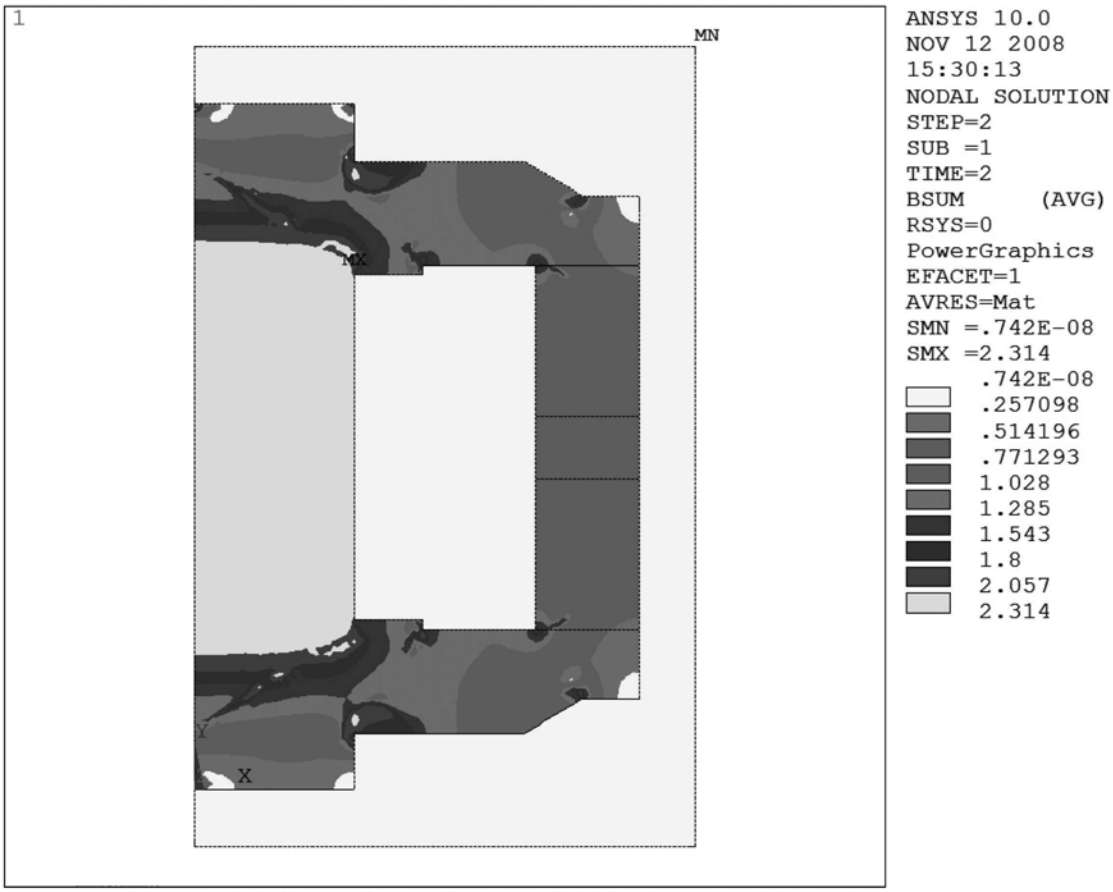

Figure 2.3-6 Magnetic flux density of MR brake under 1.5 A coil current

Compared to the above-mentioned MR brake, the magnetic circuit of the new MR actuator should be thinner in the axis direction since DC motor will be attached to the MR actuator in this direction. So the magnetic circuit should be made as thin as possible in axis direction but can be made slightly larger in the radius direction. As stated previously, electric pure iron is used as core material instead of Fe-Co alloy. Since the magnetic saturation of electric pure iron is smaller than that of Fe-Co alloy, the diameter of the coil core should be relatively larger. For convenience of assembling, a gap of 0.1 mm is left between the core and the side plates. The magnetic circuit is analyzed and designed with FEM, Figure 2.3-7 shows the FEM model of the final design.

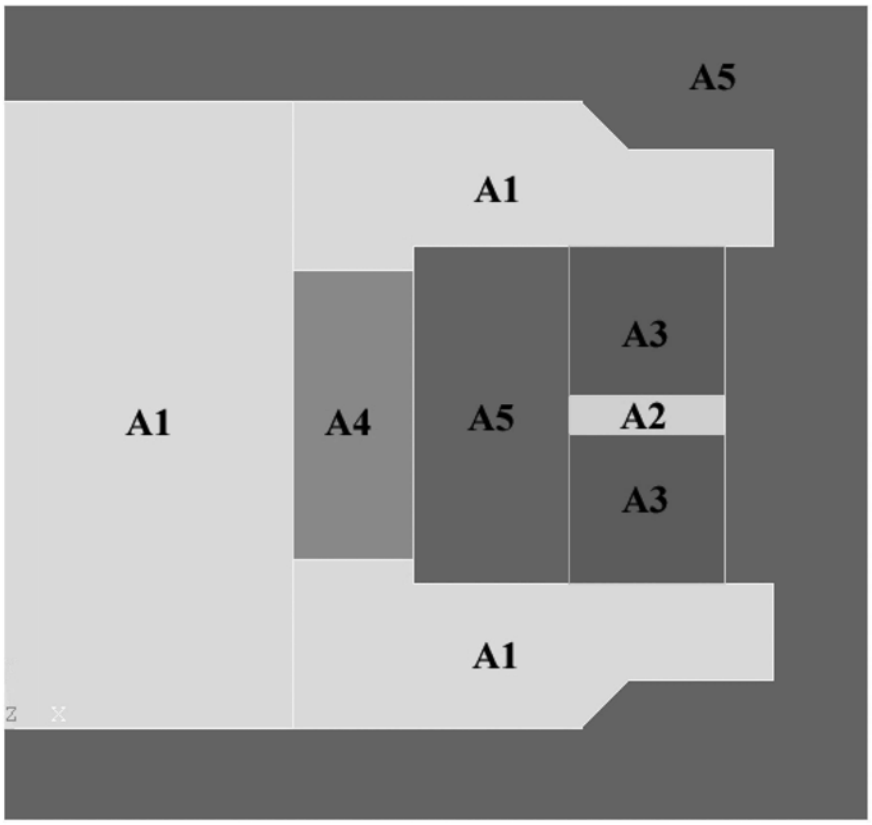

Figure 2.3-7 FEM model of MR actuator

The diameter of the core is 24 mm, and the length is 26 mm. The dimensions of the disks: R_1 = 23.5 mm, R_2 = 30 mm. The height of A2 is 1.6 mm. The magnetic flux density of the MR actuator under 1.5 A, 2.0 A, 2.4 A are shown in Figures 2.3-8 ~2.3-10.

From Figure 2.3-8, the magnetic flux density at the MR fluid is between 0.344 T and 0.516 T. The corresponding magnetic field is about 75 kA/m, and the yield stress is about 23 kPa. The calculated torque is 27 Nm. From the figure it can be seen that no saturation happened.

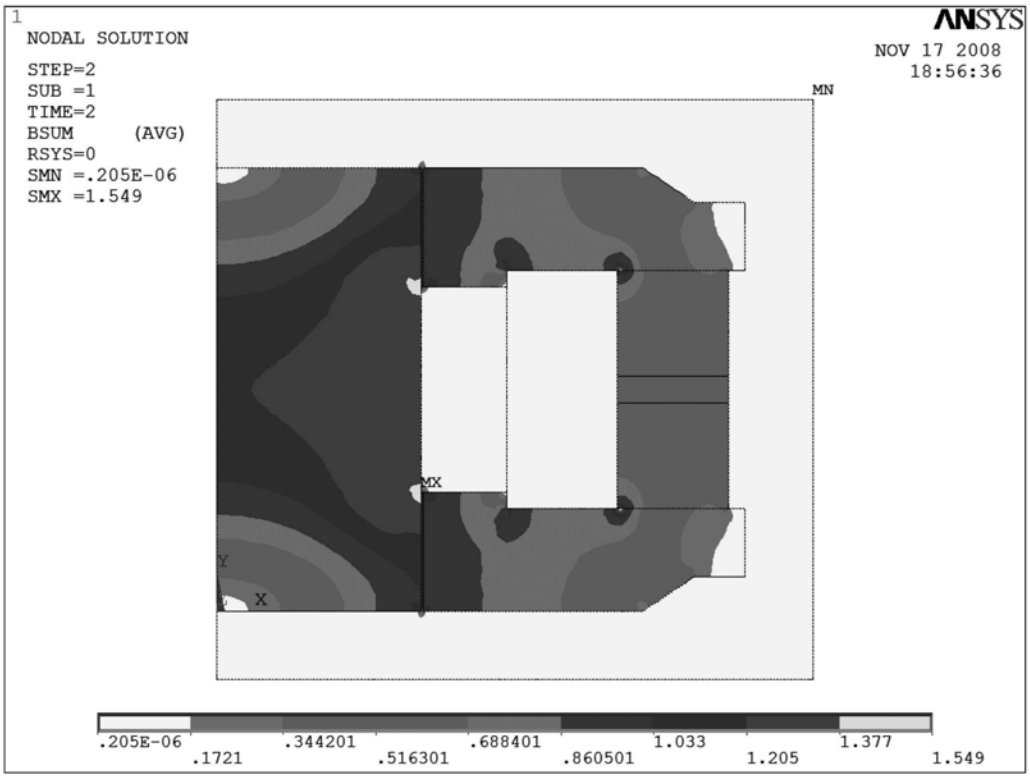

Figure 2.3-8 Magnetic flux density under 1.5 A coil current

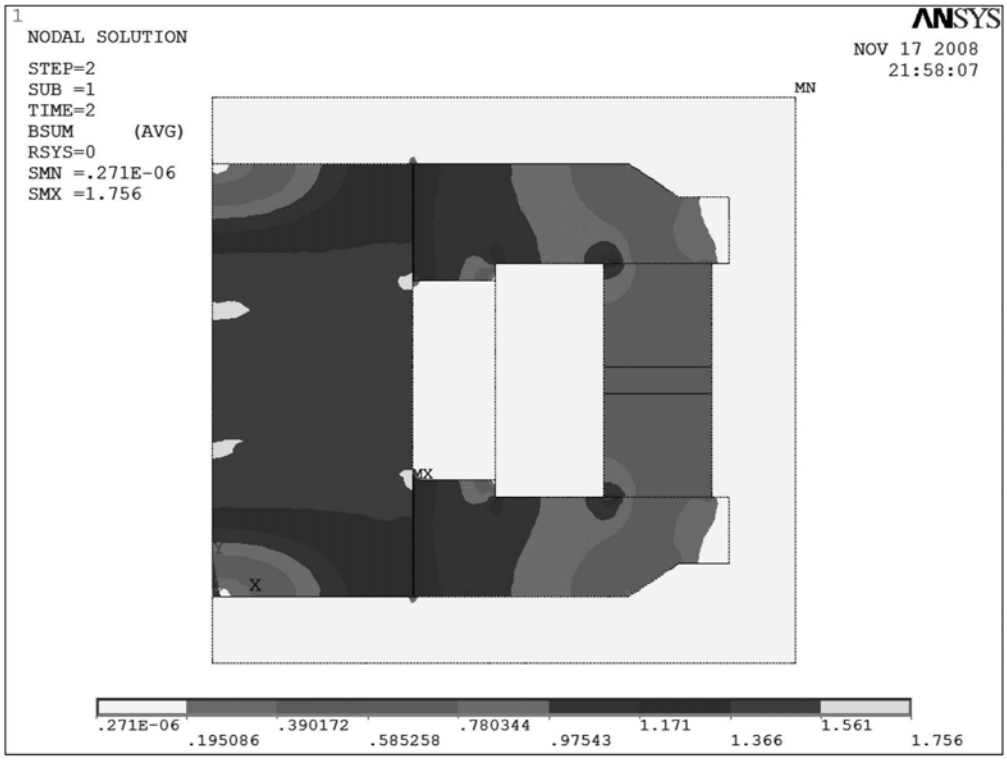

Figure 2.3-9 Magnetic flux density under 2.0 A current

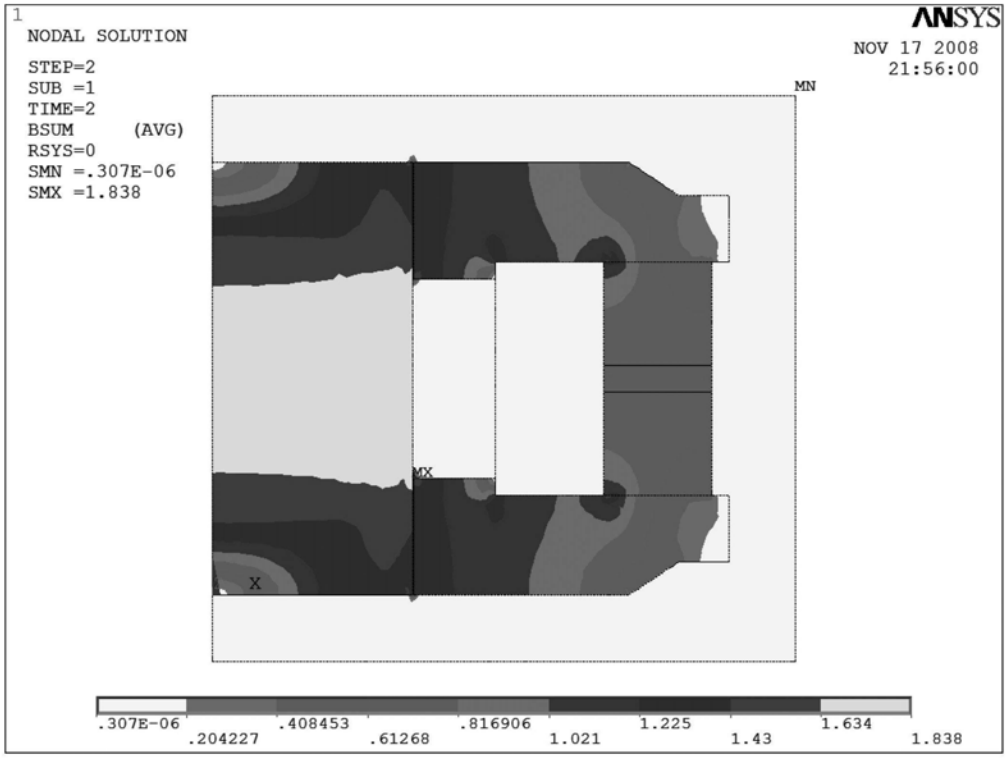

Figure 2.3-10 Magnetic flux density under 2.4 A current

From Figure 2.3-9, it can be seen that the magnetic flux density at the inner corner of core and side plate is close to the saturation of pure iron. The magnetic flux density of MR fluid is between 0.390 T and 0.6 T. The corresponding magnetic field is about 90 kA/m and the yield stress is about 27 kPa. The calculated torque of the MR actuator under 2.0 A current is 31.7 Nm.

From Figure 2.3-10, it can be seen that the magnetic flux density at the core is saturated. That means even further increase coil current can not increase the torque of MR actuator. The torque produced under 2.4 A is the maximum torque the MR actuator can produce. The magnetic flux density in the MR fluid is between 0.6 T and 0.8 T. The corresponding magnetic field is about 150 kA/m and the yield stress is 39 kPa. The calculated torque of the MR actuator is 45.8 Nm.

2.4 Design of MR actuator

For standing up or climbing stairs, the knee joint extends to provide positive torque; for sitting down or going down stairs, passive torque occurs at the knee joint to absorb energy. For normal walking, as shown in Figure 2.4-1 [Herr and Wilkenfeld, 2003] (RHS: right heel strike; RFF: right flat foot; LTO: left toe off; RHO: right heel off; LHS: left heel strike; LFF: left flat foot; RTO: right toe off; LHO: left heel off), the knee power is mainly passive, where usually happens during the bending of the knee joint; active power occurs during the extending of the knee. Based on the working conditions of knee joint, a pair of one-way bearings is used in the actuator to function as the lock/unlock mechanism as stated in Chapter 2.2. In the extending direction, the one-way bearings can rotate freely and the MR actuator can function as a clutch to transfer the torque of motor to the knee brace. In the bending direction, the one-way bearings are locked and the MR actuator can function as a brake to provide passive assistive torque.

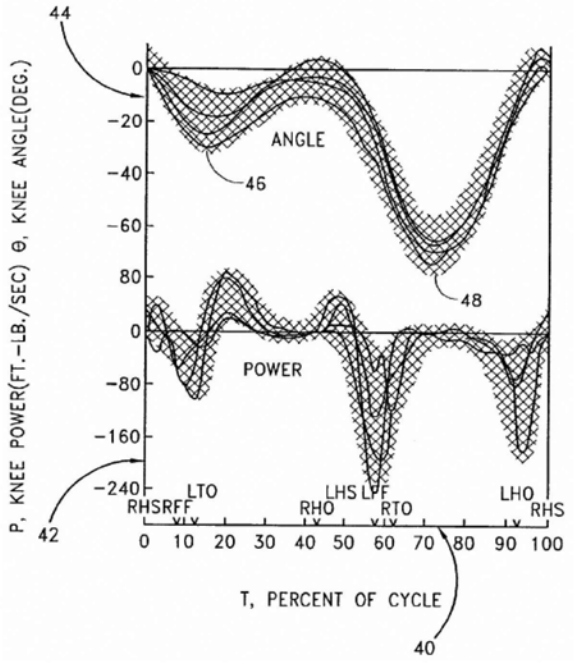

Figure 2.4-1 Knee power vs. knee joint during normal walking

[Herr and Wilkenfeld, 2003]

The section view and exploded view of the designed MR actuator are shown in Figures 2.4-2 and 2.4-3. The one-way bearings used here are model CSK 17 purchased from TBP Inc. A pair of thin wall bearings (Type: 6711, purchased from Cixi Chilong Bearing Factory) are used for mechanical transmission between outer cylinder and forks. Table 2.4-1 shows the technical data of the bearings.

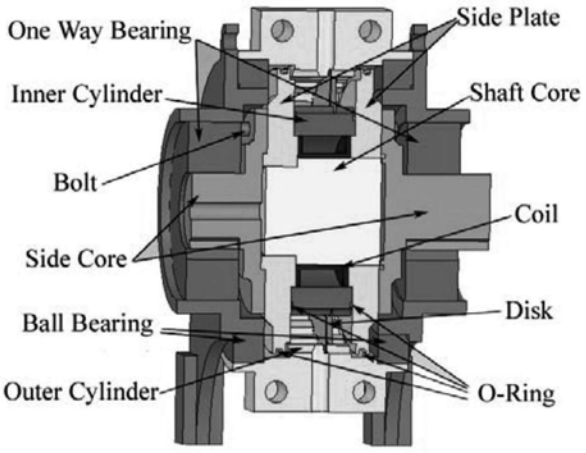

Figure 2.4-2 Section view of MR actuator

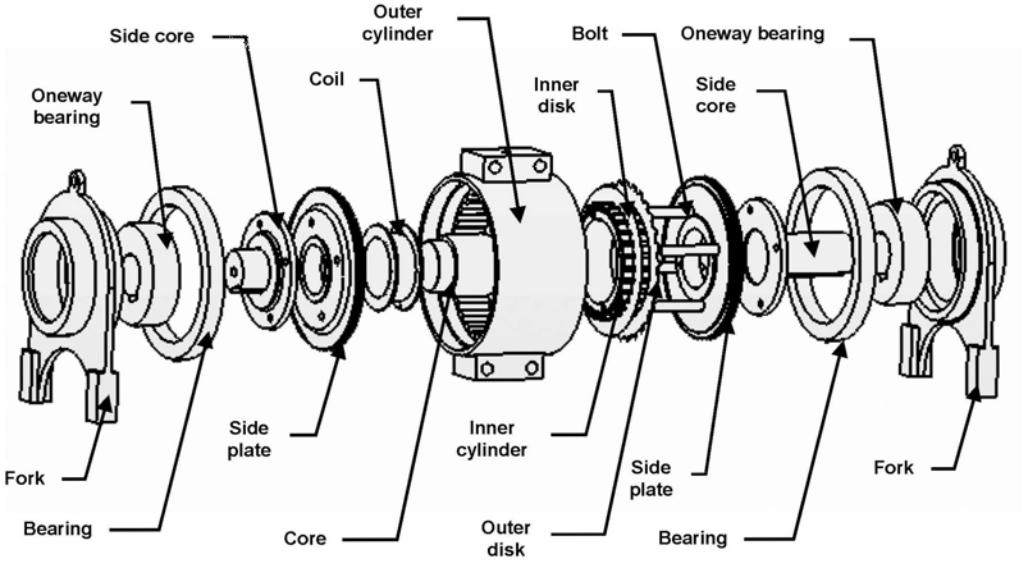

Figure 2.4-3 Exploded view of MR actuator

Table 2.4-1 Technical data of one-way bearing and thin wall bearing

Model	Boundary Dimensions (mm)			Torque (Nm)	Keyway Size (mm)		Weight (Kg)
	Inner Diameter	Outer Diameter	Width		Depth	Width	
6711	55	68	7	-	-	-	0.030
CSK 17	17	40	12	24.5	1.6	6	0.070

As stated in Section 2.2, the MR actuator consists three modules: the forks module, the core module, and the outer cylinder module.

The outer cylinder module contains the outer cylinder and outer disks, which are engaged in the spline of outer cylinder. The thin wall bearings provide supporting force to the outer cylinder module and allow frictionless motion of outer cylinder module relative to the forks module. The outer cylinder has a pair of ears for mounting to upper brace. A pair of holes on the ears allow easy MR fluid injection.

The core module contains the major part of magnetic circuit (including the core, side plates, coil and inner disks), inner cylinder, and a pair of side cores. A circular groove in the outer surface of side plate accommodates an O-ring for sealing of MR fluid. The inner disks are engaged in the splines of inner cylinder. A pair of circular grooves on both side surface of inner cylinder holds two O-rings for side sealing of MR fluid. The inner cylinder is bonded to the side cores through four bolts. A hole in one side core allows passing of wire for the coil. The core of other side core functions as input shaft that connects to the output of motor.

The forks module contains a pair of forks. It mechanically transmits with the outer cylinder module and core module through one-way bearings and thin wall bearings. It provides housing and supporting to the other two modules.

2.5 Fabrication of MR actuator and sealing of MR fluid

The inner disks and outer disks are fabricated by electrical discharge machining method. Other components are machined without any physical or chemical treatments. AWG 40 gauge copper wire is used as the coil wire. And the winding comprises 200 turns. The measured resistance of the coil is 3.8 Ω.

The outer cylinder, inner cylinder, and two side plates form a chamber that holds MR fluid. To prevent leakage of MR fluid, the contacting areas between these parts should be well sealed and Teflon O-rings are used in all these areas for sealing. Besides O-rings, more means are used to secure the seal. For static seal (between inner cylinder and side plates, which both belong the core module and no relative motion once assembled), RTV silicone gasket maker (produced by Dongbao Sealing Gum Factory Cangcheng Kaiping, China) is used as sealant. For dynamic seal (between outer cylinder and side plates, which belong to outer cylinder module and core module respectively, and relative motion is allowed during normal working), 111 Valve Lubricant & Sealant (produced by Dow Corning Corp., U.S.A) is used between O-rings and outer cylinder to provide lubrication and sealing.

Before injection of MR fluid, the MR actuator is assembled and water is filled in to check the sealing of the MR actuator. Once no leakage is observed, the MR actuator is dried and cleaned and MR fluid is injected using a syringe. Let the two holes of outer cylinder line in vertical direction and the MR fluid is injected in slowly from the lower hole. While injecting, keep the position of outer cylinder and rotate the forks module (makes the inner disks and outer disks rotate relatively) so as to make the MR fluid fill to the gaps between inner disks and outer disks. When the chamber is fully

filled with MR fluid, adhesive tapes are used to seal the holes (first seal the upper hole then the lower one).

Totally about 6 ml MR fluid is filled to the MR actuator and the weight of the MR actuator (filled with MR fluid) is about 1 kg. Figure 2.5-1 shows the disassembled and assembled MR actuator

Figure 2.5-1 Fabricated MR actuator (disassembled and assembled)

2.6 Construction of Testing Setup

The configuration of testing setup for MR actuator is shown in Figure 2.6-1. Via a 10:1 gearbox (Type B, Makishinko Inc.), an AC motor (AM 100L S4Y4, Lloyd Dynamowerke GmbH & Co. KG) is connected to the side core of MR actuator to drive the core module of MR actuator to rotate. The outer cylinder is fixed to the mounting plate through a load cell (208C03, PCB Piezotronics Inc.). Thus when the core rotates, the MR fluid will work at post-yield state. The force multiplied by the length of arm is the torque the MR actuator produced.

The force signal is conditioned by a signal conditioner (442A101, PCB Piezotronics Inc.), then is acquired by the dSPACE system (DS 1104, dSPACE Inc.), which also commands suitable control voltage signal to the MR actuator. The dSPACE system includes software and hardware. The software interfaces with MATLAB on a PC and allows the user to create a control block diagram of the system using the dSPACE Real-Time Interface in Simulink of MATLAB. When the model is built in Simulink, it will be written to the hardware of dSPACE. The hardware of dSPACE includes DS 1104 R&D Controller Board (which is mounted in a PC) and Connector and LED Panel. ControlDesk is a software that can manage and instrument real-time Simulink experiments. In the testing experiments, ControlDesk is used to build the interface that displays the experimental data and input control signals. Figure 2.6-2 shows the photo of experimental setup for testing.

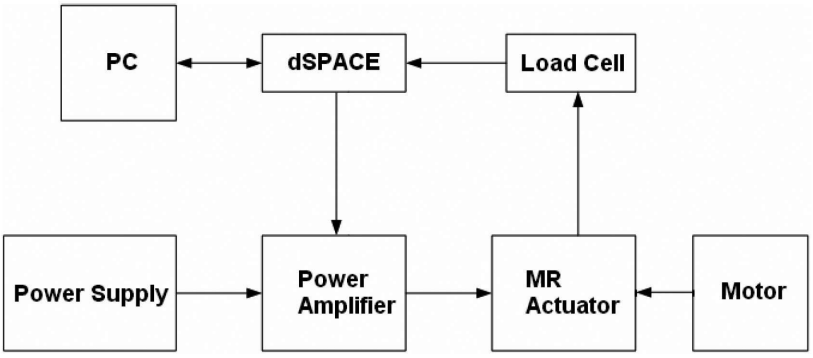

Figure 2.6-1 Configuration of testing setup for MR actuator

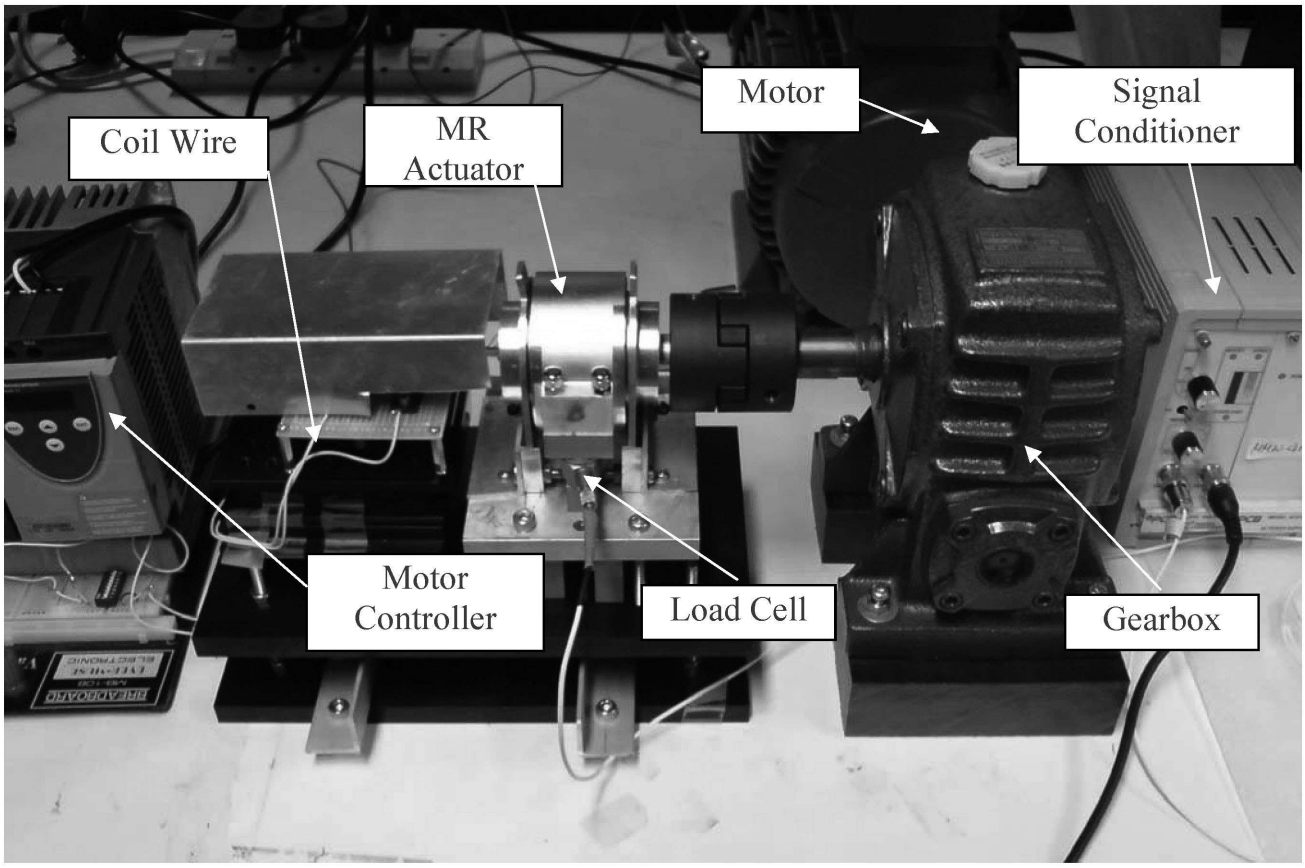

Figure 2.6-2 Testing setup for MR actuator

The current of MR actuator is regulated by the control voltage of dSPACE output, and a power amplification circuit is built, as shown in Figure 2.6-3. The relationship between control voltage (V_c) and coil current (I_{MR}) can be calculated as

$$I_{MR} = \frac{2.7}{0.33 \times (20 + 2.7)} V_c = 0.36 V_c \tag{2.8}$$

To further verify the relationship between coil current and control voltage, a sinusoidal control signal $V = (1 + \sin(2\pi t)) * 1.35$ is applied to the power amplification circuit. Figure 2.6-4 shows the experimental results. The measured relationship between coil current and control voltage is

$$I_{MR} = 0.36 V_c - 0.02 \tag{2.9}$$

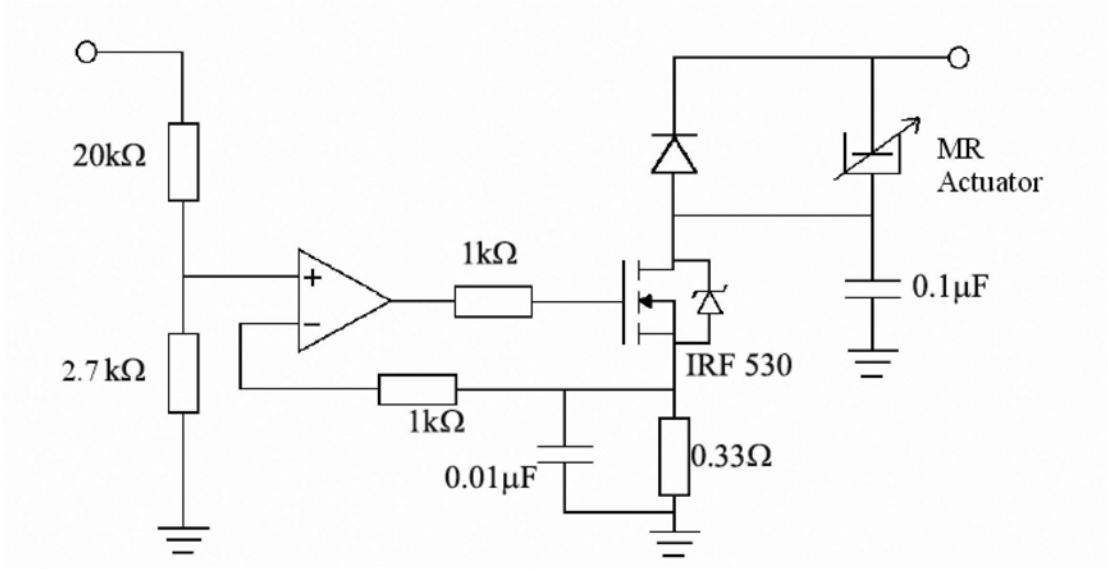

Figure 2.6-3 Power amplification circuit for MR actuator

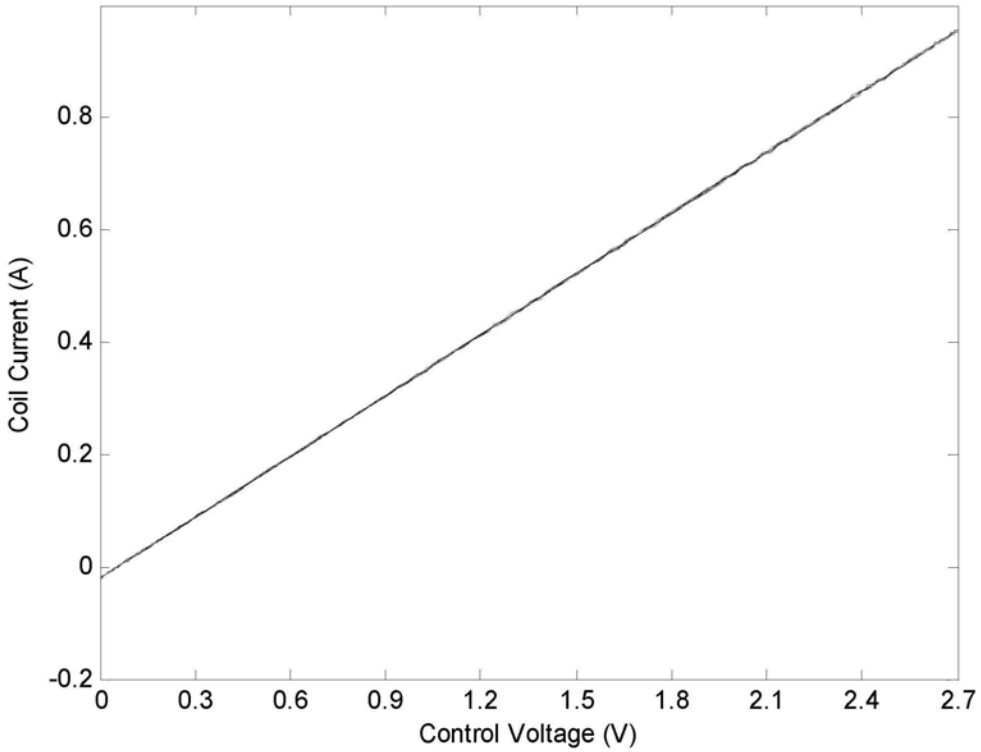

Figure 2.6-4 Relationship between control voltage and coil current

2.7 Testing Results

As mentioned in the previous section, with the experimental setup, the core module of MR actuator can be driven to rotate at various speed by an AC motor; the coil current of MR actuator can be controlled by dSPACE on the PC; the torque produced by the MR actuator is measured by a load cell, and this force information can be either collected by the dSPACE system or an FFT Analyzer. In this experiment, the torque of MR actuator under different coil currents, different MR rotating speeds is tested. The hysteresis and step response of the MR actuator are also tested.

First, the hysteresis of the MR actuator is tested. The MR actuator is driven to rotate at a constant speed of 1.4 rad/sec. Sinusoidal signals with different coil current frequency are applied to the MR actuator.

$$I_{MR} = (1+\sin(f*2\pi t))/2, f = 1,\ 1/3,\ 1/10 \qquad (2\text{-}10)$$

Since the control signal is an AC signal, the signal conditioner of load cell is switch to "AC" mode to enhance the signal/noise ratio. Figure 2.7-1 shows the experimental results. It can be seen that when the frequency of coil current is 1 Hz, large hysteresis is observed. While the frequency of coil current is about 0.1 Hz, almost no hysteresis exists. Though the hysteresis difference is significant, the amplitude of torque under different current frequency doesn't vary much.

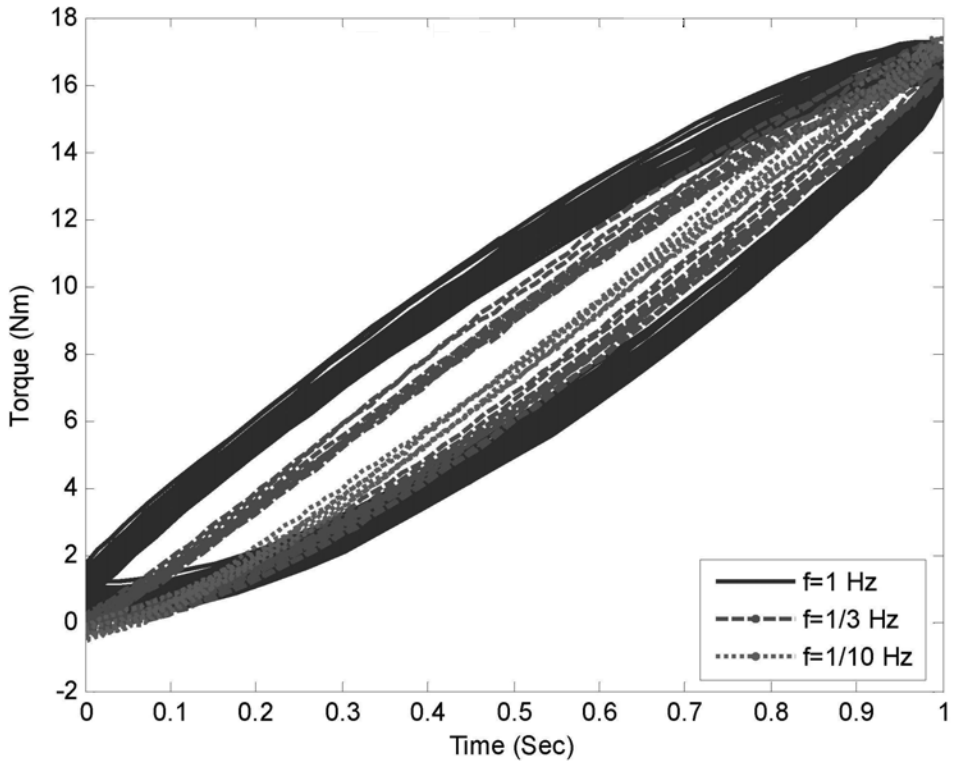

Figure 2.7-1 Hysteresis of MR actuator under different current frequency

The rotating speed of the MR actuator is changed by varying the speed of the driving motor to study the relationship between the torque of MR actuator and shear rate. The same sinusoidal control signal as Equation (2-10) with current frequency 0.2 Hz is applied to the MR actuator. The rotation speeds used for MR actuator are set as 0.48, 1.40, 5.24 rad/sec, respectively.

Figure 2.7-2 shows the experimental results. It can be seen from the figure that the difference is insignificant between the torques under different MR actuator speeds. According Bingham plastic model, the torque produced by the MR fluid includes the yield stress and the viscosity part. It means that here the yield stress dominates the viscosity part.

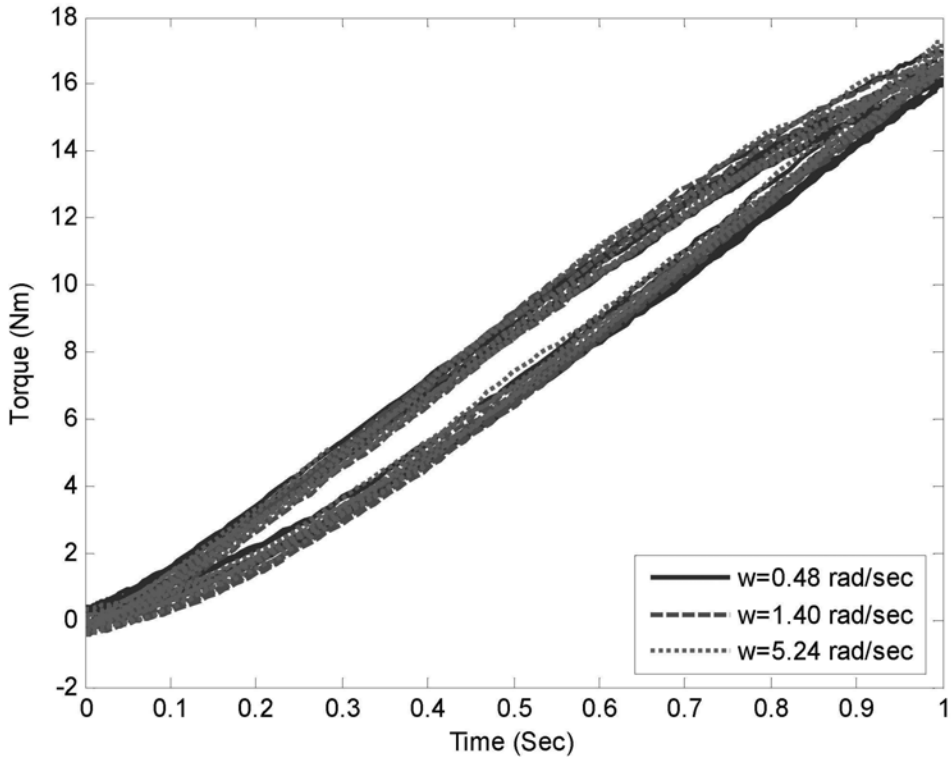

Figure 2.7-2 Measured torque at different MR actuator rotation speeds

The next experiment is to study the torque produced by the MR actuator with different coil currents. The motor drives the MR actuator to rotate at 1.4 rad/sec. As shown in previous section, the resistance of coil is 3.8 Ω, if 2.0 A current is applied, the power of the coil is 15.2 W. To prevent overheating, the maximum current used in this experiment is 1.8 A. The applied coil current is

$$I_{MR} = I_A(1+\sin(0.2*2\pi t)),\ I_A = 0.1,\ 0.2,\ \ldots,\ 0.9 \qquad (2\text{-}11)$$

The experimental results are shown in Figure 2.7-3 and Figure 2.7-4. From the figure, we can see that the torque produced by the MR actuator significantly increases with applied coil current (Noted that the DC components of the torque signals are not shown in Figure 2.7-3).

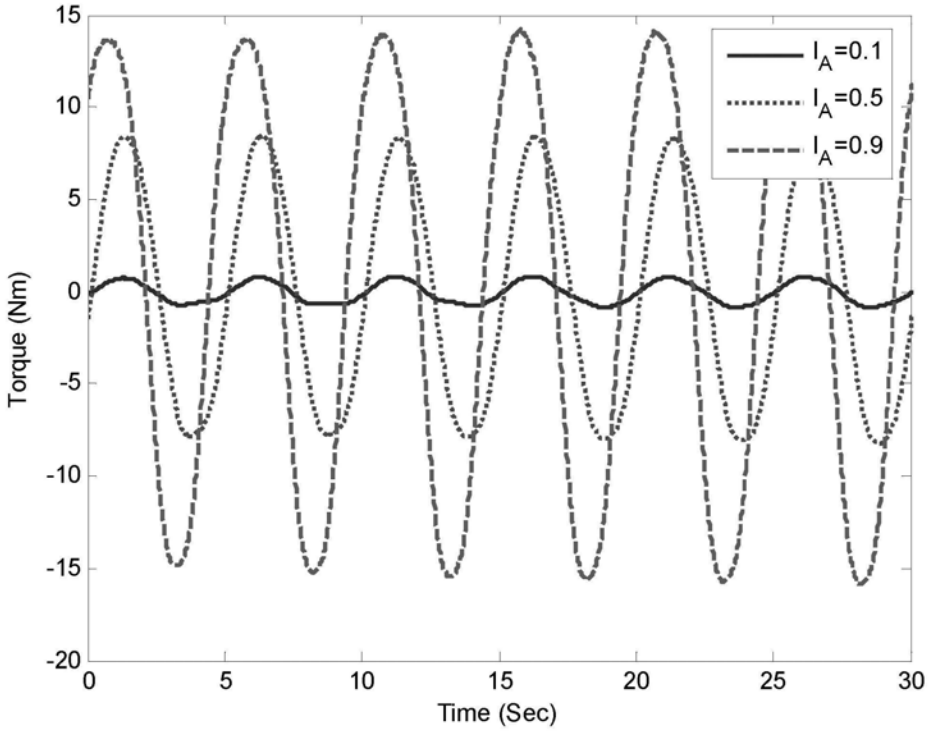

Figure 2.7-3 Measured torque at different coil currents

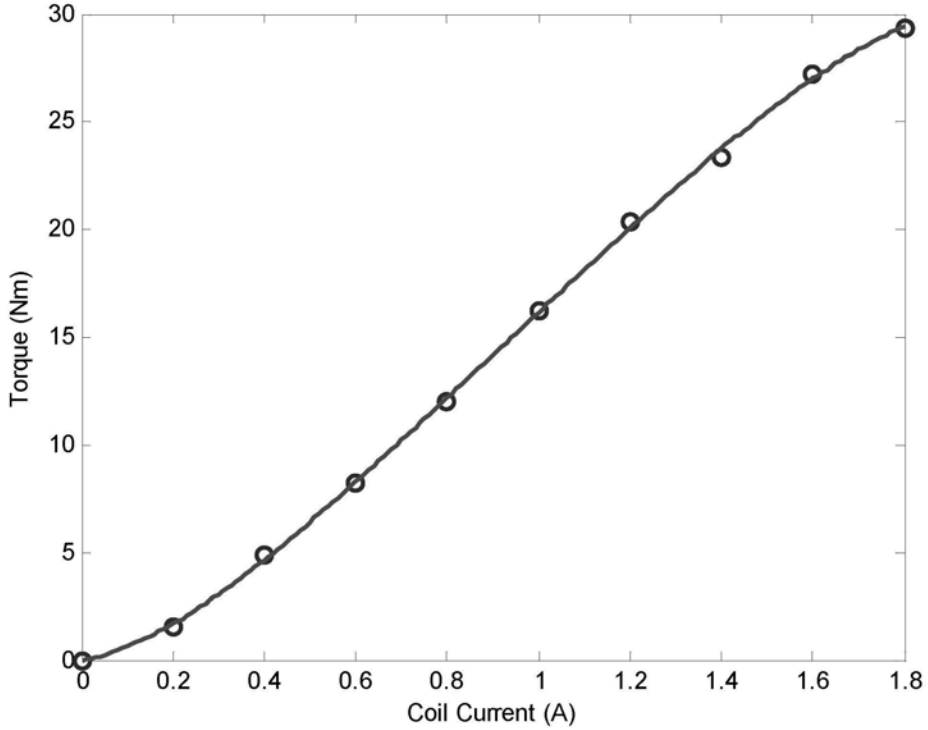

Figure 2.7-4 Measured torque vs. applied coil current

As shown in section 2.3, the torque calculated from simulation for current 1.5 A and 2.0 A is 27 Nm and 31.7 Nm, respectively. These results are close to the experimental results in Figure 2.7-4.

The step response of the MR actuator is tested in the following experiment. The motor drives the MR actuator to rotate at a constant speed of 1.4 rad/sec. A pulse current (pulse width: 5 sec) with different amplitude of 0.5, 1.0, 1.5 and 1.8 A is applied to the coil of MR actuator. The signal conditioner is switched to "DC" mode and the force signal is received by dSPACE, no filter is used for the signal. Figure 2.7-5 is the experimental result at current amplitude of 1.0 A.

It can be seen from the figure that the response time of MR actuator is about 0.1 sec. As comparison, the reaction time of normal human is between 0.15 sec and 0.40 sec. So it is capable of providing assistance in time. The experiments with different coil currents show that the response time doesn't rely on the amplitude of applied current.

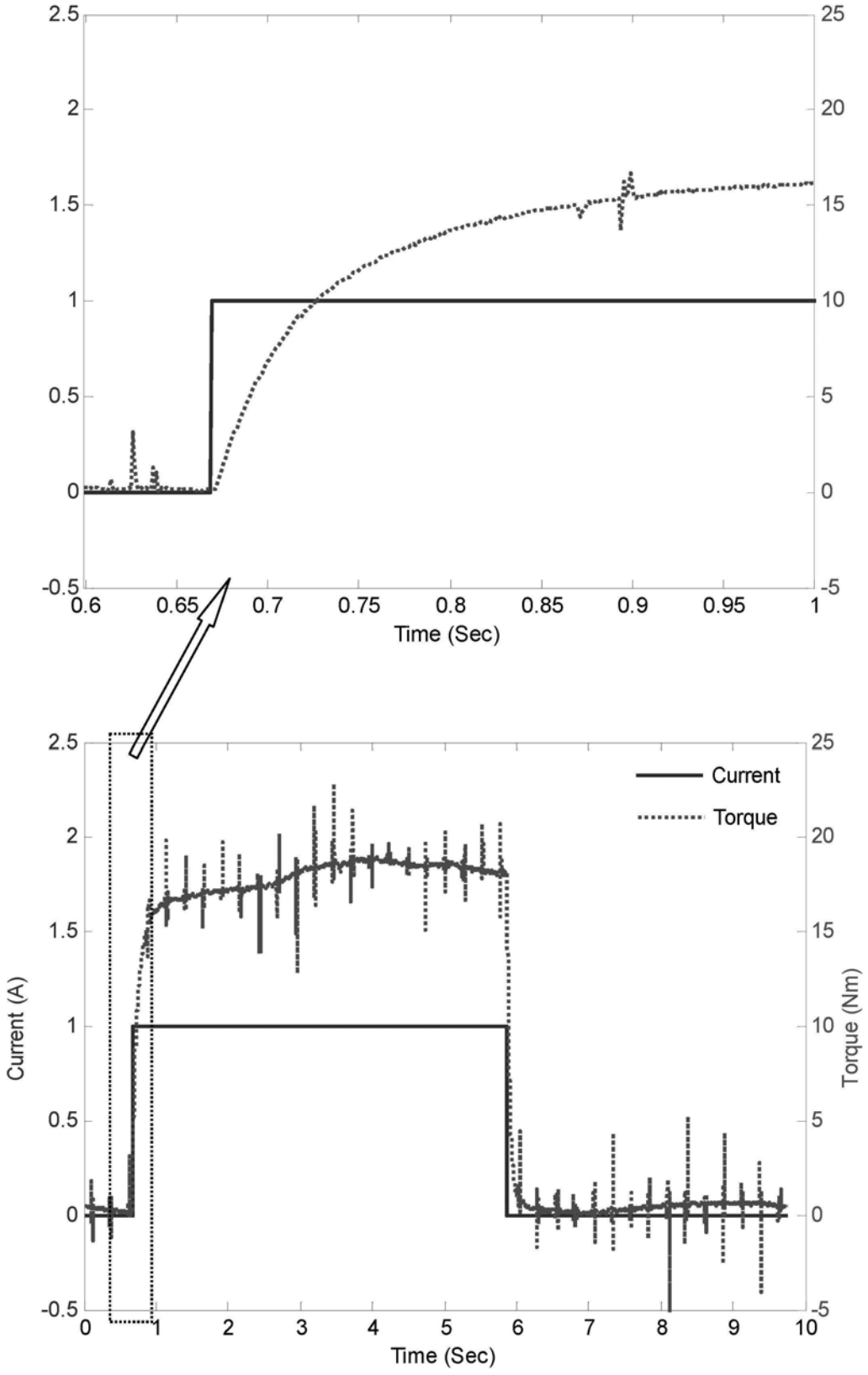

Figure 2.7-5 Step response of MR actuator

2.8 Chapter Summary

Based on the working conditions of knee joint, the MR actuator that can function as a brake or a clutch is considered. The magnetic circuit of the MR actuator is analyzed. With the help of FEM, the torque of the proposed MR actuator is calculated. The first prototype of the MR actuator is designed and fabricated. Testing apparatus and method for evaluating the developed MR actuator are also introduced. Experimental results show that the torque of the MR actuator increases as coil current increases. The measured torque of the MR actuator is close to calculated one, and it is adequate to provide assistance for the knee joint. The response time of the MR actuator is acceptable for application to human body. Experimental results also show that the torque of MR actuator does not rely on the rotation speed of MR actuator. However, when the coil current changes fast, significant hysteresis is observed.

CHAPTER THREE

CONTROL OF MR ACTUATOR

Either as a clutch to transfer energy to drive human leg or as a brake to dissipate energy of moving human leg, the MR actuator will directly interact with human body. So the control of MR actuator so as to provide proper assistive torque is a very important issue. As discussed in Chapter Two, the MR actuator is a non-linear device; in which hysteresis exists. These would add the difficulty for the control of MR actuator.

PID controller is the mostly used controller in industry applications. It attempts to correct the error between a measured process variable and a desired set point and then adjust the process accordingly. The most important thing for PID controller is the choice of controller gains. In this Chapter, the MR actuator is modeled and experiments are carried out to find the model parameters. The controller parameters are chosen based on the model. Anti-windup strategy is used to prevent instability. Experiments are carried out to test the torque tracking performances of the MR actuator under control.

The model parameters of MR actuator may vary as time or environment changes (such as abrasion of MR fluid etc.), so parameter adaptive controller is also proposed for the control of MR actuator. Experiments are also carried out for torque tracking of MR actuator under adaptive control.

3.1 PID Controller

PID controller was first placed to the market in 1939, and now is still widely used in process control. Investigation indicated that more than 90% of the controllers used in process industries are PID controllers and their advanced versions. "PID" is an acronym for "proportional, integral and derivative". It includes three terms: proportional term, integral term and derivative term. Let $u(t)$ be the controller output, the PID controller can be expressed as

$$u(t) = K_p e(t) + K_i \int_0^t e(\tau) d\tau + K_d \frac{de(t)}{dt} \tag{3.1}$$

where e(t) is the error between the plant output and set value; K_p, K_i and K_d are proportional gain, integral gain, and derivative gain, respectively. Larger proportional gain means faster response, but too large value can make the system unstable and oscillating. Larger integral gain means quicker elimination of steady state error, but brings larger overshoot. Larger derivative gain can decrease overshoot, but slows down the response time. Sometimes only one or two terms of PID controller are required, and other terms are set to zero. A PID controller can be called a PI, PD, P or I controller when other terms are set to zero. PI controller is particularly common because the derivative action is very sensitive to noise.

If the parameters of PID controller are chosen inappropriately, the controlled process can be unstable. The parameters can be manually tuned; the tuning method is to first set K_i and K_d zero, increase K_p until the output oscillate, then set K_p to half of that value. Then increase K_i until the offset is correct in sufficient time. Finally increase K_d until the output is acceptably quick to reach its reference value. This method is not

efficient and experience is required. Ziegler-Nichols method is a well known proven tuning method. Like the manual tuning method, first set K_i and K_d zero, increase K_p until the output oscillate, record this critical gain K_c and the oscillation period P_c, the control parameters are set as given in Table 3.1-1. Like the manual tuning method, Ziegler-Nichols method has trial-and-error and very aggressing. PID tuning software is also used for parameter tuning. But cost and training are needed. The most effective method is to develop a process model and choose the parameters based on the model.

Table 3.1-1 Parameter setting for Ziegler-Nichols method

Control Type	K_p	K_i	K_d
P	$0.50K_c$	-	-
PI	$0.45K_c$	$1.2K_p/P_c$	-
PID	$0.60K_c$	$2K_p/P_c$	$K_pP_c/8$

3.2 IP Controller for MR Actuator

Takesue et al. used IP controller for the torque control of MR actuator [Takesue et al., 2001]. The IP controller is an advanced version of I controller where the control parameters are determined based on process model. It is demonstrated that this controller can achieve good performance and the control parameters can be easily determined. So IP controller is used here for the torque control of MR actuator. The plant is modelled as:

$$T_O = T\dot{T}_O + KI \tag{3.2}$$

where T_o is the torque output of MR actuator, I is the coil current of MR actuator, T and K are parameters.

The transfer function of the plant can be written as

$$P(s) = \frac{T_O(s)}{I(s)} = \frac{K}{Ts+1} \tag{3.3}$$

The closed loop control system is described in Figure 3.2-1.

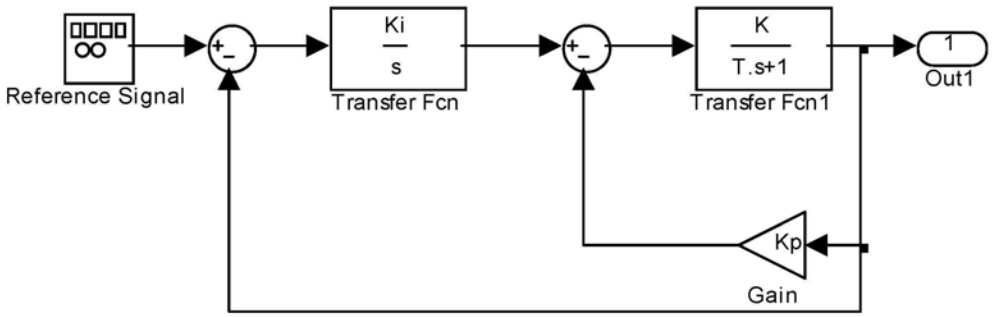

Figure 3.2-1 IP control system for MR actuator

To find proper control parameters for K_i and K_p, experiments are carried out to find the plant parameters K and T. The MR actuator is rotating at a constant speed of 1.2 rad/sec, then apply a sinusoidal current with different frequency to the coil of MR actuator and measure the torque output of the MR actuator. The coil current is

$$I_{MR} = (1.5 + 0.5\sin(\omega t))/3.7,\ \omega = 0.5,1,2,4,8,16,32,50,80 \qquad (3\text{-}4)$$

Figure 3.2-2 shows the torque output under current frequency of 8 rad/sec and 80 rad/sec. It can be seen that when the current frequency increases, the amplitude of torque output decreases. Figure 3.2-3 shows the relationship between torque/current gain and coil current frequency. With curve fitting, the plant parameters can be obtained as $K = 14.3623$, $T = 0.0283$.

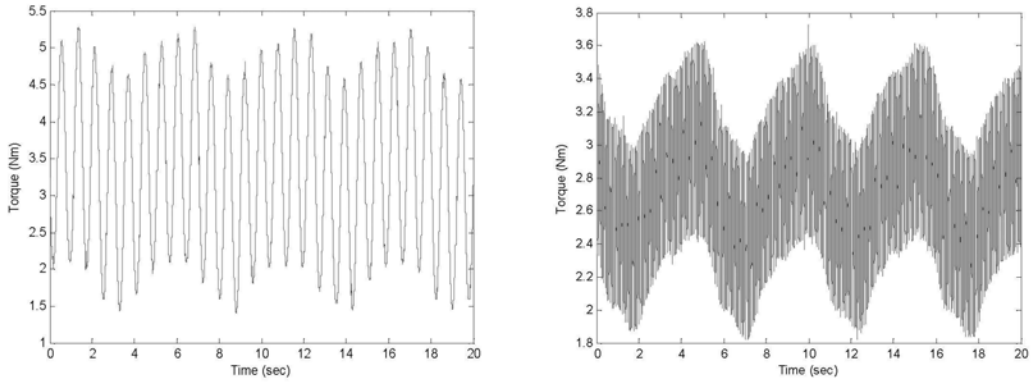

(a) w=8 rad/sec **(b) w=80 rad/sec**

Figure 3.2-2 Torque of MR actuator under different current frequency

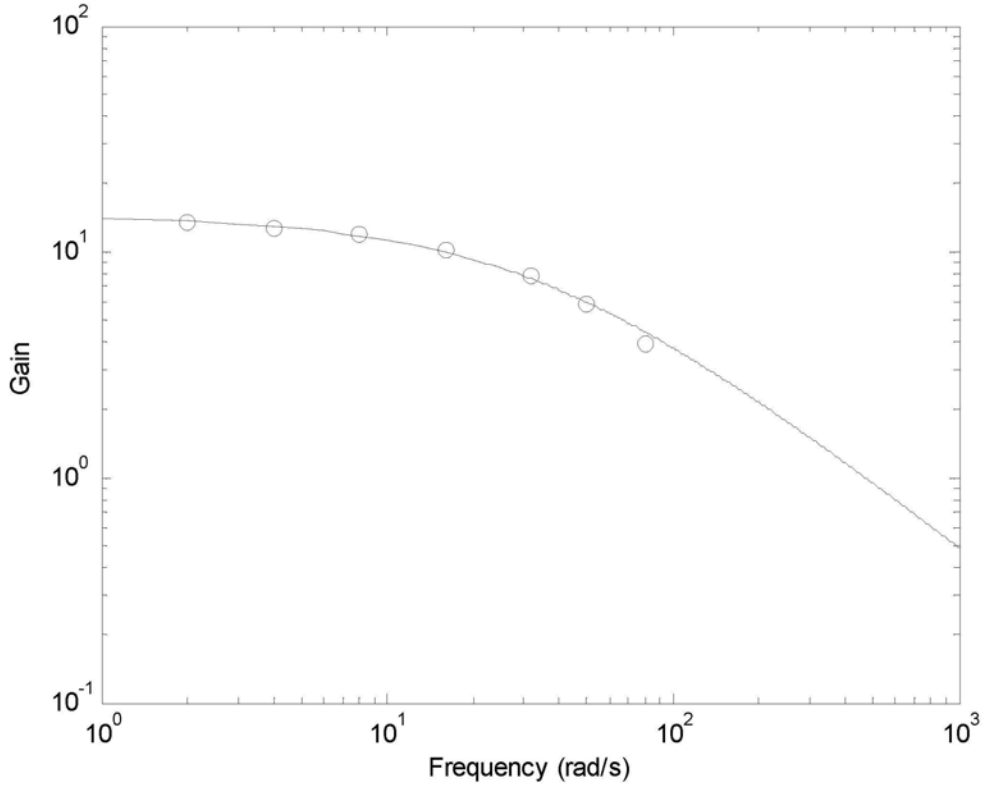

Figure 3.2-3 Curve fitting of gain vs. frequency

The transfer function of the IP control can be written as:

$$\frac{T_o(s)}{T_r(s)} = \frac{KK_i}{Ts^2 + (1KK_p)s + KK_i} \tag{3.5}$$

It can be written in other form as

$$\frac{T_o(s)}{T_r(s)} = \frac{\omega^2}{s^2 + 2\xi\omega s + \omega^2} \tag{3.6}$$

where $K_i = \frac{\omega^2 T}{K}$, $K_p = \frac{2\xi\omega T - 1}{K}$.

Set the damping ratio as 0.85 and frequency as 100 rad/sec, the control gains are calculated as: K_i = 19.7 A/(Nms) and K_p = 0.2653 A/(Nm).

Physically, the power supply can only provide a current of 0~2 A. When the controller gives a command beyond this limit, the output of the actuator will not be influenced by the input, which means saturation. Thus the error is kept very large, and the output of *I* term becomes very large. This phenomenon is called "windup" of *I* element. Once windup happens, it will take a long time to recover to normal state. The following anti-windup strategy is adopted for better control performance:

- $I \le 0$ and $T_o \ge T_r$, stop integration of IP controller
- $I \ge 2$ and $T_o \le T_r$, stop integration of IP controller

3.3 Torque Tracking under IP Control

Experiments are carried out for torque tracking of MR actuator under the IP control. The experimental setup is the same as the previous setup for testing MR actuator. The MR actuator is driven to rotate at a constant speed of 1.2 rad/sec. Figure 3.3-1 shows the Simulink model for the IP controller with anti-windup strategy. Two kinds of reference signals are used for torque tracking of MR actuator: one is sinusoidal signal and the other is pulse signal.

The sinusoidal signal used is:

$$T_r = 10 + 4\sin(2\pi t) + 2\sin(4\pi t) \tag{3.7}$$

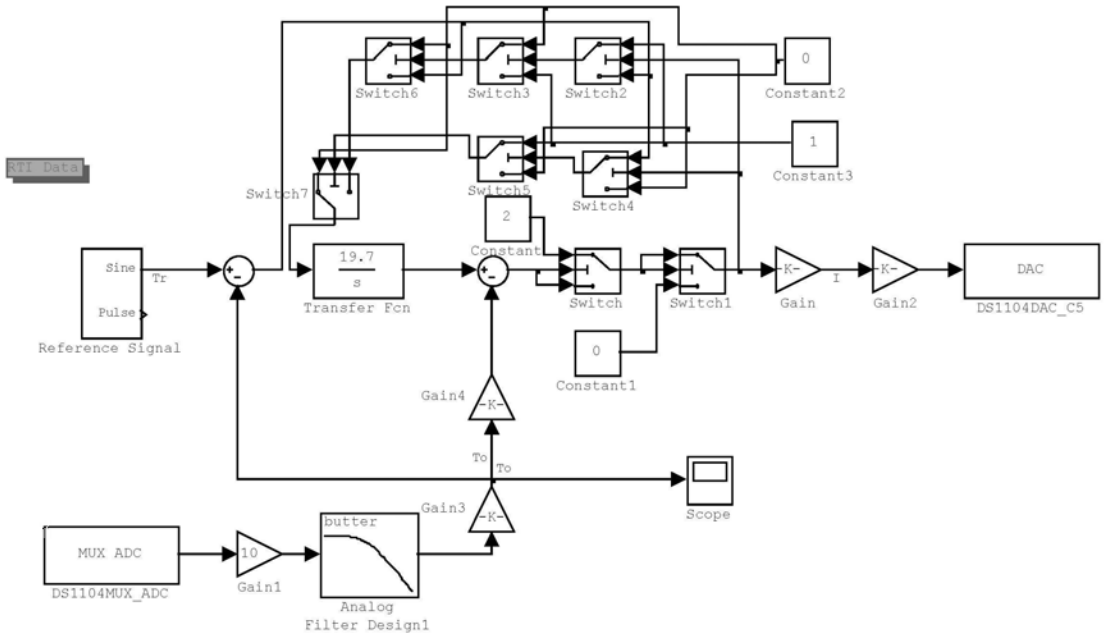

Figure 3.3-1 Simulink model of IP control

Figure 3.3-2 shows the experimental result of torque tracking for the sinusoidal signal. It can be seen that the tracking performance is very good. Figure 3.3-3 is the coil current under tracking experiment. Experiments of IP control without anti-windup strategy are also carried out and no difference is observed as compared to results that with anti-windup strategy. It is because that for the sinusoidal signal tracking, no windup phenomenon happened.

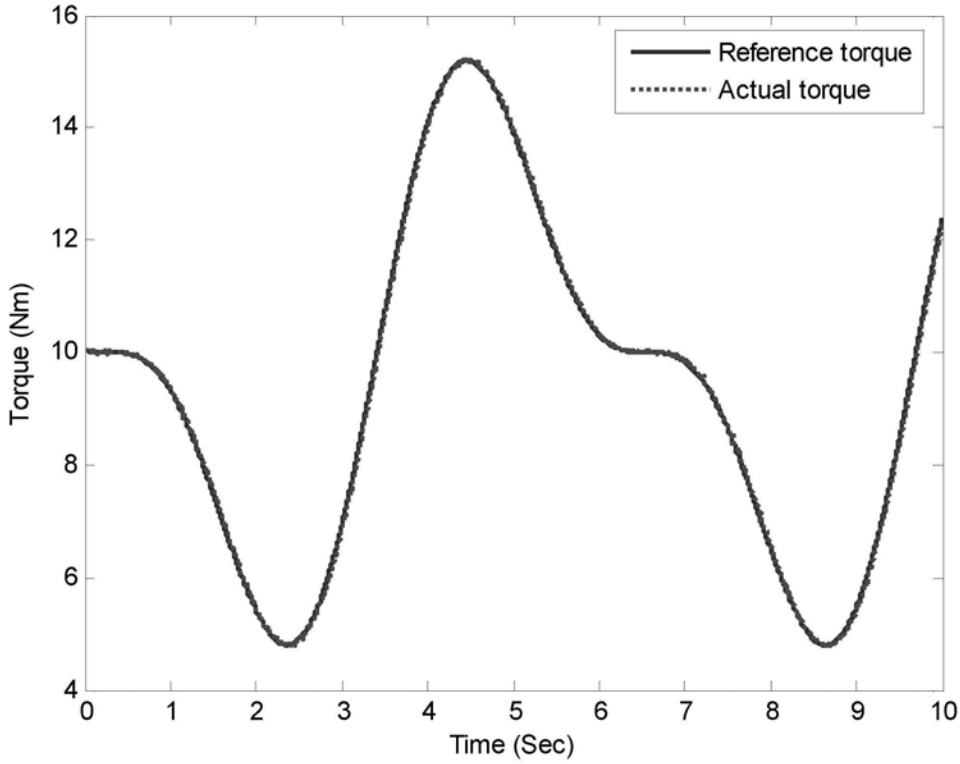

Figure 3.3-2 Torque tracking for sinusoidal signal

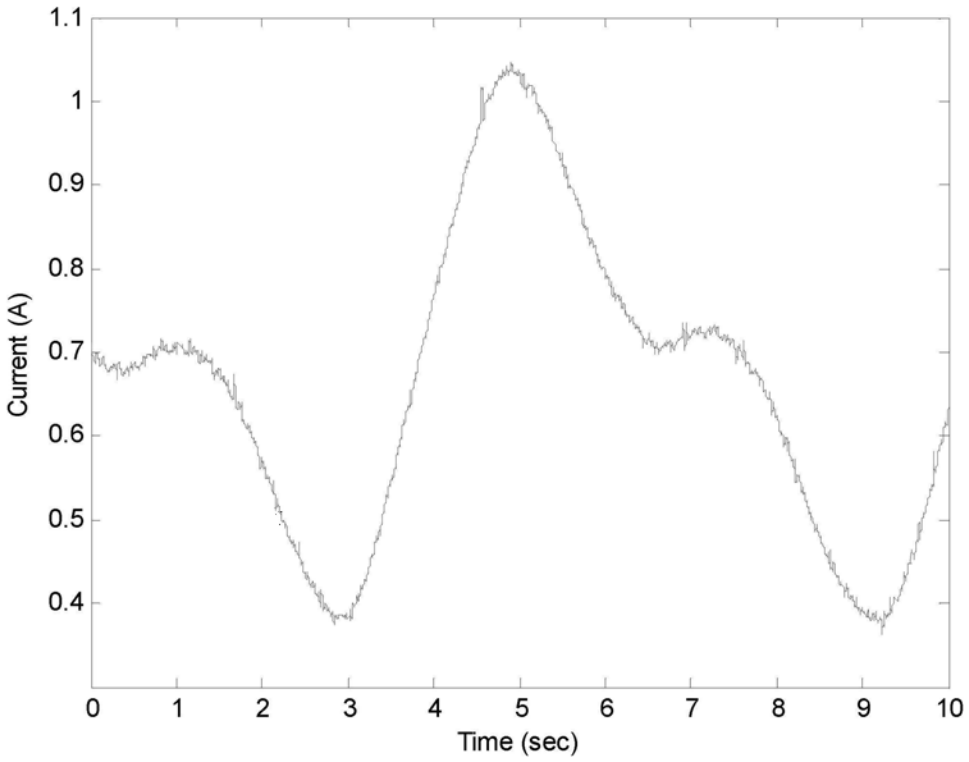

Figure 3.3-3 Coil current under sinusoidal signal tracking

Pulse signal tracking under IP control without and with anti-windup strategy are carried out. Figure 3.3-4 and Figure 3.3-5 show the experimental results, respectively. As seen from the figures, overshoots are observed for pulse signal tracking. With anti-windup strategy, the overshoot problem is greatly relieved.

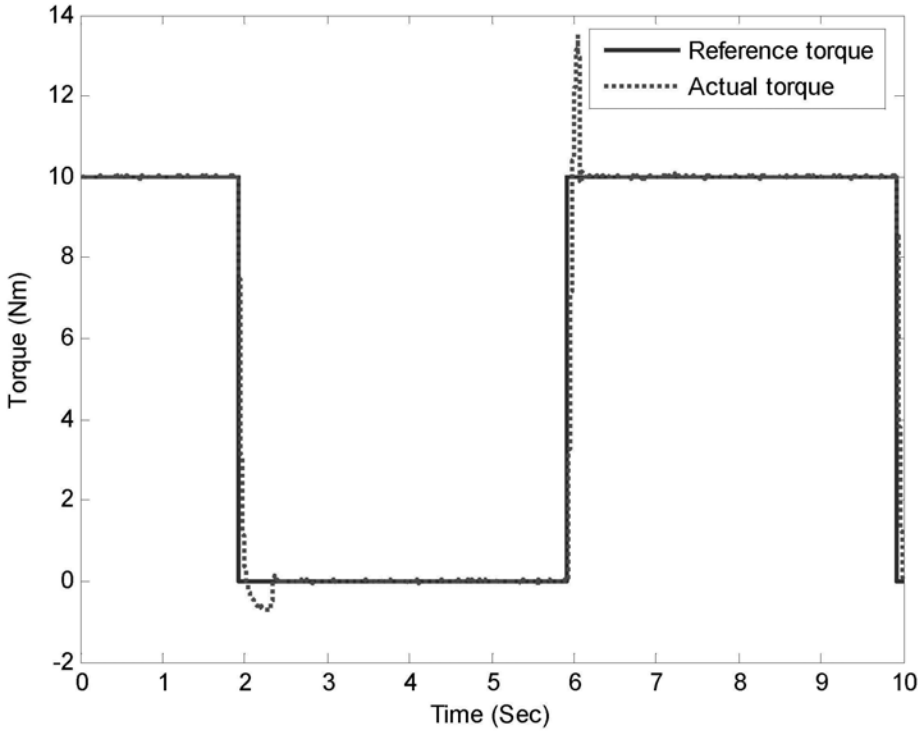

Figure 3.3-4 Pulse signal tracking without anti-windup strategy

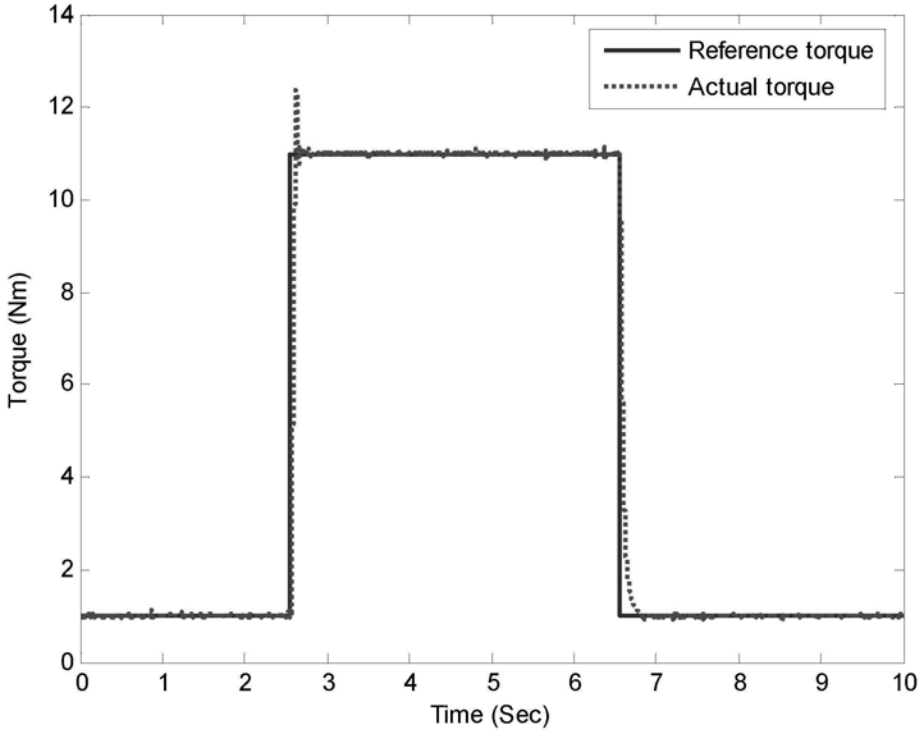

Figure 3.3-5 Pulse signal tracking with anti-windup strategy

3.4 Adaptive Control

Adaptive control is a technique of applying some system identification technique to obtain a model of the process from input-output experiments and using this model to design a controller. The parameters of the controller are adjusted during the operation of the plant as the amount of data available for plant identification increases. In practice, the adaptive techniques are applied to slowly time-varying and unknown plants. Approaches to adaptive control include gain scheduling, model reference adaptive systems, self tuning regulators, stochastic control, etc.

As discussed in previous sections, the MR actuator can be modeled as a first order single-input single-output linear time invariant plant. While controlled by IP controller, the plant parameters can be identified off-line and the controller parameters are derived based on the plant parameters. It is noted that these control parameters are fixed. The plant parameters may change slowly as time and environment change (such as temperature variation, abrasion of iron particles in the MR fluid, etc.).

The system is described as

$$y_{k+1} = ay_k + bu_k \tag{3.8}$$

where y denotes the torque output, u is the control voltage, k is the sample index, a and b are unknown gain parameters.

$$y_{r,k+1} = r_k \tag{3.9}$$

where y_r is the target torque output, r is the reference torque input. Let the control input be given by

$$u_k = c_k r_k + d_k y_k \tag{3.10}$$

where c and d are control gain parameters. There exist nominal parameter values

$$c^* = \frac{1}{b} \qquad d^* = -\frac{a}{b} \tag{3.11}$$

such that the torque output matches the target torque output

$$y_{k+1} = a y_k + b(c_k r_k + d_k y_k) = (a + b d_k) y_k + b c_k r_k = r_k = y_{r,k+1} \tag{3.12}$$

when $c_k = c^*$, $d_k = d^*$.

Define the output error

$$e_k = y_k - y_{r,k} \tag{3.13}$$

and the parameter errors

$$\Phi_{r,k} = c_k - c^*, \ \Phi_{y,k} = d_k - d^* \tag{3.14}$$

Choose the following parameter update laws

$$c_{k+1} = c_k - g e_k r_k$$

$$d_{k+1} = d_k - ge_k y_k \text{, g} > 0 \tag{3.15}$$

Now the error formulation can be written as:

$$\begin{aligned} \delta e_{k+1} &= e_{k+1} - e_k = -e_k + b(\Phi_{r,k} r_k + \Phi_{y,k} e_k + \Phi_{y,k} y_{r,k}) \\ \delta\Phi_{r,k+1} &= \Phi_{r,k+1} - \Phi_{r,k} = -ge_k r_k \\ \delta\Phi_{y,k+1} &= \Phi_{y,k+1} - \Phi_{y,k} = -ge_k^2 - ge_k y_{r,k} \end{aligned} \tag{3.16}$$

Note that the right-hand sides only contain states (e_k, $\Phi_{r,k}$, $\Phi_{y,k}$) and exogenous signals (r_k $y_{r,k}$). Consider the Lyapunov function

$$v_k = \frac{e_k^2}{2} + \frac{b}{2g}(\Phi^2{}_{r,k} + \Phi^2{}_{y,k}) \tag{3.17}$$

$$\delta v_{k+1} = v_{k+1} - v_k = -e_k^2 \le 0 \tag{3.18}$$

Hence, δv_{k+1} is negative semi-definite, and the parameter and output errors are upper bounded. It is demonstrated that, in the sense of Lyapunov, the adaptive system is stable. For all initial conditions, e_k, c_k, d_k are bounded. Since v_k is monotonically decreasing and lower bounded, $e_k \to 0$ as $k \to \infty$.

Similar to the anti-windup for the integral term of IP control, the same strategy should also be adopted for the parameter updating term of adaptive control. The power used for the MR actuator has a voltage limit of 0~10 V. If the controller gives a command out of this limit, saturation will happen and the output of the actuator will not be affected by the controller. The anti-windup strategy for the adaptive control is given as

- When $u_k \geq 10$ and $T_o < T_r$, stop controller gain adaptation ($c_{k+1} = c_k$, $d_{k+1} = d_k$)
- When $u_k \leq 0$ and $T_o > T_r$, stop controller gain adaptation.

3.5 Torque Tracking under Adaptive Control

Experiments are carried out to study the torque tracking performances of the MR actuator under adaptive control. The experimental conditions are the same as IP control. The Simulink model of adaptive control is shown in Figure 3.5-1 and Figure 3.5-2. To avoid oscillation, the adaptation process is stopped when the tracking error is small enough (in this experiment, the maximum permitted error is 0.5 Nm). The initial values for c and d are set as "1" and "-1". The sampling rate is 10 kHz.

Figure 3.5-3 shows the result of sinusoidal signal tracking. We can see from this figure that the MR actuator can track the reference very well under adaptive control. Obviously, the tracking error is smaller than the maximum permitted error. So in this process, the updating process for c and d is stopped. Figure 3.5-4 shows the control parameters during this period. It can be seen that the c is kept a constant of 6.2882, and d is kept as -6.0745, which are different as compared to their initial values. Figure 3.5-5 shows the control voltage to the coil during sinusoidal signal tracking. It can be seen that the shape of the control voltage is similar to that of reference torque signal. Though some small oscillations are observed, the control voltage is always within the physical limit of 0~10 V.

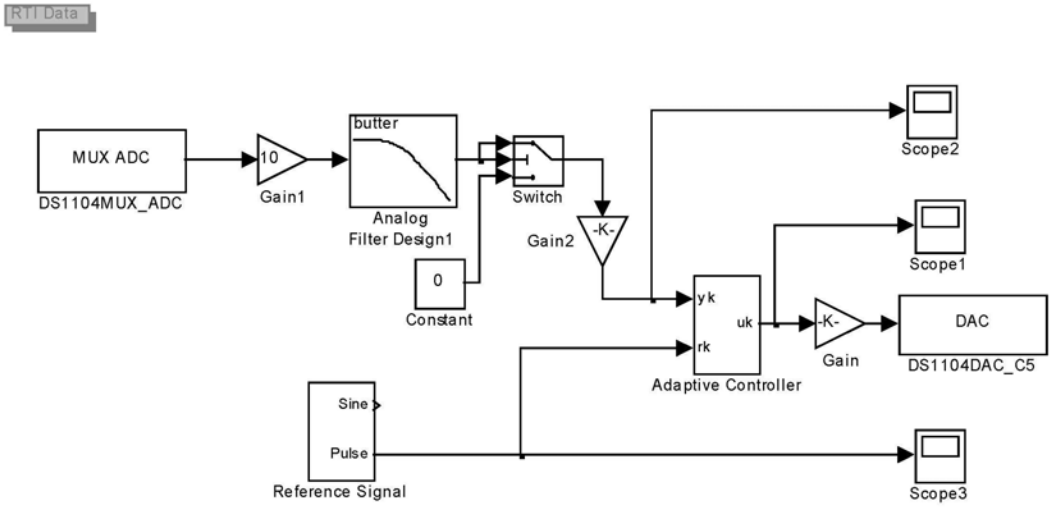

Figure 3.5-1 Simulink control model of system

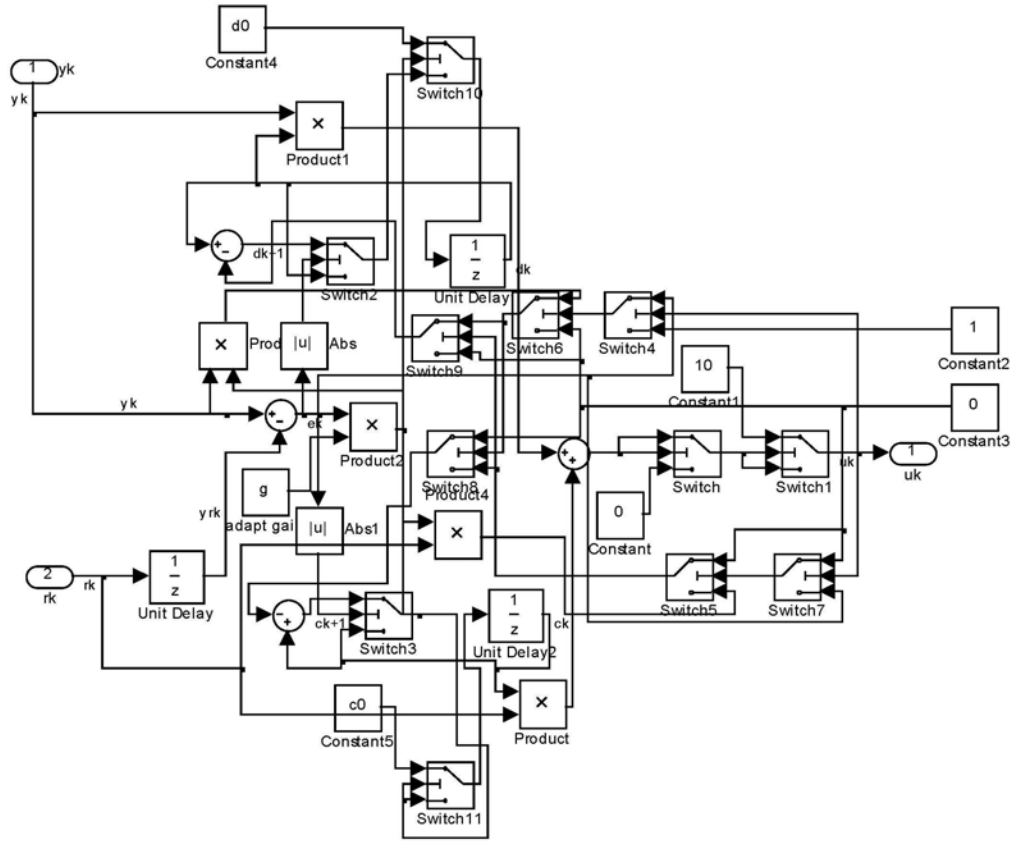

Figure 3.5-2 Simulink model of adaptive control

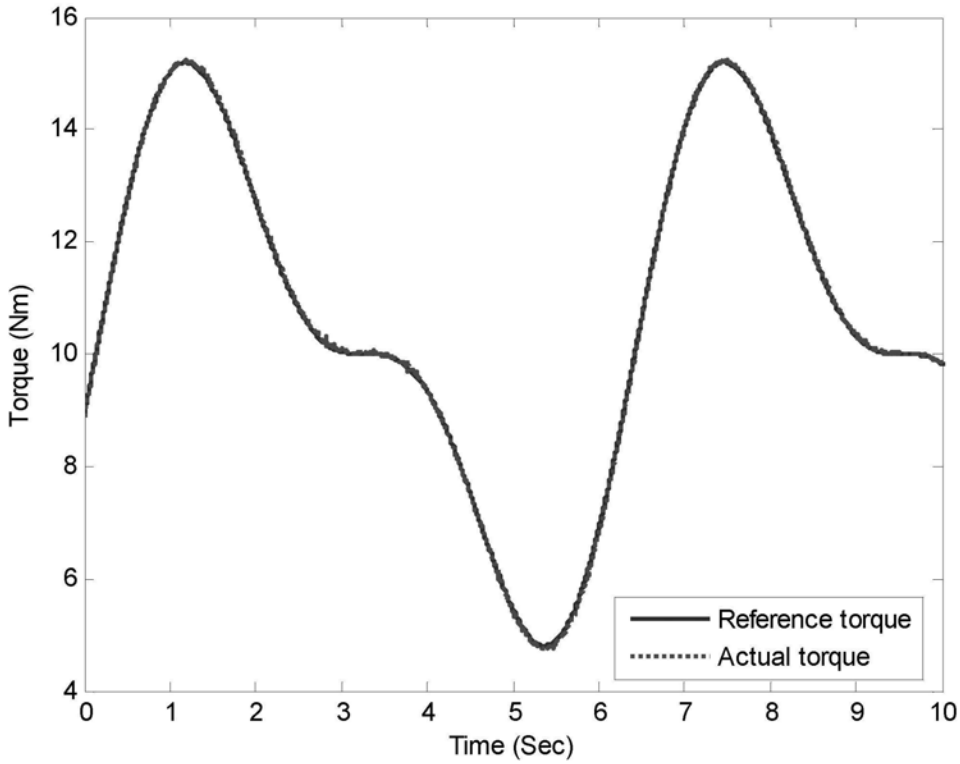

Figure 3.5-3 Sinusoidal signal tracking under adaptive control

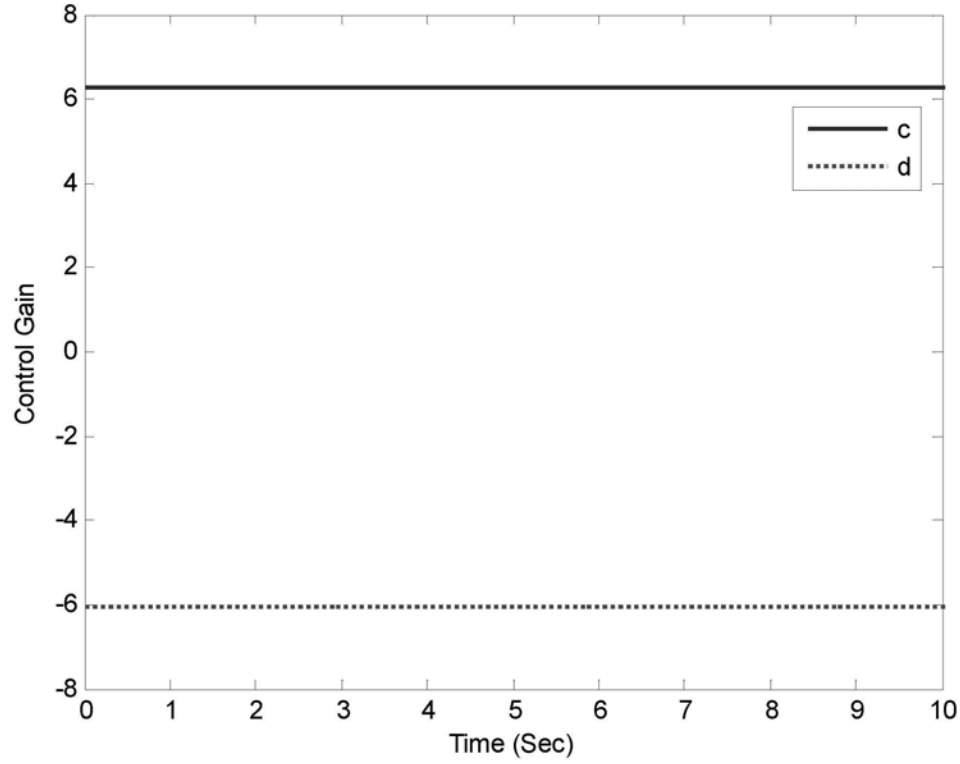

Figure 3.5-4 Control parameters under sinusoidal signal tracking

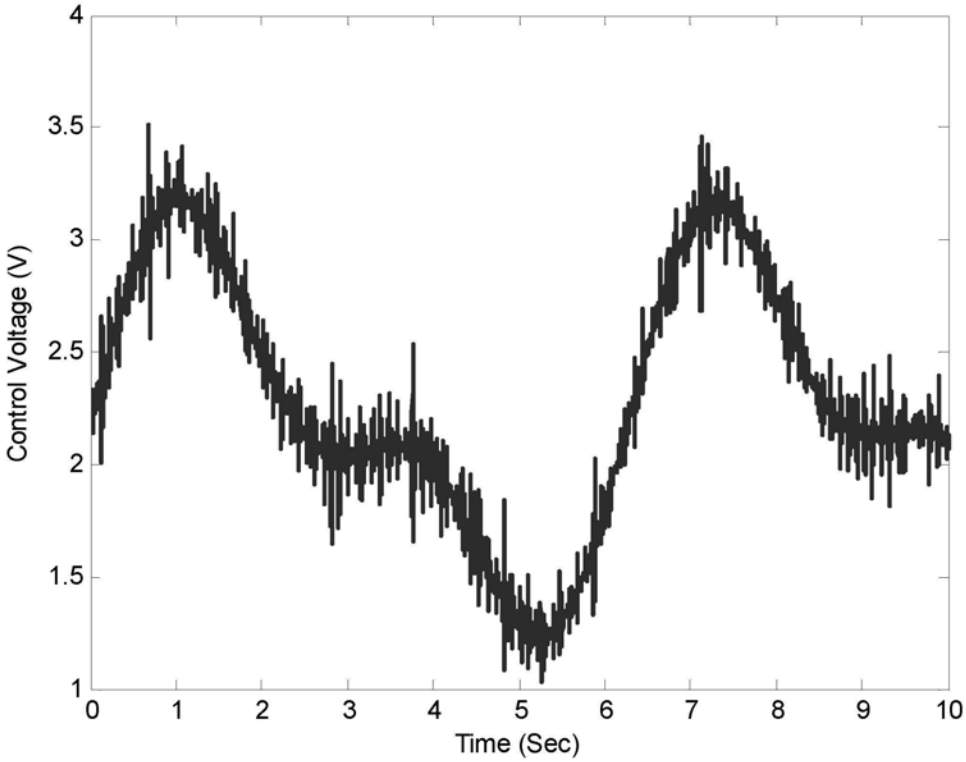

Figure 3.5-5 Coil current under sinusoidal signal tracking

Figure 3.5-6 shows the experimental results of torque tracking for pulse signal. It can be seen that the tracking performance of pulse signal is also very good. From figure 3.5-7, it can be seen that when an upright reference step signal comes, there is a step variation for each control parameter. The control voltage during the step variation also reaches both upper and lower limits, as shown in figure 3.5-8. The instant variations of signals at the upright step instance are shown in figure 3.5-9. The response time of the actuator during the step signal tracking under control is about 0.05 sec, which is quicker than open-loop response time (see Section 2.7). The variation of parameter *c* happens at the end of the period when the control voltage is saturated.

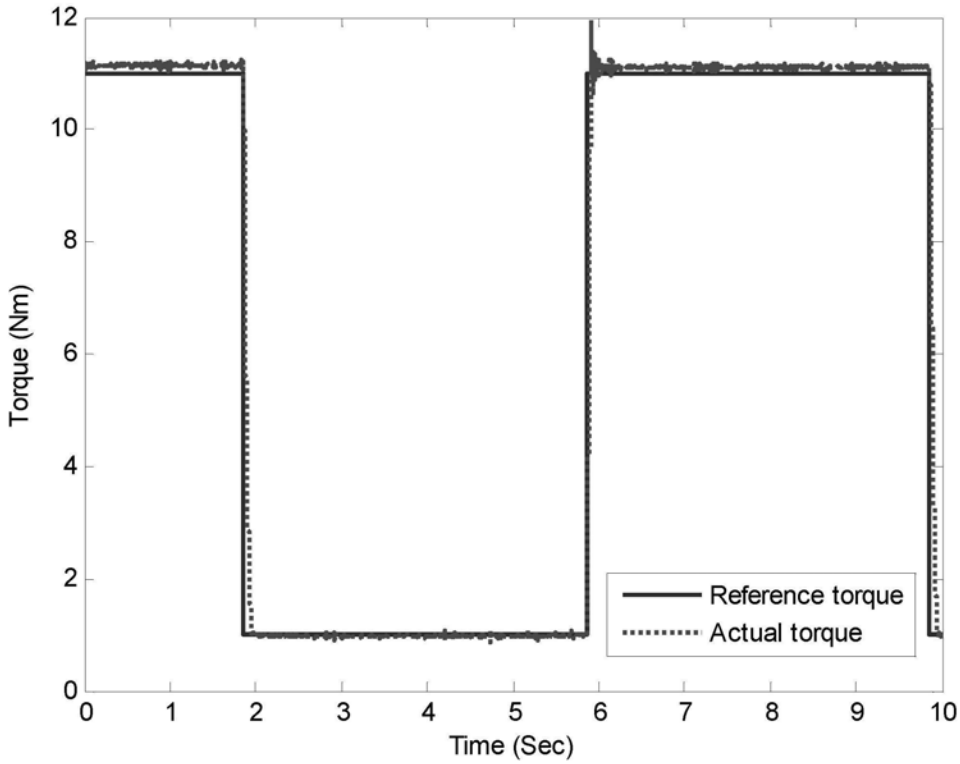

Figure 3.5-6 Pulse signal tracking under adaptive control

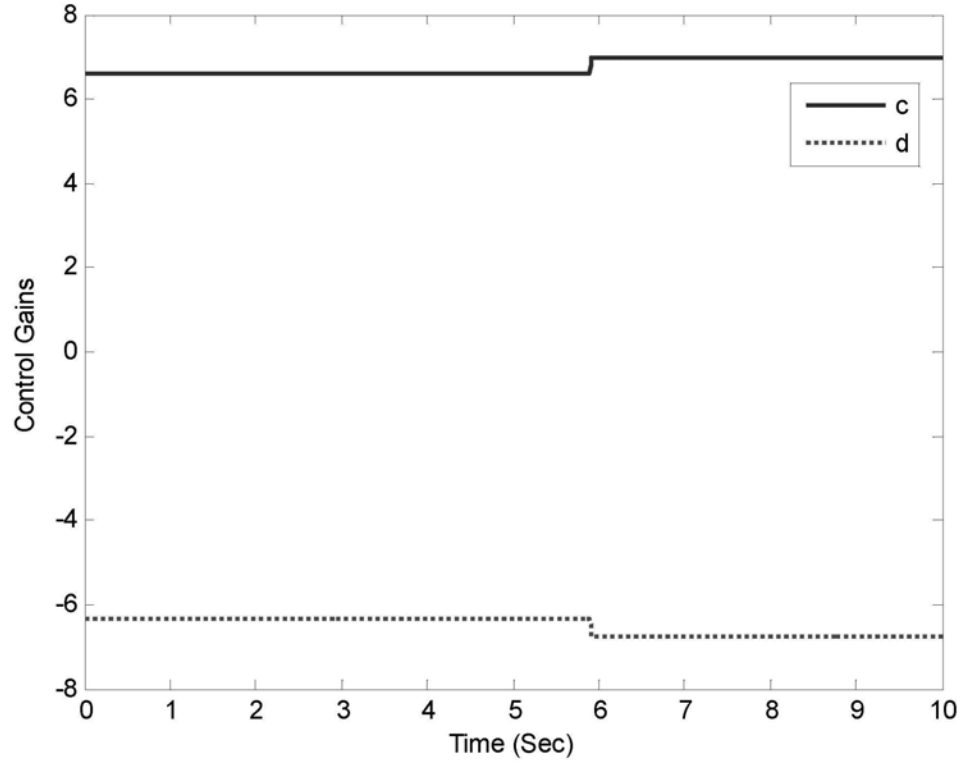

Figure 3.5-7 Control parameters under pulse signal tracking

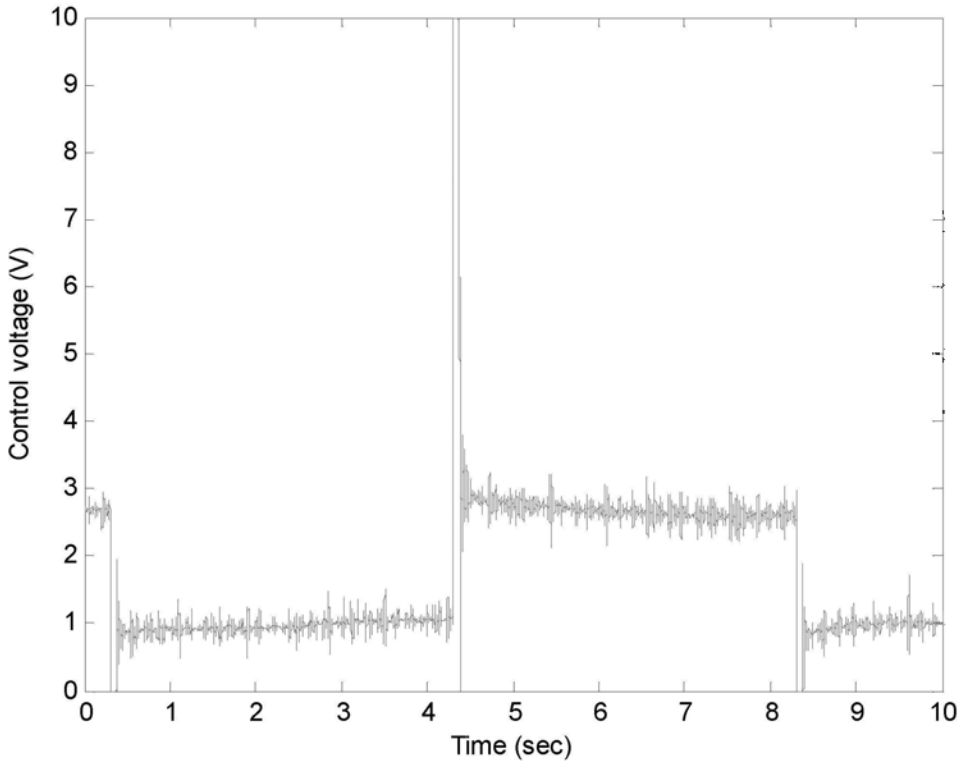

Figure 3.5-8 Control voltage under pulse signal tracking

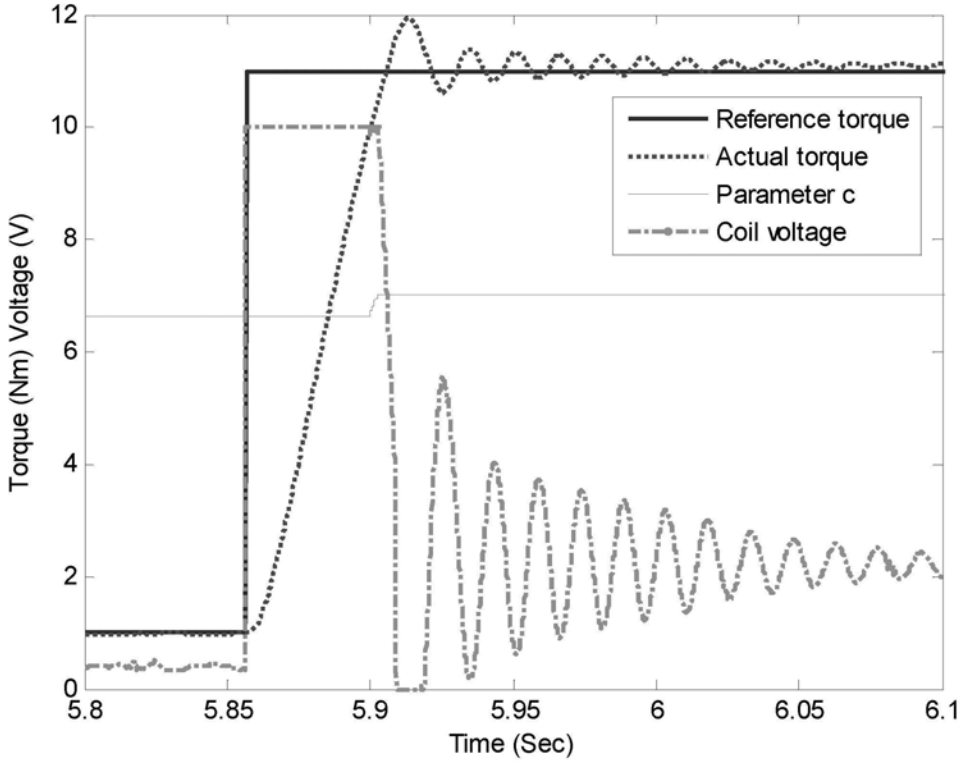

Figure 3.5-9 Signal variations at step reference change

Although the variations of the control parameters are small, they can accumulate to large values. Thus the system can become unstable. As seen in figure 3.5-10, when the parameters reach to relative large values (such as larger than 9 for *c*), obvious oscillations are observed. To avoid oscillation, an auto-reset mechanism is used. When the *c* reaches 8, *c* and *d* will be reset to 6 and -6, respectively. Figure 3.5-11 shows the experimental results with the improved control method. It can be seen that the control parameters will not increase to large values. And the auto-reset process happens at very short period of time, it will not bring any disturbance to the output torque while the long-term stability is guaranteed.

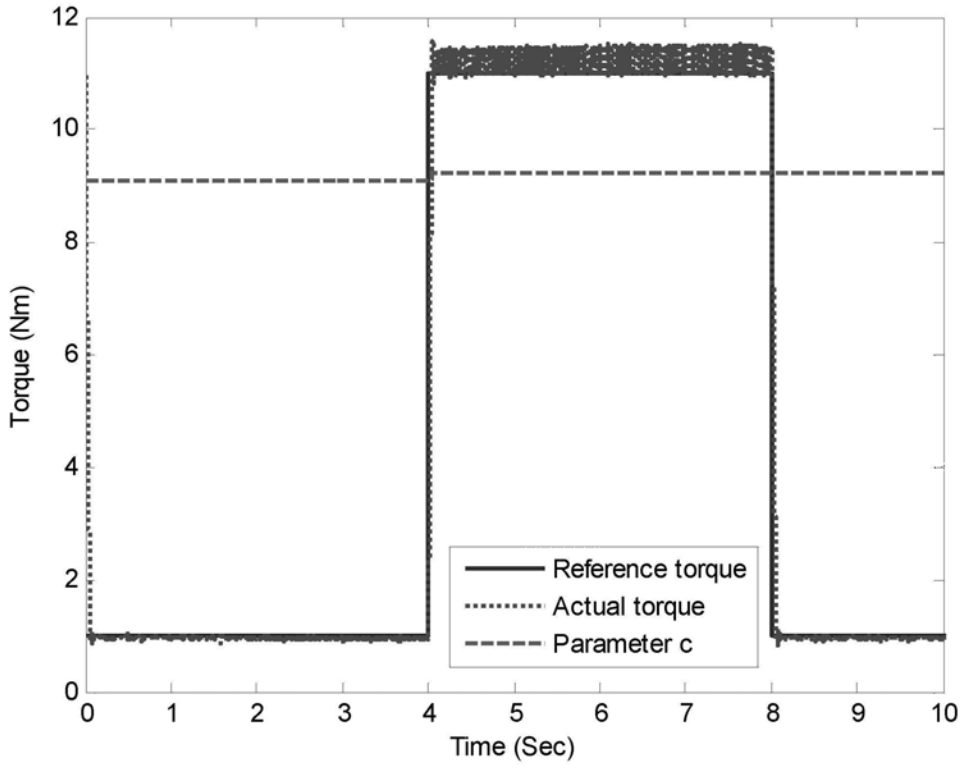

Figure 3.5-10 Pulse signal tracking under adaptive control

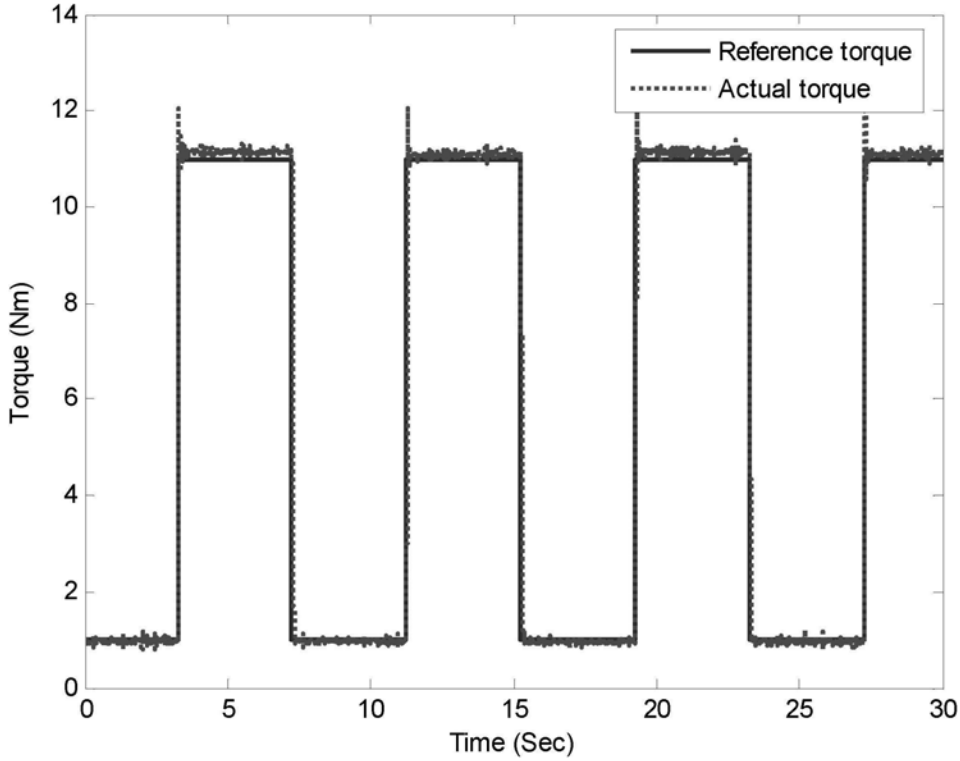

Figure 3.5-11 Pulse signal tracking under adaptive control with auto-reset mechanism

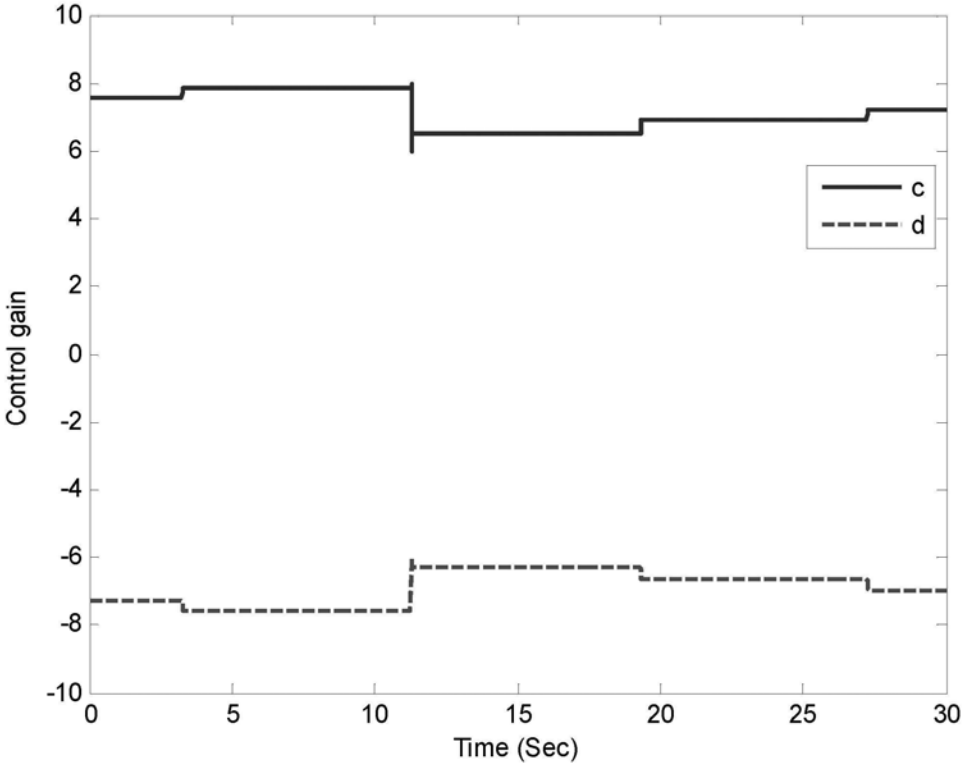

Figure 3.5-12 Parameters variation under adaptive control with auto-reset mechanism

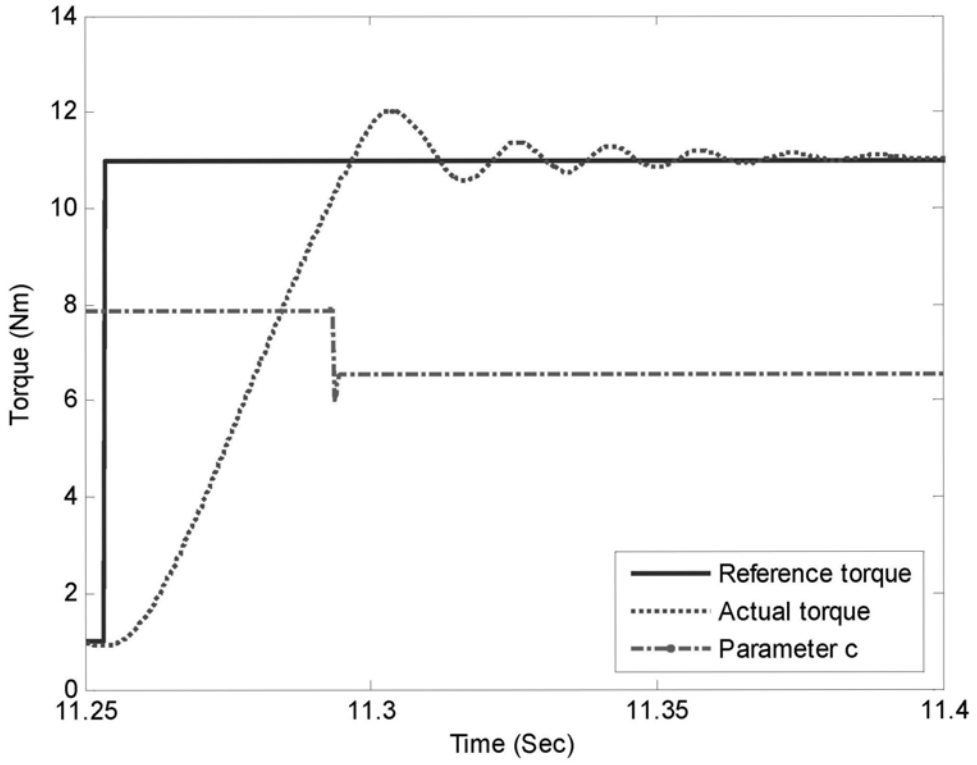

Figure 3.5-13 Auto-reset process during pulse signal tracking

3.6 Chapter Summary

IP control and adaptive control are proposed for the control of MR actuator in this chapter. The MR actuator is modeled as a first-order system. While IP control is used, the model parameters are obtained from experiments. And the control parameters are chosen based on the model parameters. Sinusoidal signal and pulse signal are used to study the torque tracking performances of the MR actuator. Anti-windup strategy is used to prevent oscillation for the torque output of MR actuator. From the experimental results, observations are summarized as follows:

1. For sinusoidal signal, the MR actuator can track the reference signal very well under IP control.
2. For pulse signal, the MR can also track the signal well, but some overshoots are observed at the step change of the reference signal. The overshoot problem can be relieved by anti-windup strategy.

As the model parameters may change with respect to time and environment, the control parameters may be not suitable when the model parameters changed. So adaptive control is proposed for the MR actuator, whose control parameters can adapt to model parameters variations. Experiments for sinusoidal signal and pulse signal tracking under adaptive control are also carried out. From the experimental results, observations are summarized as follows:

1. For sinusoidal signal, the MR actuator can track the reference signal very well too under adaptive control.
2. For pulse signal, the MR can also track the signal well, and the overshoots are smaller than those of IP control. But the control parameters can accumulate to

large values and thus the system may become unstable. This problem can be solved by an auto-reset mechanism.

CHAPTER FOUR

ASSISTIVE KNEE BRACE WITH MR ACTUATOR

In this chapter, an assistive knee brace that uses both DC motor and MR actuator will be investigated. The DC motor generates the active assistive torque. The MR actuator provides the passive assistive torque and transfers the torque from the DC motor to the knee brace when the DC motor works. A potentiometer is used to detect the angular information of the knee joint, and a pair of strain gauges are used to measure the force information. The strain gauges are calibrated with a load cell. A testing structure will be fabricated for testing the knee brace. The motion of the knee brace in the testing structure will be analysed. The dynamic force of knee brace during motion will be studied and the relationship of torque - angular position will be found. Experiments will be carried out to test the knee brace. IP based state control and adaptive control are proposed for the motion control of knee brace under the testing structure. Experiments will be carried out to study the motion of the knee brace under control in the testing structure. The performances of the knee brace motion under different control methods will be evaluated.

4.1 Assistive Knee Brace

As MR devices can not provide active torque or force, a DC motor is used together with the MR actuator in this assistive knee brace. The developed assistive knee brace is shown in figure 4.1-1. It comprises the following components:

1) DC motor
2) MR actuator
3) Braces
4) Gear pair (3:1)
5) Potentiometer
6) Strain gauge
7) Slip ring

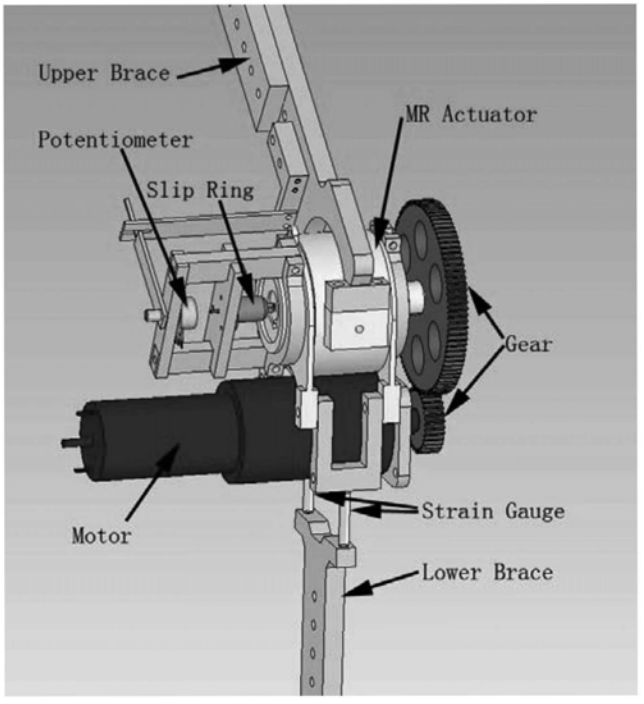

Figure 4.1-1 Assistive knee brace with MR actuator

The DC motor works to provide active torque, the MR actuator functions as a clutch to transfer the torque produced by the motor or a brake to provide controllable resistive torque. The upper brace and lower brace will be bonded to upper leg and lower leg, respectively. A pair of gears are used to transfer the torque of motor to the MR actuator. A potentiometer is used to measure the angular position of the knee joint. Strain gauges are used to measure the force and torque of the knee brace.

The data of the DC motor (Type RE 40, Maxon Motor Inc.) is shown in table 4.1-1. To increase the torque output, a gearbox (Type GP 52 C, Maxon Motor Inc.) is used. The reduction ratio of the gearbox is 156:1. A servoamplifier (Type ADS 50/5, Maxon Motor Inc.) is used for the control of DC motor. The servoamplifier has four working modes: speed control using tacho signals, speed control using encoder signals, $I \times R$ compensated speed control and torque or current control. $I \times R$ compensated control is used for the control of motor. Figure 4.1-2 shows the wiring for the control of motor.

Table 4.1-1 Motor data

	Unit	Value
Assigned power rating	W	150
Nominal voltage	V	24
No load speed	min^{-1}	7580
Stall torque	mNm	2280
Max. continuous torque	mNm	170
Speed / torque gradient	min^{-1} / mNm^{-1}	3.33
No load current	mA	137
Starting current	A	75.7

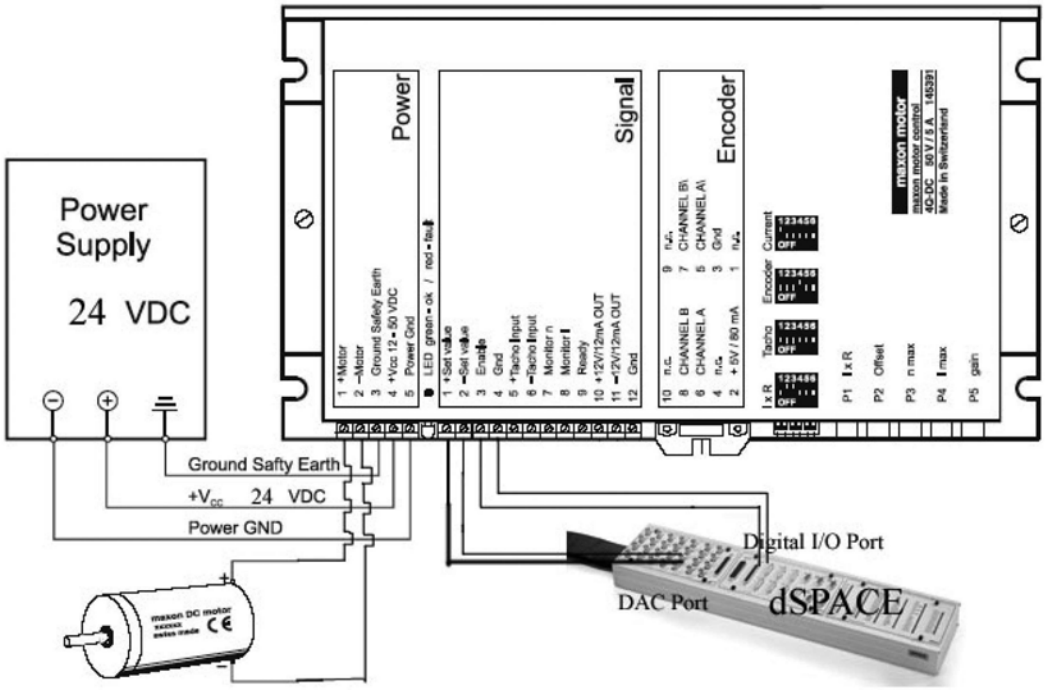

Figure 4.1-2 Wiring for motor control

There are several independent power systems for the knee brace, such as power of DC motor, power of MR actuator, power of dSPACE, etc. If these power systems are connected, noises will be introduced from one system into another, especially when different power systems have different electric potential for ground. So signal isolating is required for good measurement and control. High-linearity analog opto-couplers HCNR201 is used for signal isolating. Figure 4.1-3 shows the isolating circuit. The output voltage of the isolating circuit is

$$\frac{V_{OUT}}{V_{IN}} = K\frac{R_2}{R_1} \tag{4.1}$$

where K is photodiode current ratio and $K = 1 \pm 5\%$.

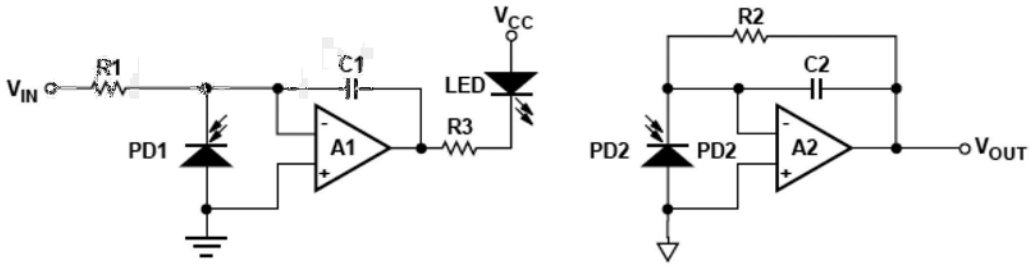

Figure 4.1-3 Signal isolating circuit

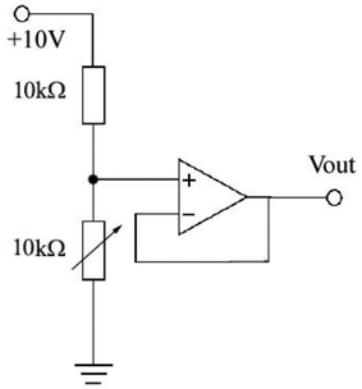

Figure 4.1-4 Circuit for potentiometer

A 10 KΩ potentiometer is used for measuring the angular information. The circuit for potentiometer is shown in figure 4.1-4.

Strain gauges are used to measure the force information. Strain gauges have the advantages of small size and low cost. The configuration and connection of the strain gauges are shown in figure 4.1-5. Strain gauges are used in full bridge so as to increase the signal/noise ratio. Both pillars of the knee brace have strain gauges to measure the force and torque information.

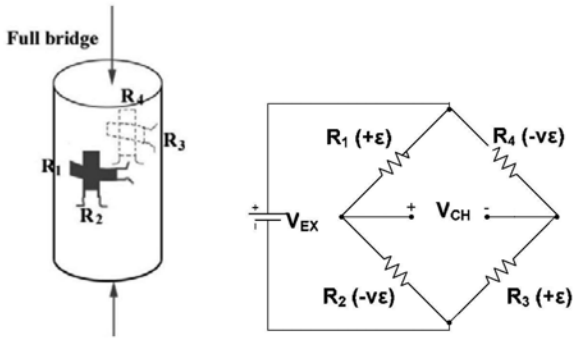

Figure 4.1-5 Configuration and connection of strain gauges.

The gauge factor GF of strain gauge is defined as:

$$GF = \frac{\Delta R / R_0}{\varepsilon} \tag{4.2}$$

where R_0 is the original resistance of strain gauge, ε is the strain.

The signal output V_{CH} is

$$V_{CH} = \frac{V_{EX} GF(1+v)\varepsilon}{2} \tag{4.3}$$

where V_{EX} is the excitation voltage, v is the poisson's ratio.

The measured force F is

$$F = \frac{2ESV_{CH}}{V_{EX} GF(1+v)} \tag{4.4}$$

where E is the modulus of elasticity, S is the area of cross-section.

The gauge factor of the strain gauge (Type FCA-1-17, TML Inc.) is 2.14. The pillar that the strain gauges are attached to is made from stainless steel with radius of 2 mm. The excitation voltage is 2.0 V, thus the relationship between force and output signal is

$$F = \frac{2ESV_{CH}}{V_{EX}GF(1+v)} = 0.903 \times 10^6 V_{CH} \tag{4.5}$$

The strain gauges are calibrated using a load cell (Type 208C03, PCB Piezotronics, Inc.). The calibration setup is shown in figure 4.1-6. The load cell is in series with the pillar that the strain gauges are attached to. A clamp is used to manually apply normal force. The signal of the strain gauges is collected by dSPACE. Before acquisition, the signal is amplified using a 6-channel strain amplifier (Type YE3817C, Sinocera Inc.). A gain of 1000 is chosen for the signal amplification. Thus the force can be expressed as

$$F = 903 * V_O \tag{4.6}$$

where V_O is the output of strain gauge.

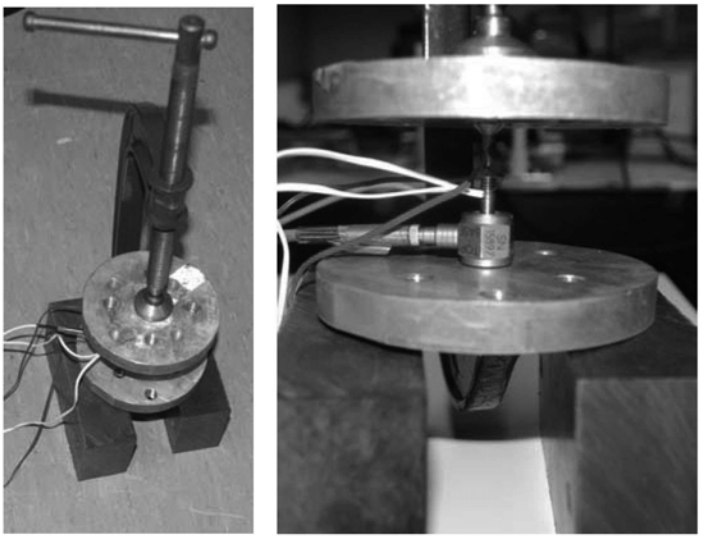

Figure 4.1-6 Strain gauge calibration setup

Calibrating experiments are carried out for both pillars. Figure 4.1-7 and figure 4.1-8 show the experimental results. It can be seen that when the applied force is low (smaller than 800 N), the signal of strain gauge has good linearity to the force signal; but when the force is large (larger than 900 N), the force-signal is no longer linear. For the assistive knee brace, the distance of the two pillars is 81 mm. So 800 N is corresponding to a torque of 64.8 Nm, which is much larger than the nominal torque of the knee brace. So the strain gauges are suitable for the measuring force signal of the knee brace. Also, the calibrated force for these pillars can be obtained.

For pillar 1, the force can be expressed as,

$$F = 350 * (V_O + 1) \tag{4.7}$$

For pillar 2, the force can be expressed as,

$$F = 900 * (V_O - 6.22) \tag{4.8}$$

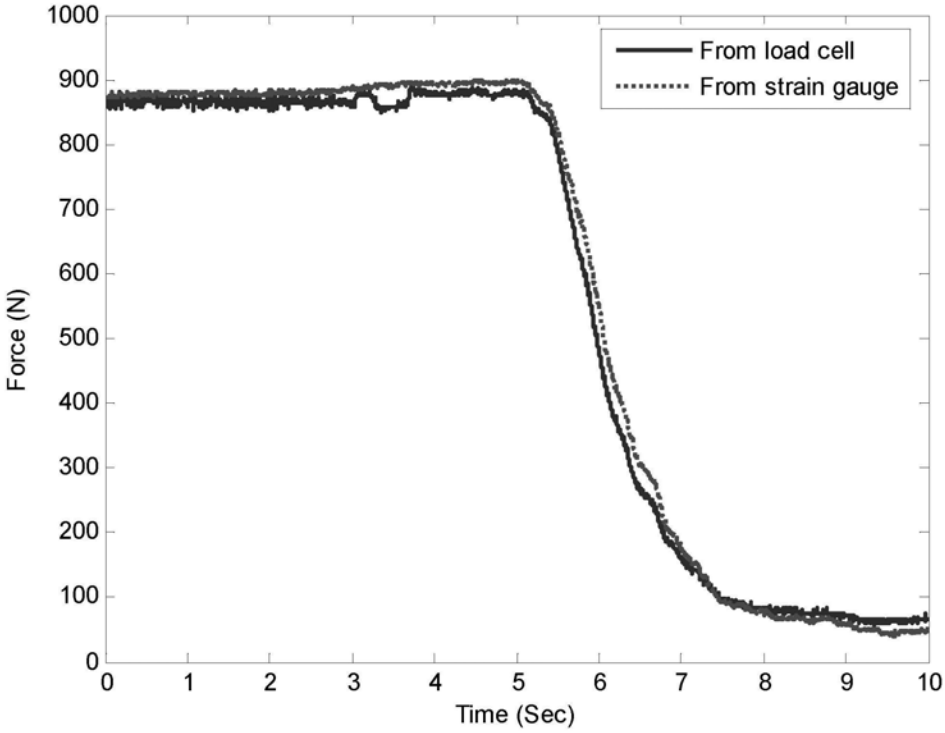

Figure 4.1-7 Calibration of pillar 1

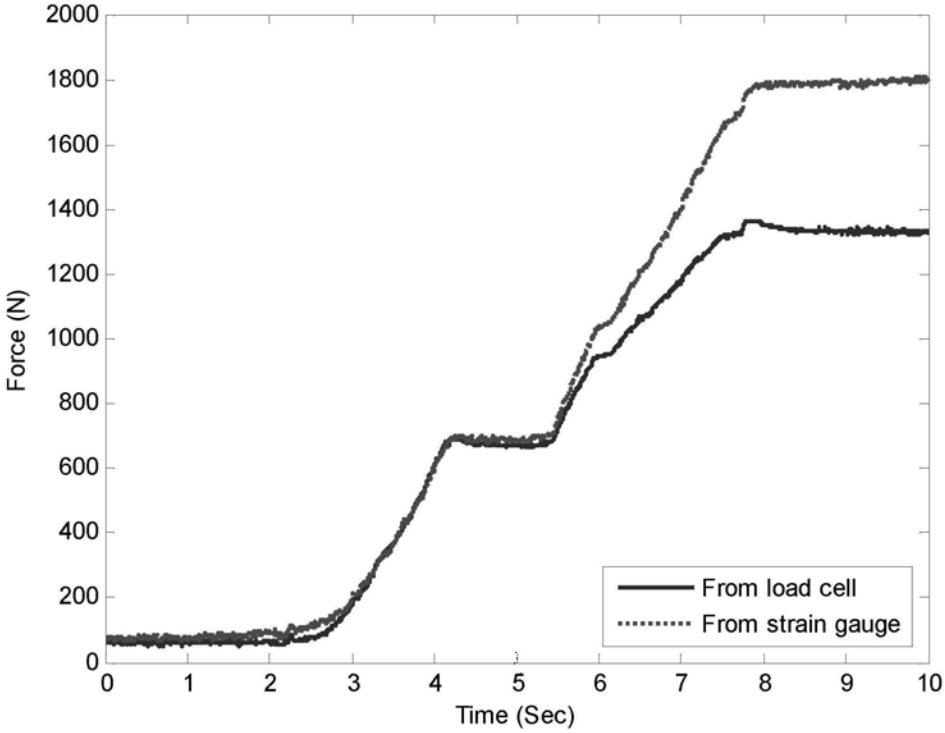

Figure 4.1-8 Calibration of pillar 2

4.2 Motion Analysis

It would be dangerous to directly apply the assistive knee brace to human body. So a testing structure is developed for testing the knee brace, which is shown in figure 4.2-1. The load disks are used to mimic the weight of human body. The load disks can move up and down along the guide poles under the torque from the knee brace and gravity force. The weight of the first load disk (which combined with a pair of linear bearings to minimize the friction force between the load disks and the guiding poles) is about 6 kg. The weight of the subsequent load disk is 5 kg.

When the motor is on and the current is applied to the MR actuator, the knee brace can lift up the load disks. This motion can be regulated by both the motor and the MR actuator. For the moving down process of the load disks, the motor is turned off and only the MR actuator is used to control the motion.

The knee brace with MR actuator in the testing structure can be modeled as figure 4.2-2, where m_1 is the mass of the joint, m_2 is the mass of load disks, l_1 is the length of lower brace, and l_2 is the length of upper brace. Please note that the weight of the upper brace and lower brace are neglected since they are much lighter than m_1 and m_2.

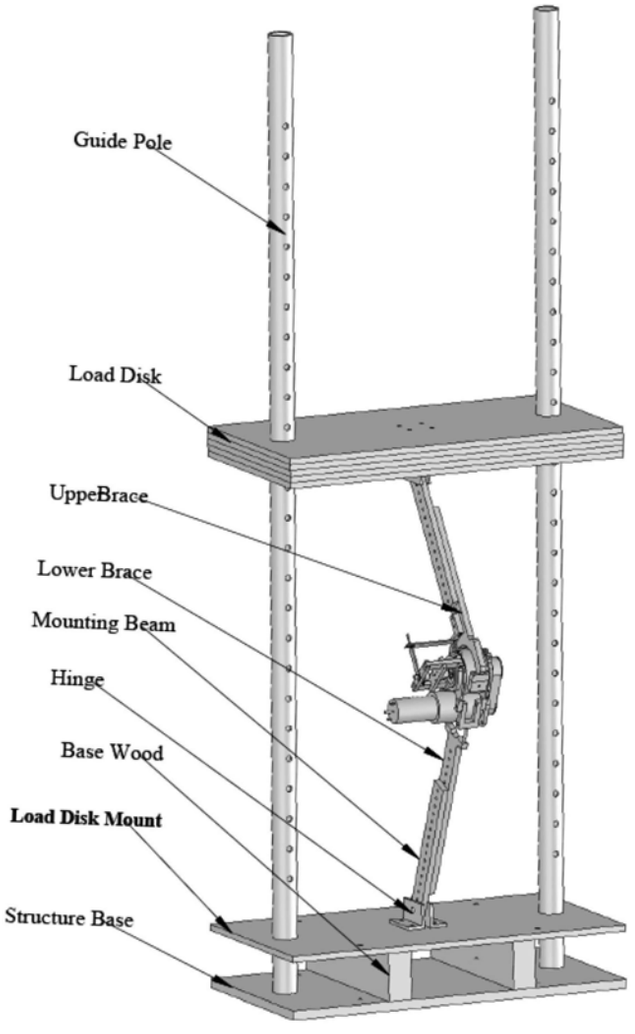

Figure 4.2-1 Testing structure for knee brace

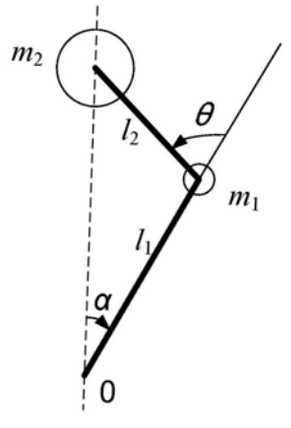

Figure 4.2-2 Simplified model of the knee brace system

The potential energy of the system is

$$V = m_1 g l_1 \frac{l_1 + l_2 \cos\theta}{\sqrt{l_1^2 + l_2^2 + 2 l_1 l_2 \cos\theta}} + m_2 g \sqrt{l_1^2 + l_2^2 + 2 l_1 l_2 \cos\theta} \tag{4.9}$$

The kinetic energy of the system is

$$T = \frac{1}{2} m_1 l_1^2 \left(\frac{l_2 \dot{\theta}}{l_1 + l_2 \cos\theta} \right)^2 \left(\cos\theta + \frac{l_1 l_2 \sin^2\theta}{l_1^2 + l_2^2 + 2 l_1 l_2 \cos\theta} \right)^2 + \frac{1}{2} m_2 \frac{\left(l_1 l_2 \sin\theta \dot{\theta} \right)^2}{l_1^2 + l_2^2 + 2 l_1 l_2 \cos\theta} \tag{4.10}$$

The Lagrangian function is

$$L = T - V \tag{4.11}$$

The nonconservative forces include the torque generated by the MR actuator τ, friction at the joint f_1 and the friction between the load disks and guide poles f_2. The virtual work can be express by

$$\delta W = (\tau + f_1 - \frac{f_2 l_1 l_2 \sin\theta}{\sqrt{l_1^2 + l_2^2 + 2 l_1 l_2 \cos\theta}}) \delta\theta \tag{4.12}$$

Using Lagrange's equation,

$$\frac{d}{dt}\left(\frac{\partial L}{\partial \dot{\theta}} \right) - \frac{\partial L}{\partial \theta} = \tau + f_1 - \frac{f_2 l_1 l_2 \sin\theta}{\sqrt{l_1^2 + l_2^2 + 2 l_1 l_2 \cos\theta}} \tag{4.13}$$

The equation of motion can be obtained with the help of Matlab symbolic toolbox,

$$\tau = \ddot{\theta}\left[\frac{2m_1 l_1^2 (l_2\cos\theta/h + l_1 l_2^2 \sin^2\theta/h^3)^2}{1-l_2^2\sin^2\theta/h^2} + m_2 l_1^2 l_2^2 \sin^2\theta/h^2\right]$$
$$+\dot{\theta}^2\left[\begin{array}{l} m_1 l_1^2 (l_2\cos\theta/h + l_1 l_2^2\sin^2\theta/h^3) \\ *\dfrac{(-l_2\sin\theta/h + 3l_1 l_2^2\sin\theta\cos\theta/h^3 + 3l_1^2 l_2^3\sin^3\theta/h^5)}{1-l_2^2\sin^2\theta/h^2} \\ +\dfrac{m_1 l_1^2 (l_2\cos\theta/h + l_1 l_2^2\sin^2\theta/h^3)^2 (l_2^2\sin\theta\cos\theta/h^2 + l_1 l_2^3\sin^3\theta/h^4}{\left(1-l_2^2\sin^2\theta/h^2\right)^2} \\ + m_2 l_1^3 l_2^3\sin^3\theta/h^4 + m_2 l_1^2 l_2^2\sin\theta\cos\theta/h^2 \end{array}\right] \quad (4.14)$$
$$- m_1 g l_1 \frac{h^2 l_2^2\sin\theta\cos\theta + l_1 l_2^3\sin^3\theta}{h^3\sqrt{h^2 - l_2^2\sin^2\theta}} - m_2 g l_1 l_2\sin\theta/h - f_1 - f_2 l_1 l_2\sin\theta/h$$

For normal walking, the variation of the knee joint is between 0~1 rad [Kawamoto et al., 2002]. In this testing structure, if the knee joint angle is close to 0, the load disks can not move down under gravity force due to friction force. So we set the motion range of the knee joint as 22~55 °, i.e., 0.384~0.96 rad.

Let the motion equation of the knee joint be

$$\theta = \begin{cases} \dfrac{(38.5 + 16.5\cos(2\pi t/4.4))\pi}{180} & \text{Extending phase} \\ \dfrac{(38.5 + 16.5\cos(2\pi t/1.2))\pi}{180} & \text{Bending phase} \end{cases} \quad (4.15)$$

Initial condition: m_2 = 8 kg, l_1 = 0.48 m, l_2 = 0.35 m, $f_1 = \begin{cases} 2Nm, \dot{\theta} > 0 \\ 0Nm, \dot{\theta} < 0 \end{cases}$

$f_2 = 14\,\mathrm{sgn}(\dot{\theta})$ N.

The simulation results are shown in figure 4.2-3 to figure 4.2-5. Figure 4.2-3 shows that the torque of the knee joint for the extending phase (θ decreases from 0.96 rad to

0.384 rad) is larger than that of the bending phase under the same knee joint angle. It is reasonable since, for the extending phase, the knee joint should provide additional torque to overcome the friction force, while for the bending phase the friction force help balance the gravity force.

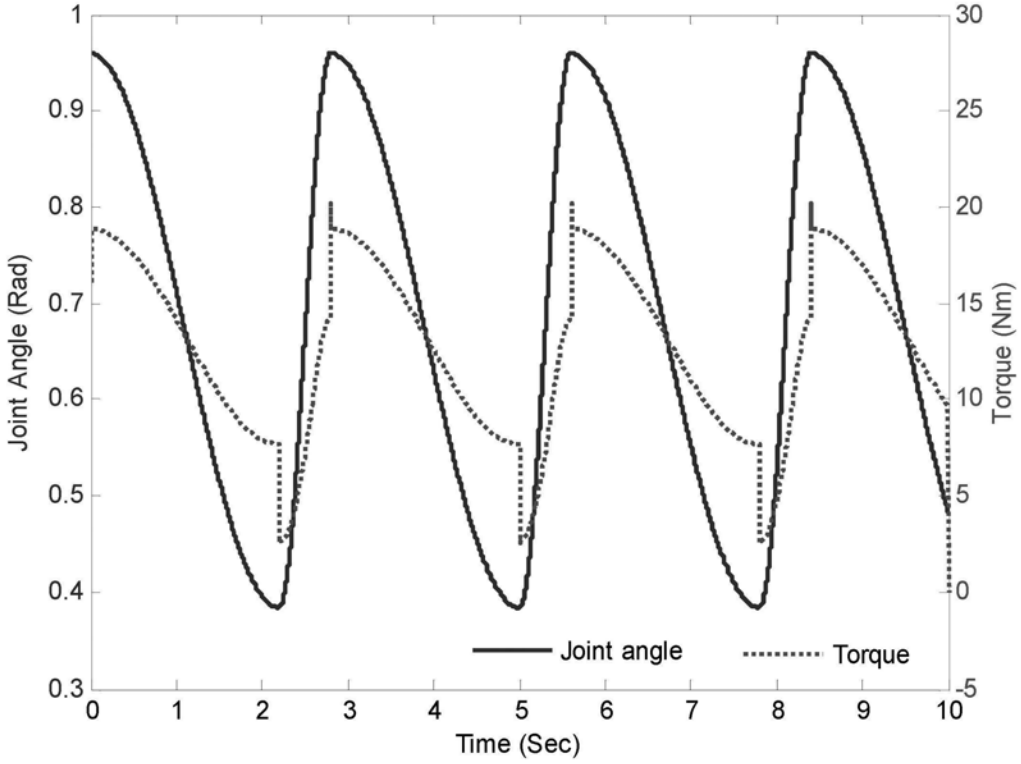

Figure 4.2-3 Knee joint angle and torque of the knee brace with slow motion

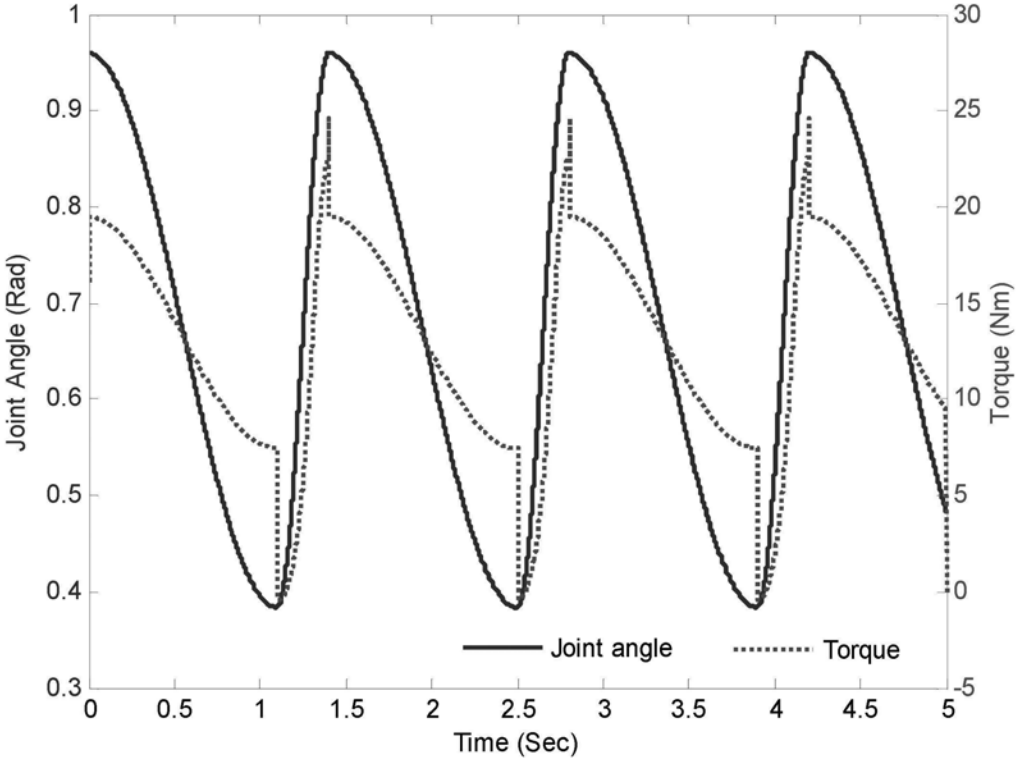

Figure 4.2-4 Knee joint angle and torque of the knee brace with fast motion

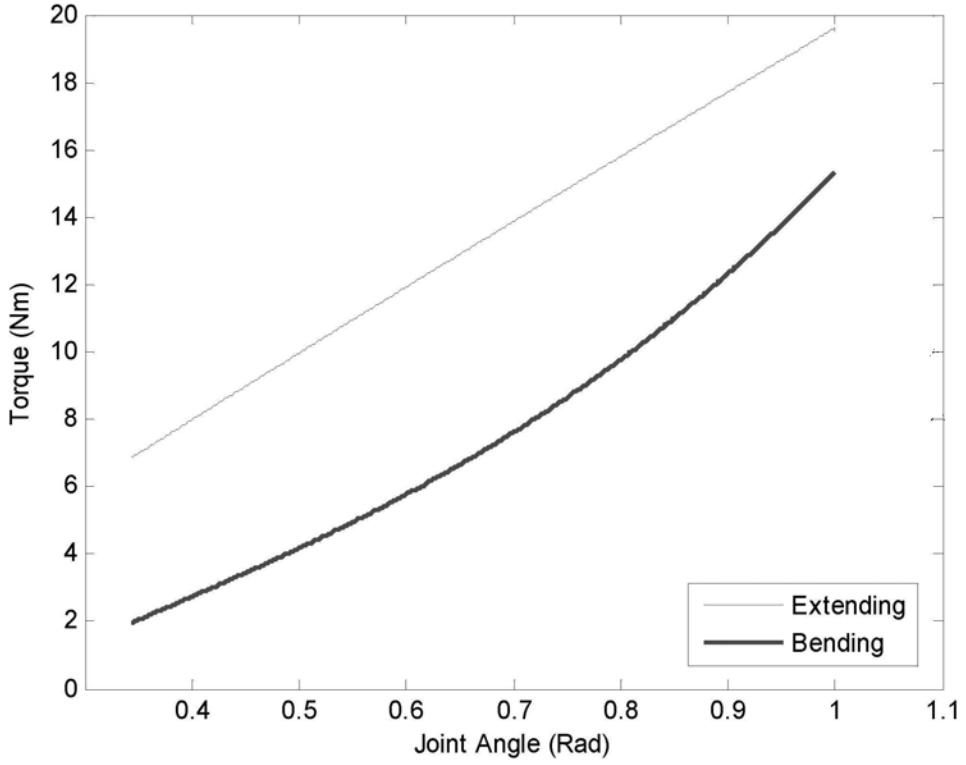

Figure 4.2-5 Torque vs. knee joint angle at slow motion

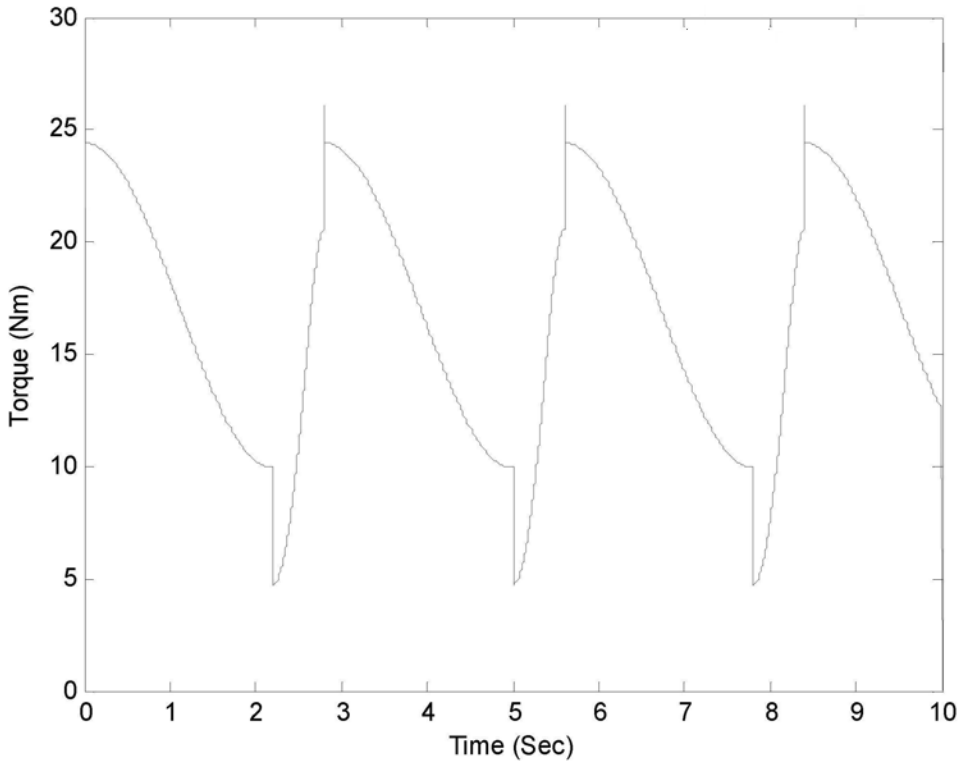

Figure 4.2-6 Knee joint torque with 11 kg load

Figure 4.2-4 shows the result under the same condition as figure 4.2-3 but at two times faster speed. While compared these two simulation results, it can be seen that, for the extending phase, the increase of speed does not bring obvious torque increase; while for the bending phase, the increase of speed brings significant increase of torque. It proves that when the motion is slow, dynamic force is negligible; while the motion is fast, the dynamic force will be significant. Figure 4.2-5 shows the relationship between the knee joint angle and required knee torque during bending and extending phases under a load of 8 kg. It can be seen that for the extending phase, the torque is linear to the joint angle. But for the bending phase, nonlinearity exists. Figure 4.2-6 shows the torque of the knee joint during motion with a load of 11 kg (i.e., two load disks). It can be seen that the maximum torque is smaller than 30 Nm, which is the upper limit of the MR actuator under coil current of 1.8 A.

4.3 Testing and Control of Knee Brace

Experiments are carried out to test the knee brace with the developed testing structure. The initial condition is the same as the simulation with m_2 = 15 kg. The motor rotates at constant speed. A pulse current input of 0.5A, 1.0A, 1.5 A, 2.0 A is applied to the MR actuator and the knee brace is at the start position $\theta = 1$, where bolts are used in the guiding poles to prevent the load disks from falling. When the knee brace rotates to its end position $\theta = 0$, the power of the MR actuator is turned off. The experimental results are shown in figure 4.3-1. It can be seen that the torque of the knee brace increases as the coil current increases. Also it is found that the measured torque using strain gauges are close to the measured results using load cell (refer to Chapter Two). It is noted that when the coil current is equal or larger than 1 A, the measured torque increases with time, although the coil current and rotating speed of MR actuator are kept constant. When the load is lighter, the knee brace can lift up the disk. Figure 4.3-2 shows the experimental results at condition m_2 = 15 kg and 1.1 A coil current. It is seen that at the time around $t = 4$ second, the measured torque begins to decrease. It is because that the knee brace starts to extend and the force arm is becoming smaller. It is noted that the torque the knee brace starts to extend is about 20 Nm, which is close to the simulation result in figure 4.2-5. Once the knee brace starts to extend, the torque of the knee joint drops below the yield torque of the MR actuator and the MR fluid is not at yield state now. Once the knee brace reaches the end position, the knee brace can not rotate anymore due to restrict structure and the MR actuator works in yield state again. During the whole process, the maximum torque the DC motor applied to the knee brace is limited by the yield torque of MR actuator.

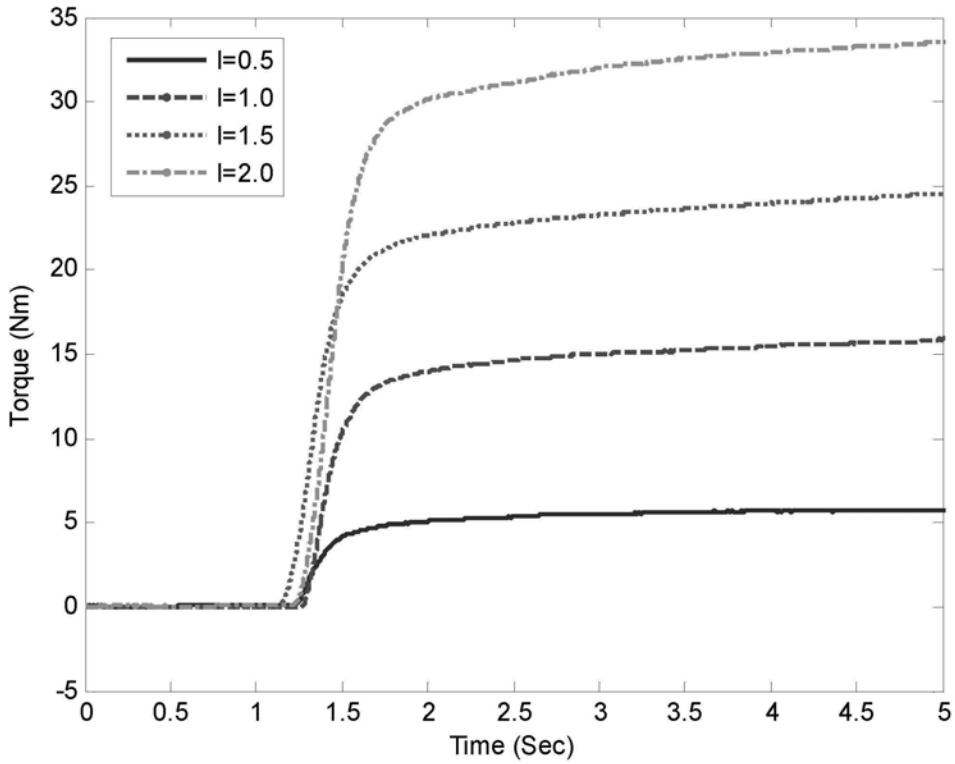

Figure 4.3-1 Knee brace torque under different coil current

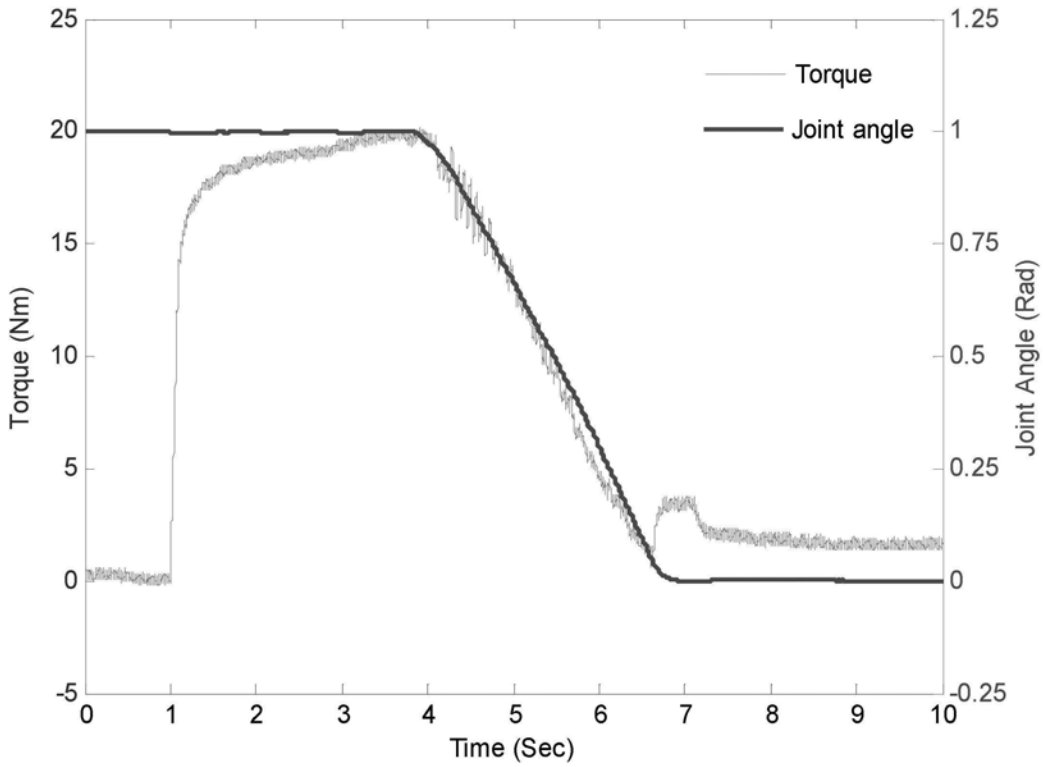

Figure 4.3-2 Joint angle and torque during knee brace extending

To further study the performance of the knee brace, a simple control algorithm is applied to the system. The flow chart of the control algorithm is shown in figure 4.3-3. The start position is $\theta_0 = 1$. θ_1, θ_2 are the allowable lower position and upper position, respectively. These two parameters are set to 0.95 (slightly smaller than the initial position of 1.0) and 0.4 as the previous simulation. Since the working space is well defined in the testing structure, position control is used for the control of this knee brace. The experiment is carried out on a dSPACE system. The system model is built in Matlab and then uploaded into dSPACE. A virtual panel is built in the ControlDesk of dSPACE. When the flag "Start" on the panel is set, the knee brace will begin to extend to lift up the load disks. While the upper position is reached, the motor is turned off and only the MR actuator regulates the motion of the structure.

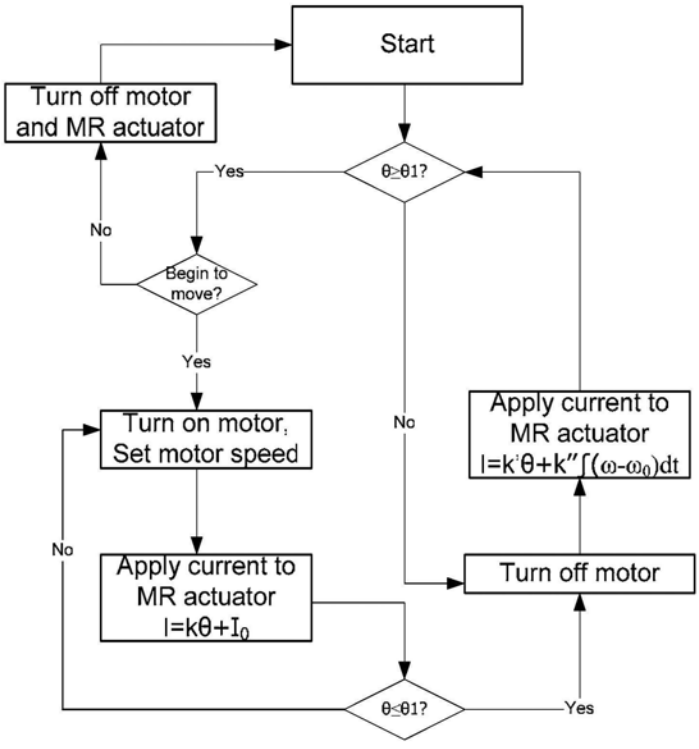

Figure 4.3-3 Flow chat of IP-based state control algorithm

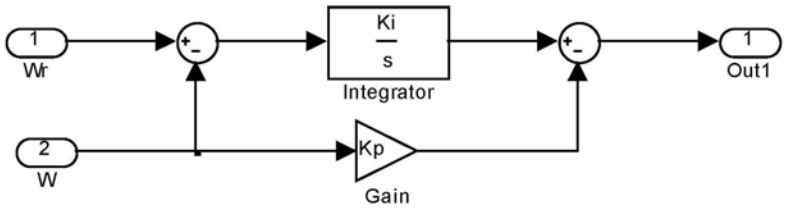

Figure 4.3-4 IP control of MR actuator during knee bending

For the extending phase (i.e. motor switching on phase), only the motor is used to regulate the motion of the knee brace, and the current applied to the MR actuator is $I = k\theta + I_0$, where k and I_0 are manually adjusted to make I as small as possible while make sure that the MR actuator can fully transfer the torque produced by the motor to the knee brace during extending process, so as to reduce the energy consumption of the MR actuator. For the knee bending phase (i.e. motor switching off phase), an IP controller is used to adjust the output of the MR actuator, as shown in figure 4.3-4.

Experiments are carried out with the above controller under the load of 8 kg. The condition and target motion trajectory are the same as the simulation in figure 4.2-3. The control parameters of IP controller are set as: $k_i = 2$, $k_p = 0.6$. The control parameters are set small to avoid oscillation. Figure 4.3-5 shows the experimental results. From the figure, it can be seen that both the moving up and down processes can be controlled. As the simulation, the measured torque of extending process is larger than that of the bending process at the same angular position. The torque variation of the experiment is similar to the simulation although the trajectory under control cannot exactly follow the target one.

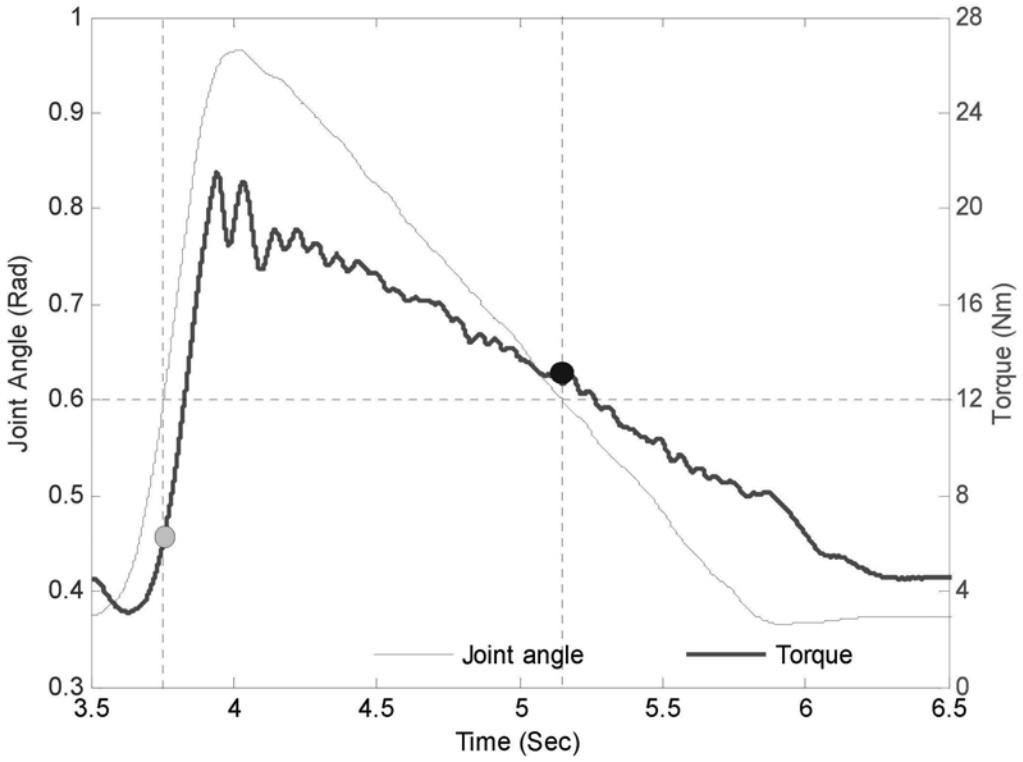

Figure 4.3-5 Torque and joint angle during motion

Adaptive control is also proposed for controlling the bending process of the knee brace. From the simulation results we can see that when the knee motion is slow, the torque of the knee joint is proportional to the knee joint angle. Speed control is used for the motion of the knee brace. Through Newton second law, the motion equation can be simply expressed as

$$\frac{\dot{\theta}_{y,k+1} - \dot{\theta}_{y,k}}{\Delta t} = \frac{T}{I} = \frac{k_a U - (mg - f_2)L + f_1}{I} \tag{4.16}$$

where Δt is the sampling time, T is the torque of the knee brace, I is the rotational inertia of the knee brace, U is the control input, L is the force arm, m is the equivalent mass, f_1 and f_2 are the rotational and linear friction forces. When the knee joint

angle is small, the force arm is linear to the joint angle. I is a constant. f_1 is omitted since it is small and f_2 can be combined in the mass of the knee brace. Thus the speed of the knee brace at some instant is determined by its previous speed, the voltage applied to the MR fluid, and the angular position. The system model can be expressed as

$$\dot{\theta}_{y,k+1} = a\dot{\theta}_{y,k} + bU_k - c\theta_{y,k} \tag{4.17}$$

Let the control input be given by

$$U_k = l_k r_k + m_k \dot{\theta}_{y,k} + n_k \theta_{y,k} \tag{4.18}$$

where l, m, n are control parameters. There exist nominal values

$$l^* = \frac{1}{b},\ m^* = -\frac{a}{b},\ n^* = \frac{c}{b} \tag{4.19}$$

such that $\dot{\theta}_{y,k+1} = r_k$.

Define the output error

$$e_k = \dot{\theta}_k - \dot{\theta}_{r,k} \tag{4.20}$$

Choose the following parameter adaptation law:

$$l_{k+1} = l_k - ge_k r_k$$

$$m_{k+1} = m_k - ge_k \dot{\theta}_{y,k} \tag{4.21}$$

$$n_{k+1} = n_k - ge_k \theta_{y,k}$$

It can be proved that the system is stable with Lyapunov stability criterion.

The current applied to the MR actuator is smaller than 2.0 A, so $0 \le U_k \le 7.5$. The diagram of the control system is shown in figure 4.3-6 and figure 4.3-7.

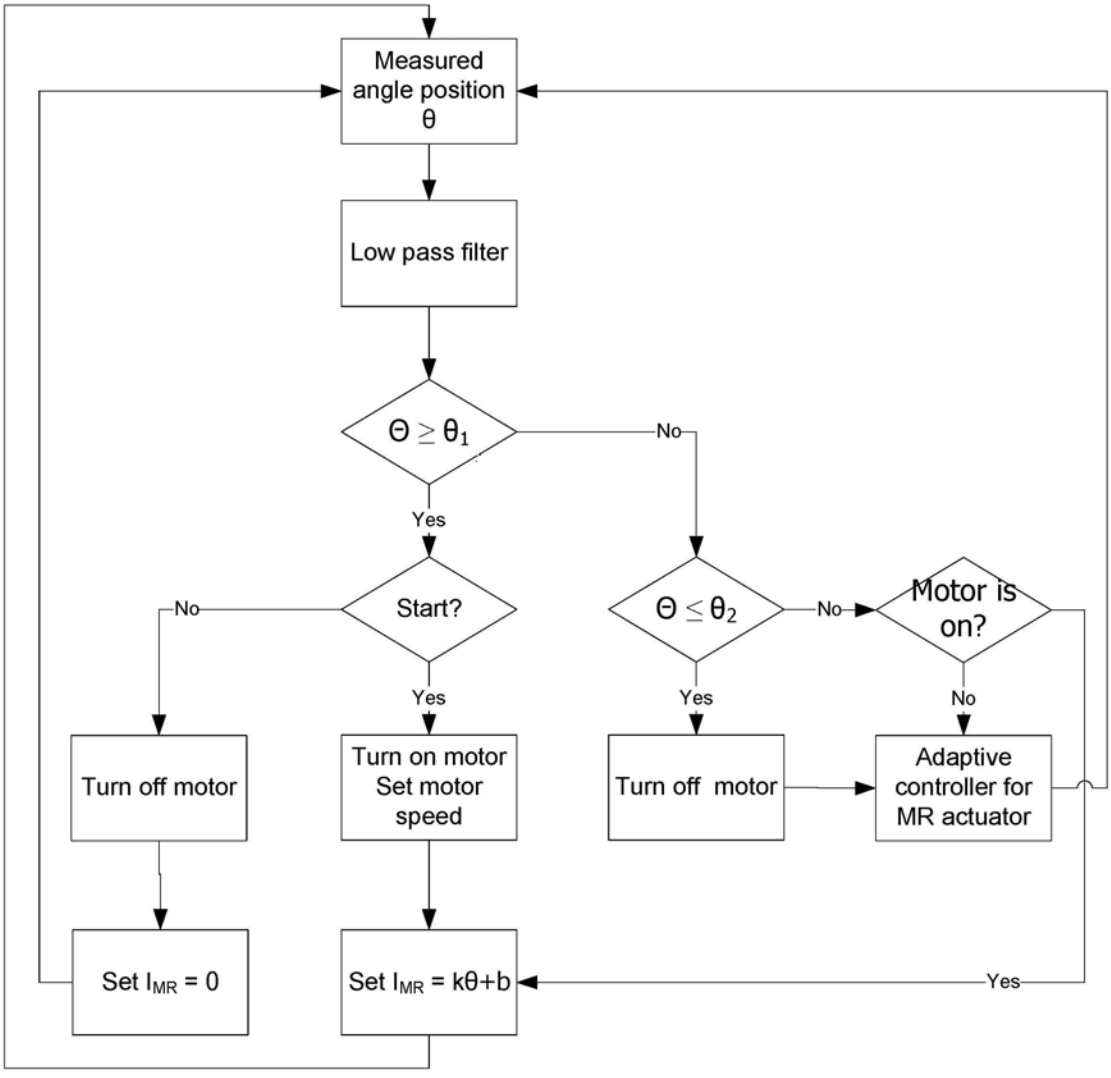

Figure 4.3-6 Block diagram of control system of knee brace

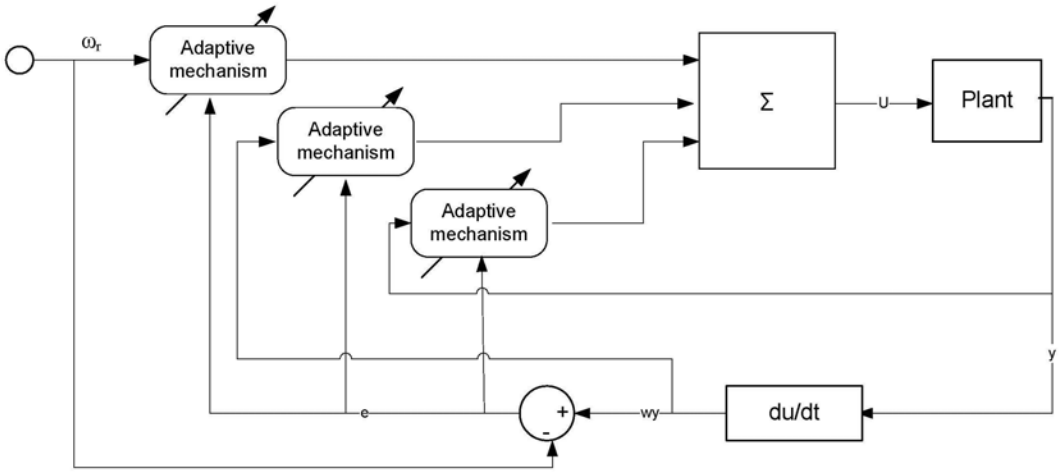

Figure 4.3-7 Block diagram of adaptive controller

Experiments are carried out to study the performances of knee brace under control. The experimental conditions are the same as those in the previous IP control experiments. Figure 4.3-8 and figure 4.3-9 show the experimental results at the start up of experiments. The reference speed for bending down is set as 0.25 rad/sec. The control parameters *l*, *m*, *n* are set as -1, 1, and 1, respectively. Figure 4.3-10 and figure 4.3-11 show the experimental results of about 6 minutes after start.

It can be seen from the figures that at the beginning, the falling down speed is not very accurate and the overshoot is a bit large, but several minutes later, the performance of the controller is much better, the average speed is close to the reference speed, and the overshoot is much smaller. The control parameters change fast at the beginning and become stable after several minutes.

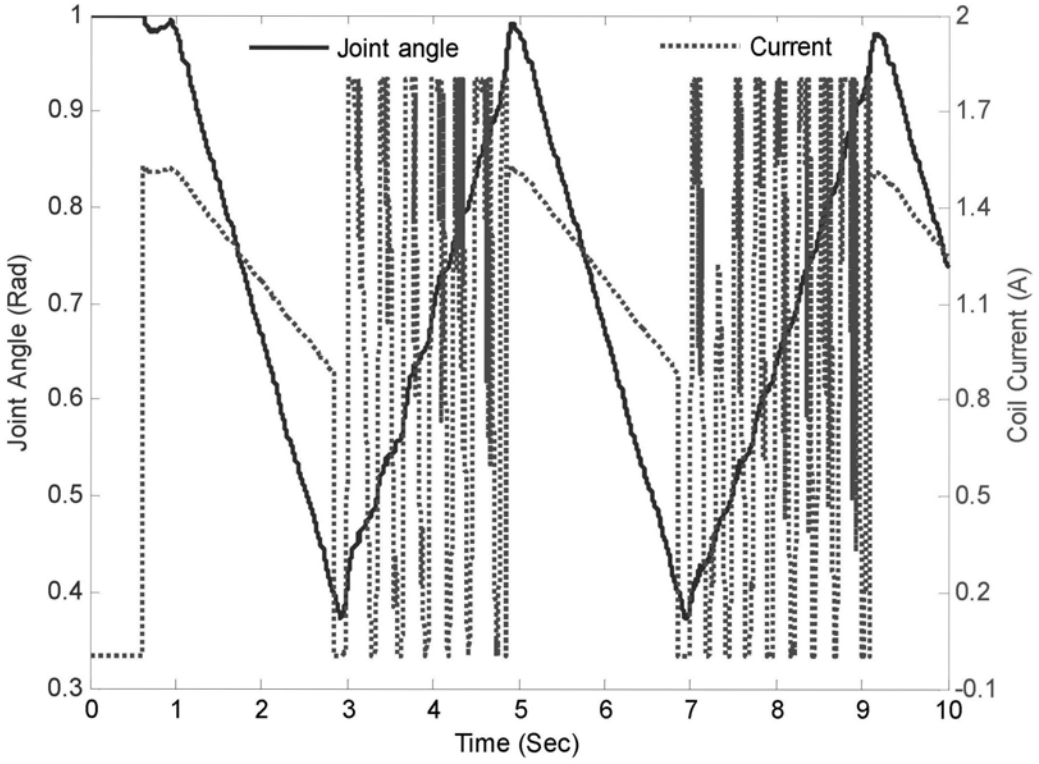

Figure 4.3-8 Start of knee brace motion under adaptive control

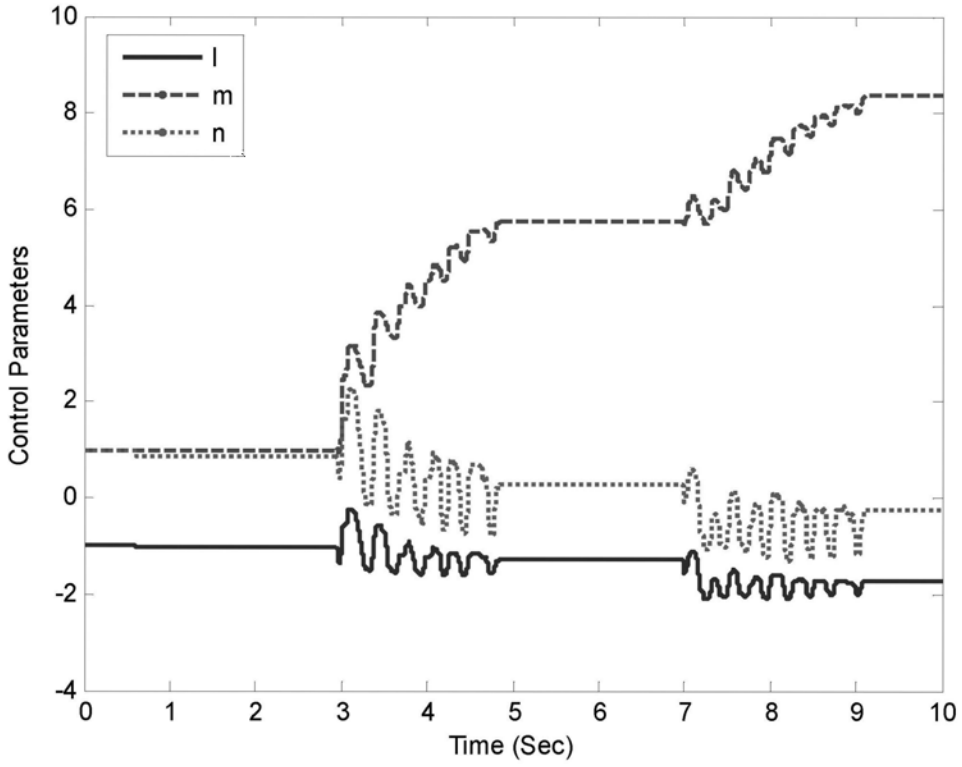

Figure 4.3-9 Control parameters at start up of adaptive control

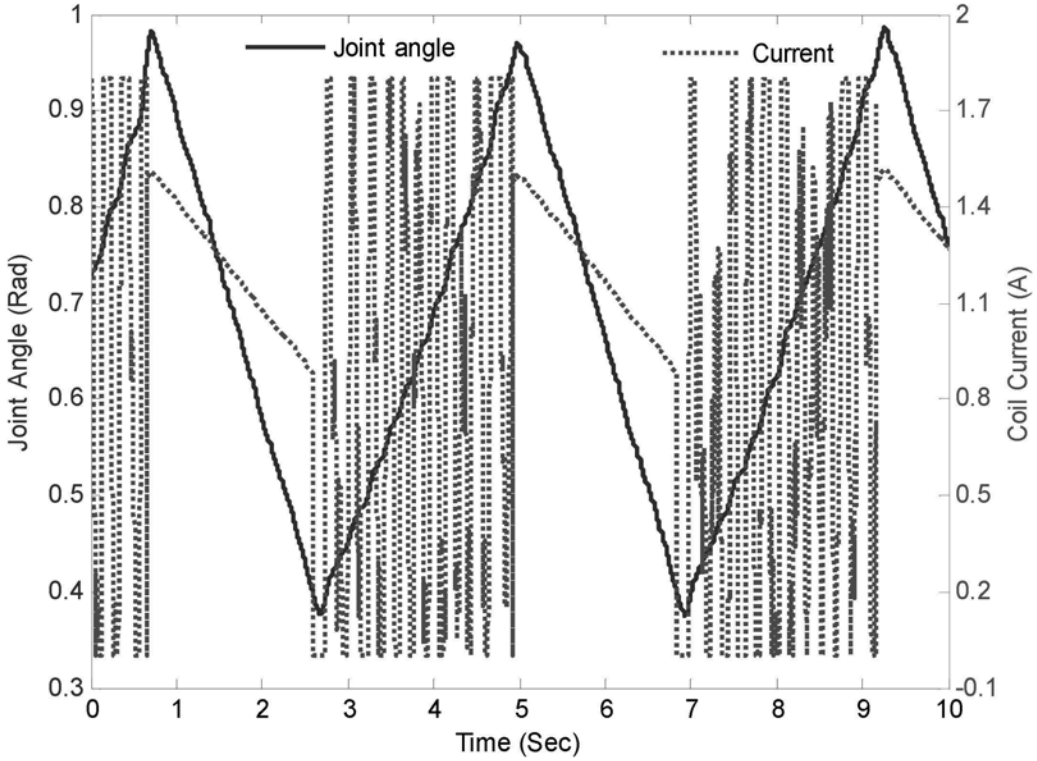

Figure 4.3-10 Steady state knee brace motion under adaptive control

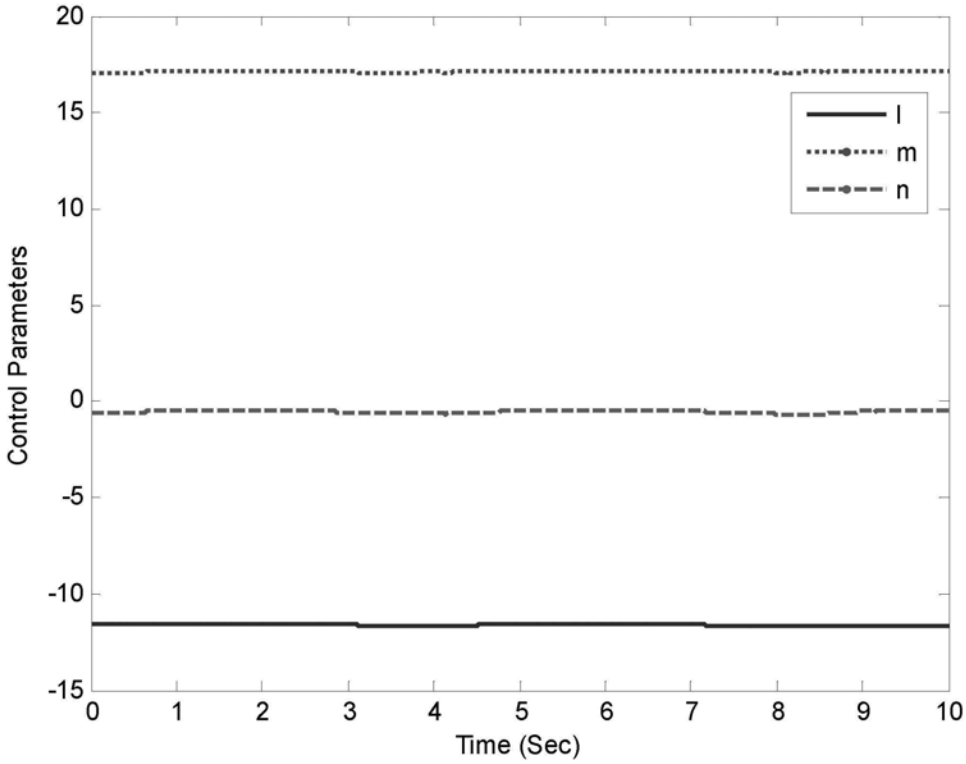

Figure 4.3-11 Steady state control parameters under adaptive control

The performances of IP controller and adaptive controller are compared experimentally. The control gains of IP controller are set small to avoid oscillation; however, small controller gains render slow response time. In the following experiments, the integral gain is changed from 10 to 500. The experimental conditions are the same as the previous experiment, but the reference speed changes to 0.50 rad/sec. Figure 4.3-12 shows the experimental results under IP control and adaptive control. It is seen that larger overshoot is observed for IP control.

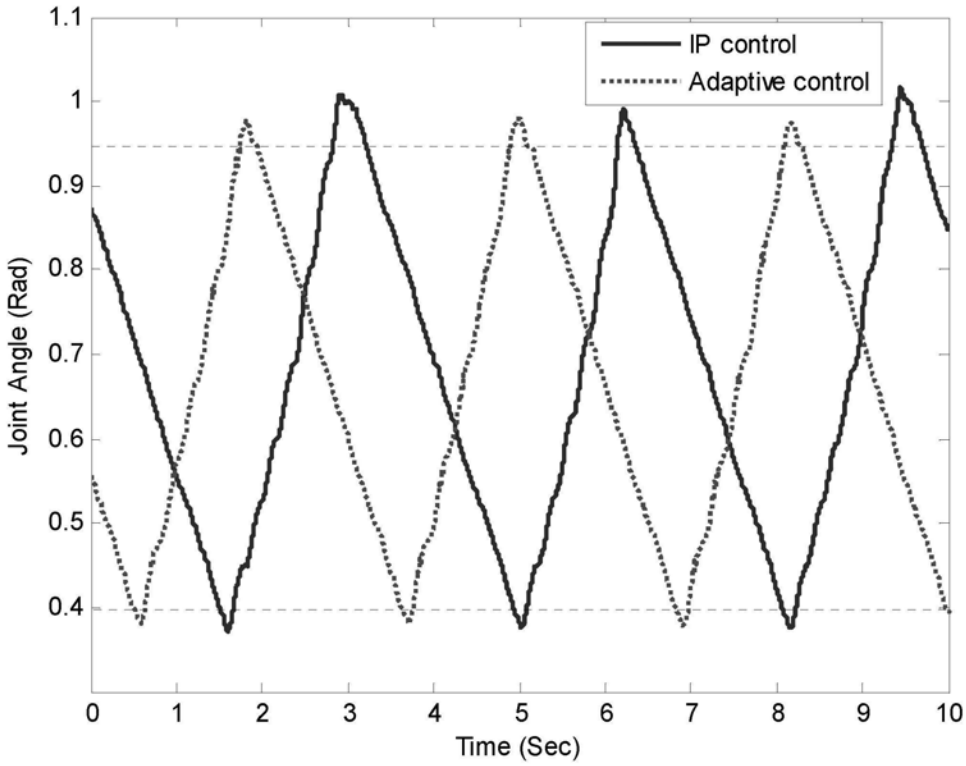

Figure 4.3-12 IP control vs. adaptive control with fast motion speed

4.4 Chapter Summary

In this chapter, the knee brace with both MR actuator and DC motor is developed and tested in a custom-built testing structure. The DC motor can provide active assistive torque while the MR actuator provides passive assistive torque. With the angular and force information from the potentiometer and strain gauges, the knee brace can shift its working modes according to working condition.

The motion of the knee brace under the testing structure is analyzed. From the simulation results, it can be seen that when the motion is slow, the dynamic force of the knee brace can be omitted. The torque of the knee brace is almost linear to the joint angle when the angle variation is between 0~1 rad. The measured values of torque under different coil currents using strain gauges are consistent with the values measured by load cell in Chapter Two. And the knee brace is capable of lifting up 8 kg load with 1.1 A coil current.

IP-base state control and adaptive control are used for control of the knee brace. Experimental results demonstrate that the motion of knee brace can be well controlled by both controllers. However, significant oscillations are observed for both controllers. Under adaptive control, the motion of knee brace has smaller overshoot as compared to that under IP control when the motion speed is fast.

CHAPTER FIVE

EVALUATION OF KNEE BRACE WITH MR ACTUATOR

In this Chapter, the characteristics of the knee brace with MR actuator will be evaluated in three aspects: power consumption, performance, and safety.

A knee brace without MR actuator will be fabricated as compared to the knee brace with MR actuator. Some connecting components will be used to replace the MR actuator and both active and passive torques are provided by the DC motor. The knee brace without MR actuator will be tested and controller for this knee brace will also be developed.

The power consumption of the knee brace with MR actuator and without MR actuator will be investigated. Experiments will be carried out to study the energy consumption of both knee braces during bending and extending processes. The power consumption of knee brace during normal walking cycle will also be analyzed and compared.

Low impedance, good force controllability and fast response time are desired features for assistive knee braces. The inertia of knee brace, force controllability, and response time will be studied for both knee braces.

Safety is the most important aspect for devices that directly acting on human body. The safety of the knee braces under some extreme conditions (such as the actuators are out of control) will be studied.

5.1 Knee Brace without MR Actuator

To better evaluate the hybrid assistive knee brace with MR actuator, a knee brace that uses only DC motor is developed, as shown in figure 5.1-1. The whole system is almost the same as the previous knee brace except that a joint (replaces the MR actuator). The joint comprises: (1) a wing shape part, which is connected to the upper brace; (2) an "n" shape part, which is connected to the lower brace; (3) a shaft core, which is connected to the big gear and wing part; (4) A ball bearing (Type 16003, size $17 \times 35 \times 8$ mm), which is housed in the "n" shape part. The motion of the knee brace is fully controlled by the DC motor. Figure 5.1-2 shows the photo of the fabricated knee brace without MR actuator.

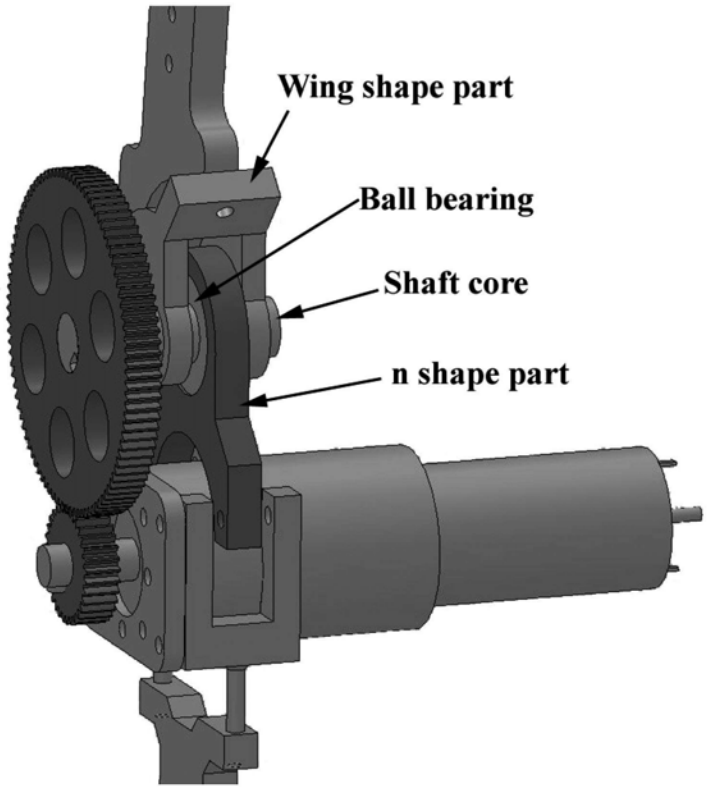

Figure 5.1-1 Knee brace with motor only

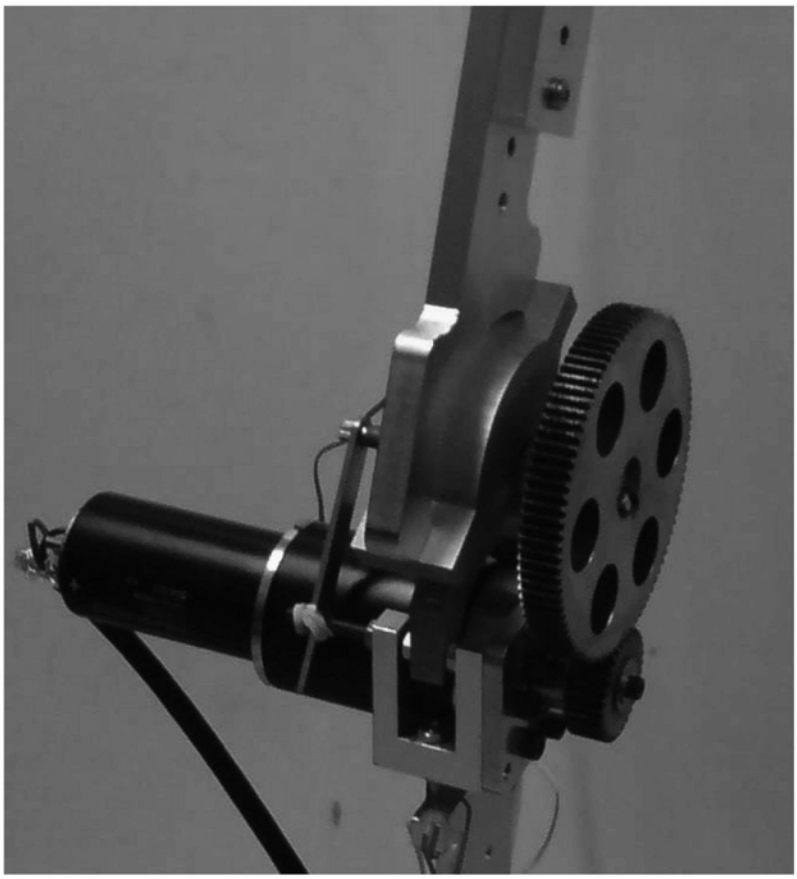

Figure 5.1-2 Photo of knee brace with motor only

The knee brace is tested in the testing structure. The experimental condition is: mass of load m_2 = 8 kg, knee brace motion range 0.4 ~0.95 rad. The motor rotates at constant speed and changes its rotation direction once the knee brace reaches the upper or lower limit positions. The speed control signal is set as 1, 2, 3, 4, 5, respectively. Figure 5.1-3 shows the knee motion under control signal of "1" and "3". It can be seen that though the absolute speed control signal is the same, the bending speed and extending speed under control signal "1" are different. Figure 5.1-4 shows the relationship between the control signal and knee brace motion speed.

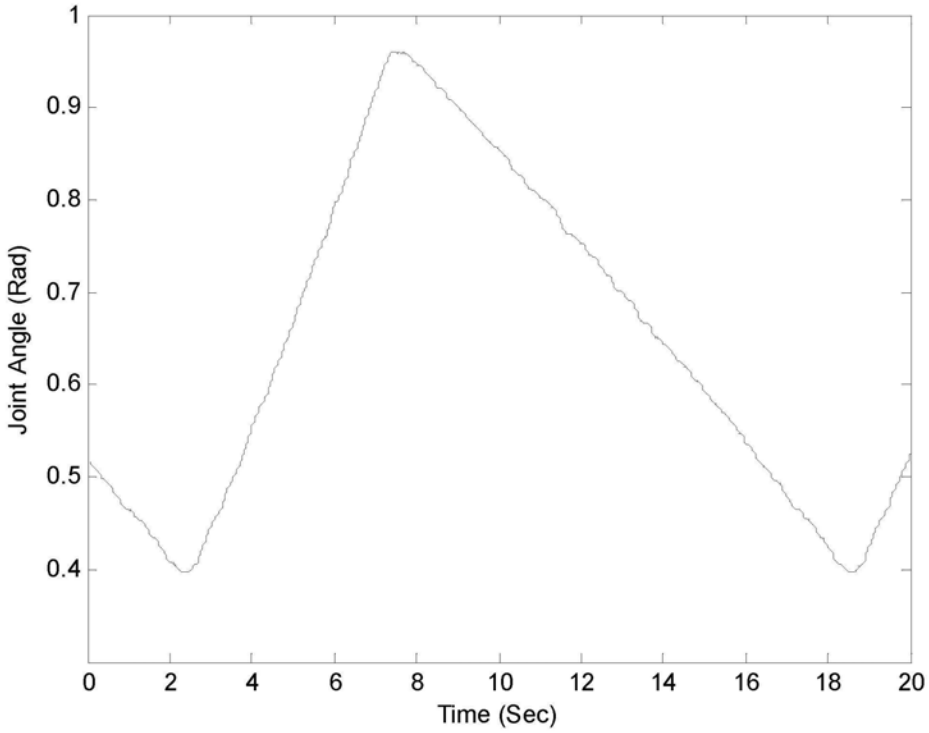

(a) Speed control signal is "1"

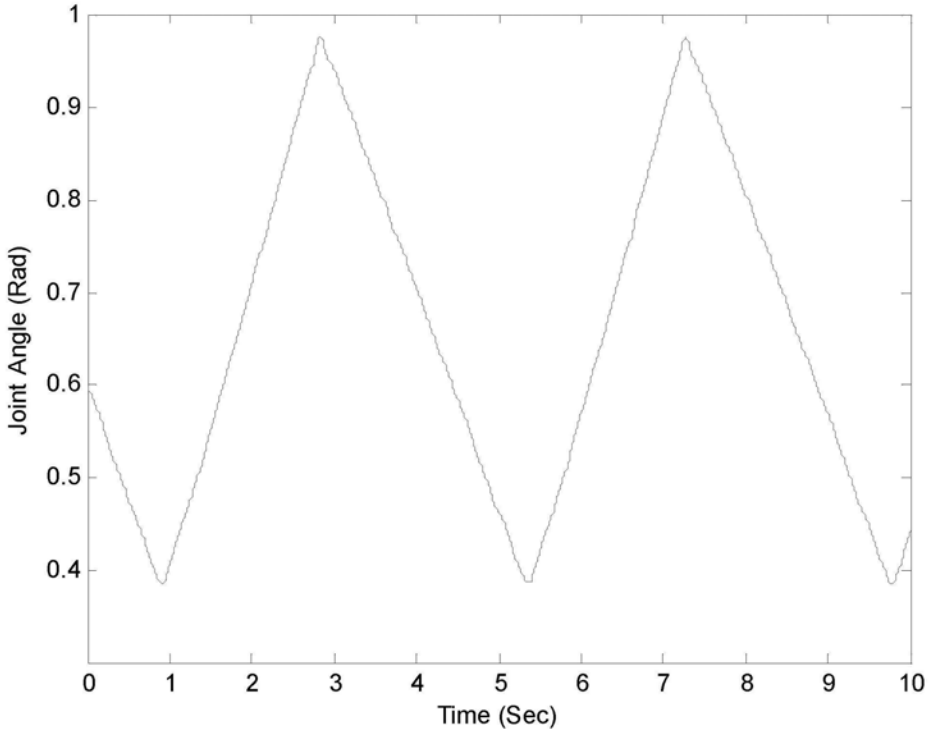

(b) Speed control signal is "3"

Figure 5.1-3 Knee motion under different speed

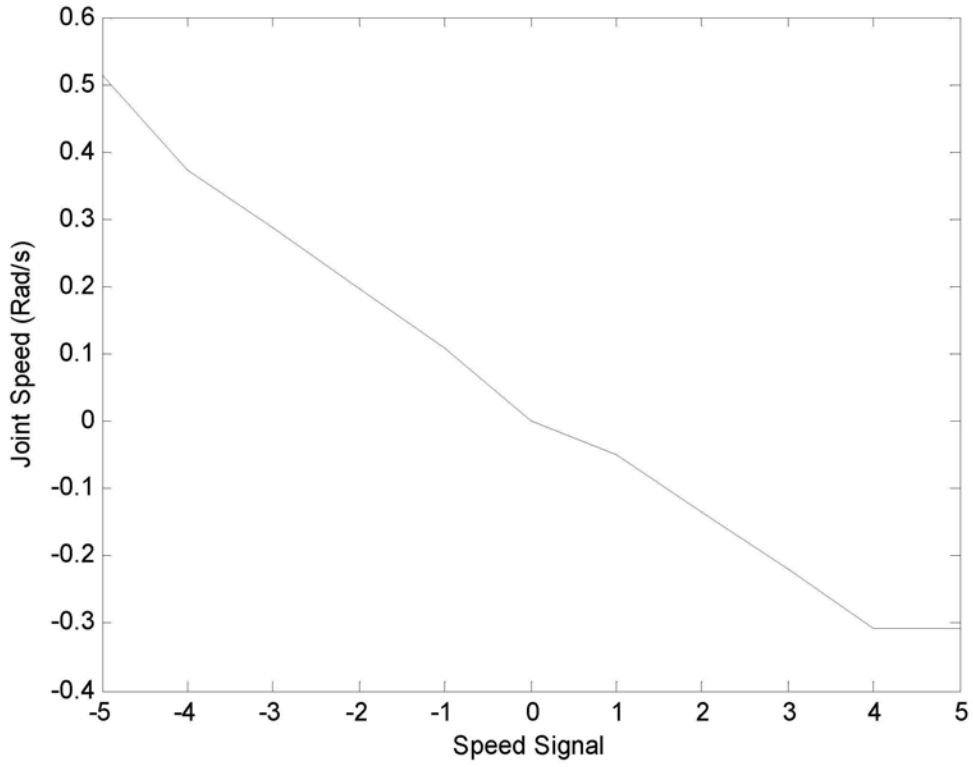

Figure 5.1-4 Relationship between control signal and knee brace speed

For the range of 1~4 and -1 ~ -4, the speed signal has good linearity to the joint speed. The relationship between knee brace speed and control signal can be expressed as

$$\omega = \begin{cases} -0.0884x + 0.021, \text{ when } x > 0 \\ -0.0858x + 0.0369, \text{ when } x < 0 \end{cases} \tag{5.1}$$

where x is the speed control signal. When x is positive, the motor drives the knee brace to extend; while x is negative, the motor drives the knee brace to bend.

Based on the relationship, the exact speed of motor can be controlled. PI control is proposed for the control of knee brace without MR actuator. Figure 5.1-5 shows the

Simulink model of the controller. Only the bending phase is controlled by the PI controller and a constant speed signal is given to the extending phase. Experiments are carried out to study the motion of the knee brace under control. The motion range for the knee joint is limited in the range of 0.4~0.9 rad. Figure 5.1-6 shows the experimental results when the reference speed is 0.2 rad/sec. The actual speed is estimated to be close to the reference speed 0.2 rad/sec. However, overshoot is observed during the motion.

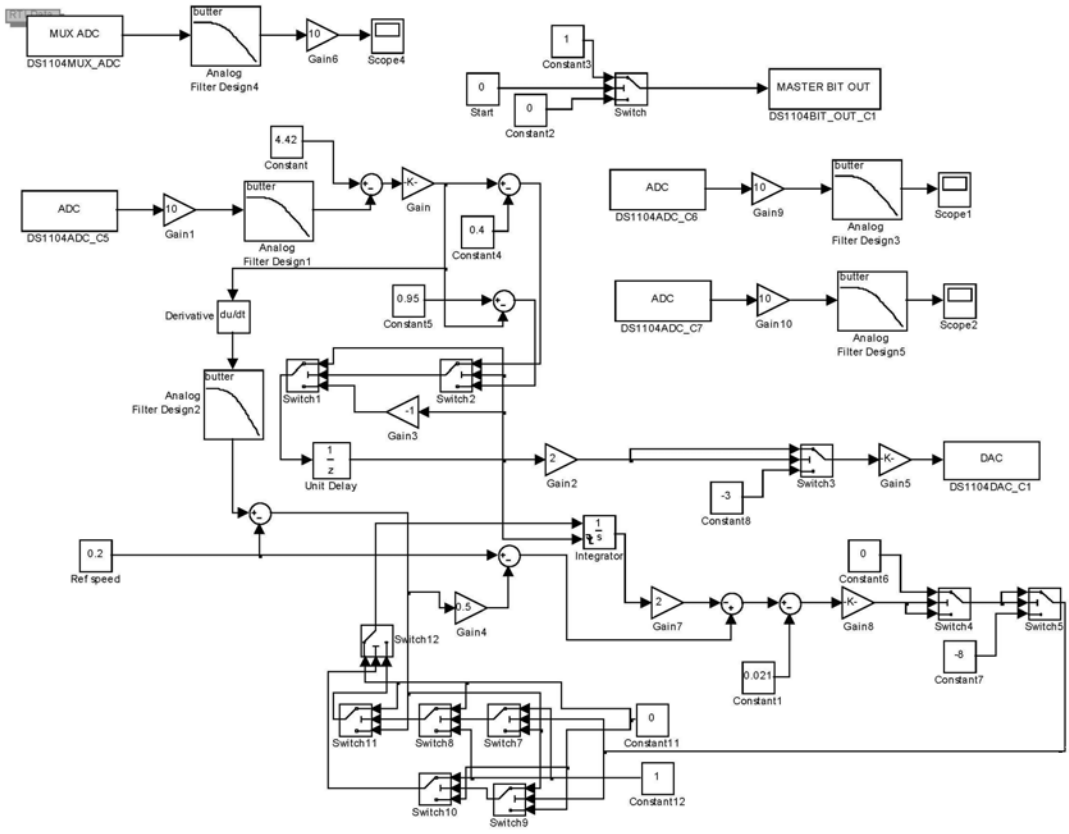

Figure 5.1-5 PI control system for knee brace without MR actuator

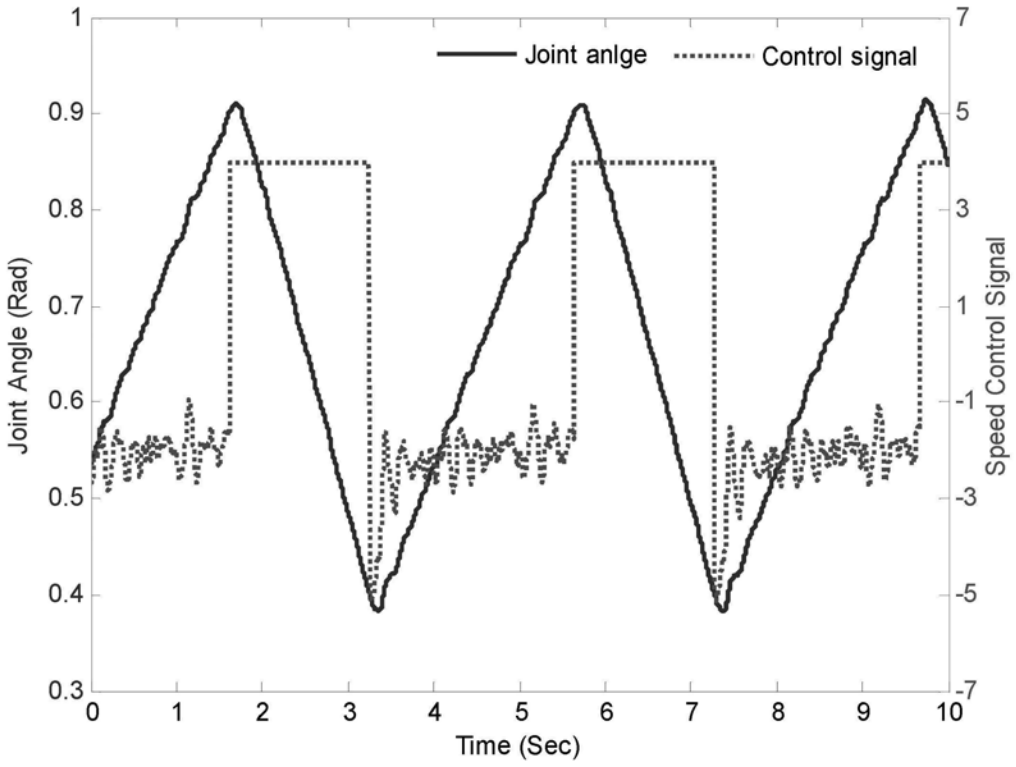

Figure 5.1-6 Knee joint motion under PI control

5.2 Study on Power Consumption

The power consumption of knee brace with MR actuator and without MR actuator is studied in this section. The power consumption includes the power for the DC motor and MR actuator. Since the voltage of DC motor is constant, the power consumption of motor is proportional to the motor current. And the motor current is proportional to the torque output, so the power of motor can be calculated from the torque of knee brace during motion. However, the efficiency of the gearbox should be considered while calculating the power since the torque transfer efficiency is not 100%. From the datasheet of the gearbox GP 52 C, only maximum torque transfer efficiency is given, which is 75%. The transfer efficiency is experimentally tested. The experimental setup is shown in figure 5.2-1.

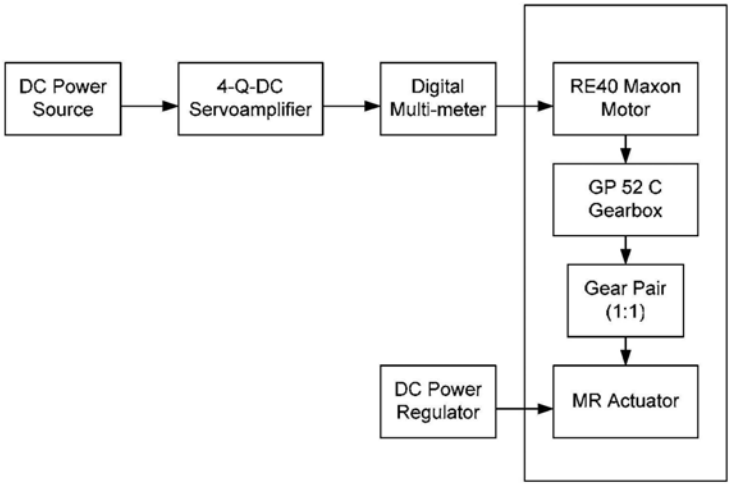

Figure 5.2-1 Diagram of experimental setup

The speed control signal is 2.0 V, the MR actuator is working at yield state. Apply currents of 0.1~0.9 A to the coil of MR actuator and measure the corresponding motor currents with digital multimeter. Figure 5.2-2 shows the experimental results.

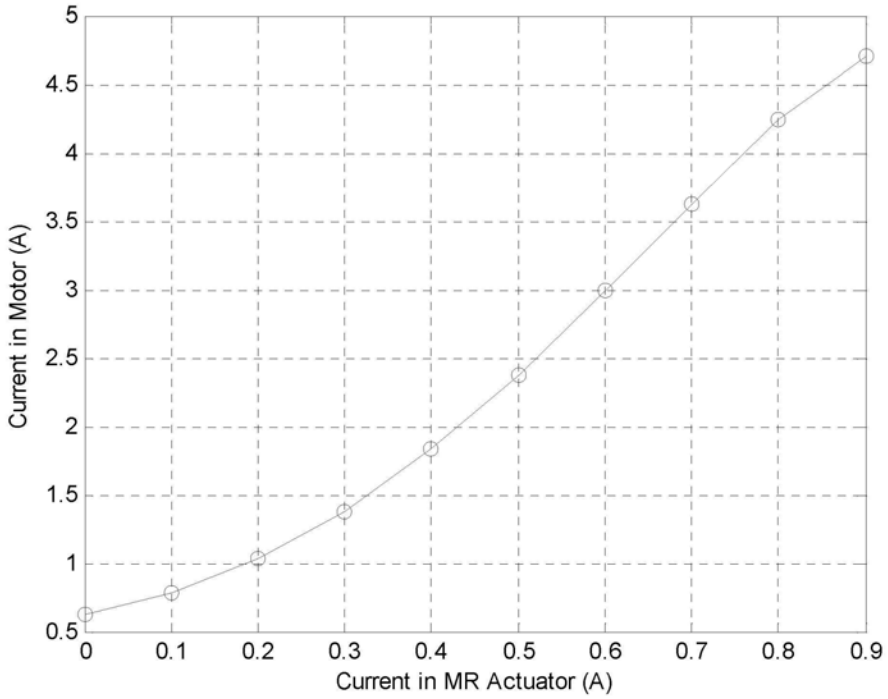

Figure 5.2-2 Current of MR actuator vs. current of motor

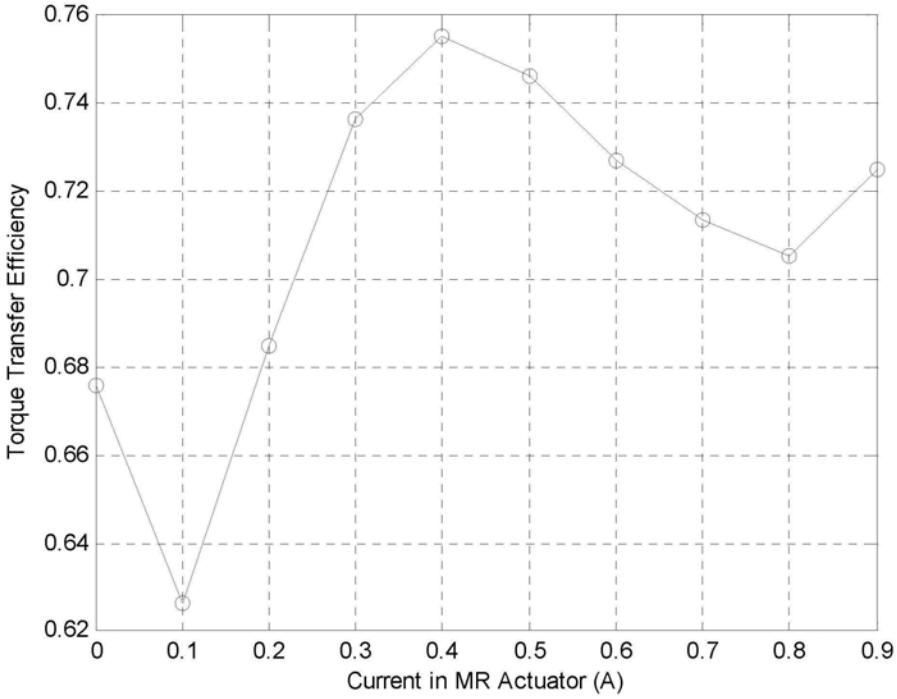

Figure 5.2-3 Transfer efficiency of gearbox at different coil currents

The torque of the MR actuator at different coil current has been measured in Chapter 2. The torque of motor can be calculated with the parameters of DC motor. So the transfer efficiency of the gearbox can be calculated, as shown in figure 5.2-3. It can be seen that the transfer efficiency is not constant, and the average torque transfer efficiency is about 71%.

Let the knee brace rotate in the range of 0.4~0.95 rad, the extending speed is 0.244 rad/sec and the bending speed is 0.25 rad/sec. The torque of the knee brace is shown in figure 5.2-4 (simulation result).

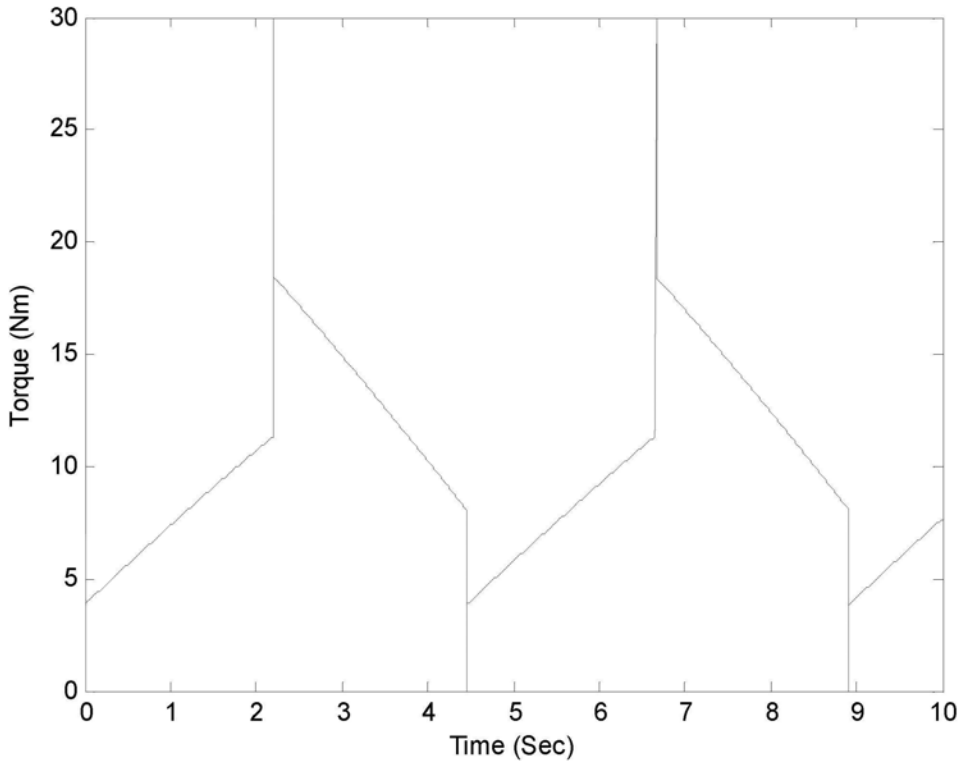

Figure 5.2-4 The torque of knee brace during bending and extending

The mean torque during the bending process is 7.65 Nm, and the mean torque of the knee brace during the extending process is 13.39 Nm. A 3:1 gear pair is used in the knee brace, so the total gear ratio for the motor is 468. The torque constant at the output can be calculated as 0.0302*468*71% = 10 Nm/A. For the knee brace with MR actuator, during the extending process, the average current of motor is 1.339 A, and the average current of MR actuator is 0.77 A. The average current of MR actuator during the bending process is about 0.5 A. The voltage of DC motor and MR actuator is 24V and 6V, respectively. The power consumption for the bending and extending can be calculated as shown in table 5.1-1. For the knee brace without MR actuator, only the DC motor consumes energy. For the bending process, the unloaded current of DC motor is 0.137 mA, so the equivalent resistance of DC motor is 1.94 Nm. It is close to the friction force of the knee brace with MR actuator. The inertia of motor

and viscosity of motor are not considered here. Assume the torque transfer efficiency in the reverse direction is also 71%, the torque constant of DC motor is 10/0.71/0.71=20 Nm/A. The power consumption during bending and extending process is calculated as shown in table 5.2-1.

Table 5.2-1 Power consumption for both knee braces

Condition	$P_{Extending}$	$P_{Bending}$	$P_{Average}$	Power Save
Without MR actuator	32.14 W	9.18 W	20.80 W	3.5%
With MR actuator	36.76 W	3.00 W	20.09 W	

As seen from table 5.2-1, the knee brace with MR actuator saves energy up to 3.5%. In fact, due to the large gear ratio, the gearbox is not backdrivable, the torque transfer efficiency should be smaller than 71% in the reverse direction, and thus the power consumption should be smaller. And the viscosity of motor may dissipate some energy during the bending process. So the energy consumption of both knee braces for the bending and extending may be not significant.

Experiments are carried out to study the power consumption for the knee brace with MR actuator. The experimental conditions are: working range: 0,40~0.95 rad, extending: open loop, reference speed 0.333 rad/sec and 0.244 rad/sec; bending: closed loop, under adaptive control, reference speed 0.1 rad/sec and 0.25 rad/sec. Figure 5.2-5 shows the experimental results with extending speed of 0.244 rad/sec and bending speed of 0.25 rad/sec. The average current of MR actuator during bending and extending is 0.76 A and 0.77 A, respectively; the average current of motor during extending is 1.31 A. The power consumption for these cases are calculated and given in table 5.2-2.

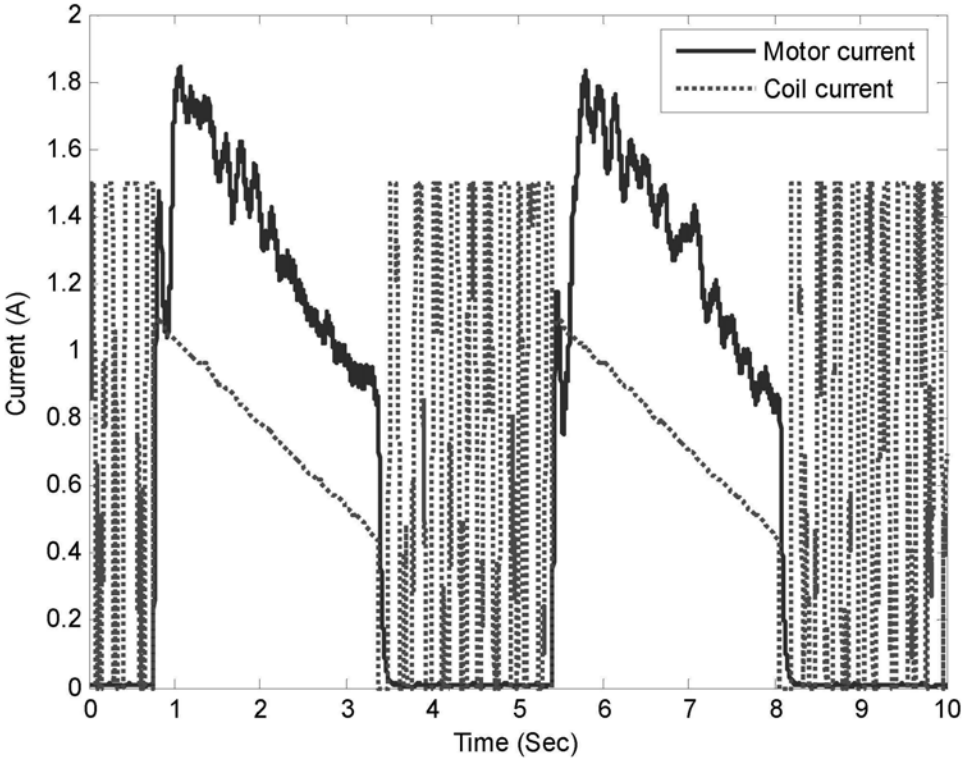

Figure 5.2-5 Current of motor and MR actuator during motion

Experiments are also carried out to study the power consumption of the knee brace without MR actuator. The experimental conditions are the same as the previous experiments. The only difference is that for the cases with bending speed 0.25 rad/sec, it is open-loop instead of closed-loop. Figure 5.2-6 shows the case with extending speed 0.244 rad/sec and bending speed 0.25 rad/sec. The mean current of the bending process is 0.25 A, and the mean current of the extending process is 1.29 A. The power consumption of these cases are calculated and given in table 5.2-2. From the experimental results, it can be seen that the difference of energy consumption for both knee braces during bending and extending processes is not significant. When the bending speed is slow and extending speed is fast, the knee brace with MR actuator is slightly more energy efficient. However, if the extending speed is slow and the bending speed is fast, the knee brace without MR actuator consumes less energy.

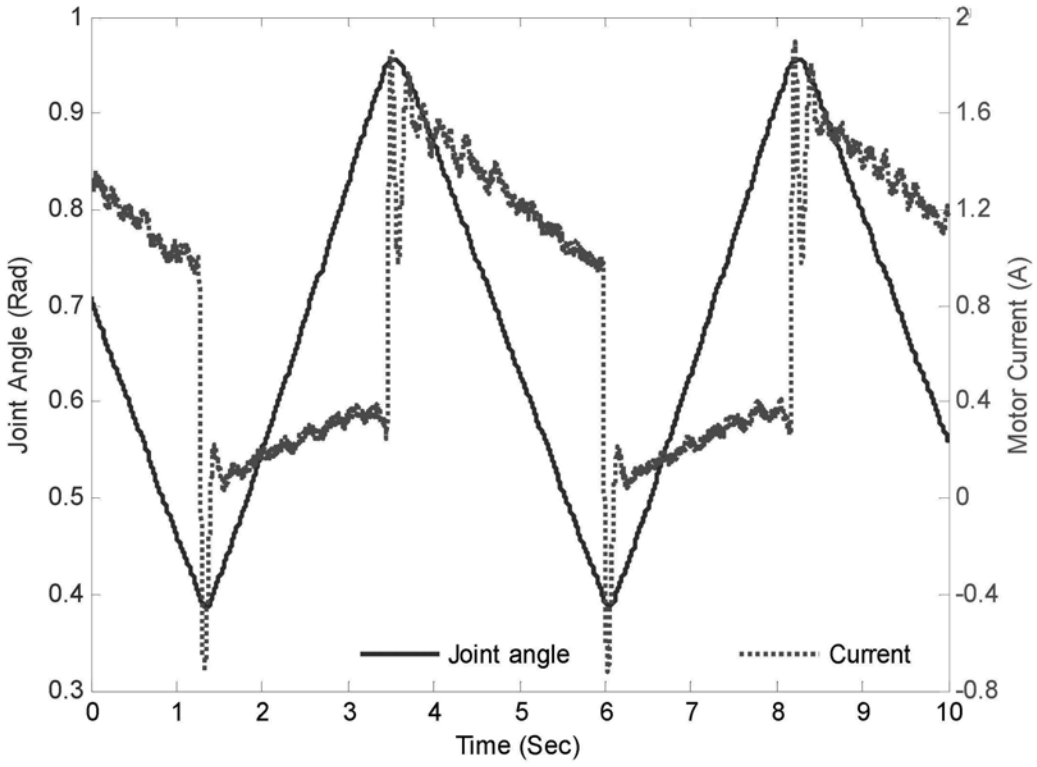

Figure 5.2-6 Motor current of knee brace without MR actuator during motion

Table 5.2-2 Energy consumption comparison between two knee braces (Unit: W)

Working condition		Bending	Extending	Total	Power saving
Extending: 0.244 Bending: 0.1	With MRA	5.052	35.598	13.93	3.06%
	Without MRA	6.209	34.243	14.36	
Extending: 0.244 Bending: 0.25	With MRA	4.566	35.952	20.45	-9.00%
	Without MRA	5.904	31.004	18.61	
Extending: 0.333 Bending: 0.1	With MRA	4.638	38.214	12.39	7.76%
	Without MRA	6.235	37.058	13.35	
Extending: 0.333 Bending: 0.25	With MRA	4.566	35.848	17.98	-6.28%
	Without MRA	6.082	31.186	16.85	

Table 5.2-3 shows the comparison between simulation results and experimental results for the case with bending speed 0.25 rad/sec and extending speed 0.244 rad/sec. In the simulation, the knee brace with MR actuator is slightly more energy efficient. But the experimental results show that the knee brace without MR actuator is slightly

more energy efficient. It is mainly caused by the difference of energy consumption of knee brace without MR actuator during bending phase (the experimental results is only 64.3% of simulation results). As analysed before, the gearbox is not backdrivable and the torque transfer efficiency is smaller than that of the forward direction. Also because of the not backdrivability, the motor should work even no torque is required for the knee brace without MR actuator. The MR actuator consumes more energy as compared to the simulation result. It is due to the oscillation of the control signal, which dissipates more energy. In fact, for the extending phase, the experimental results are very close to the simulation results.

Table 5.2-3 Energy consumption comparison between simulation and experiment (Unit: W)

Condition		Bending	Extending		Total	Power saving
			Total	MRA		
Simulation	With MRA	3.00	36.76	4.62	20.09	3.5%
	Without MRA	9.18	32.14	0	20.80	
Experiment	With MRA	4.57	35.95	4.62	20.45	-9.00%
	Without MRA	5.90	31.00	0	18.61	

For normal walking, the majority power of the knee brace is negative, as seen in figure 2.4-1. The walking pattern here can be simplified as follows:

$$\theta = \begin{cases} \frac{10*2\pi}{360}(1-\cos(\frac{20\pi t}{3})) & 0 \le t \le 0.3 \\ 0 & 0.3 < t \le 0.5 \\ \frac{35*2\pi}{360}(1-\cos(4\pi(t-0.5))) & 0.5 < t \le 1 \end{cases} \tag{5.2}$$

$$P=\begin{cases} -100\sin(\dfrac{20\pi t}{3}) & 0\le t\le 0.3 \\ 0 & 0.3<t\le 0.5 \\ -300\sin(\dfrac{20\pi}{3}(t-0.5)) & 0.5<t\le 0.65 \\ 0 & 0.65<t\le 0.85 \\ -200\sin(\dfrac{20\pi}{3}(t-0.85)) & 0.85<t\le 1 \end{cases} \tag{5.3}$$

Figure 5.2-7 shows the variation of knee joint angle and power during normal walking. The torque of the knee joint during walking can be expressed as

$$\tau=\begin{cases} 0 & \dot{\theta}=0 \\ P/\dot{\theta} & \dot{\theta}\neq 0 \end{cases} \tag{5.4}$$

Figure 5.2-8 shows the knee joint torque during normal walking.

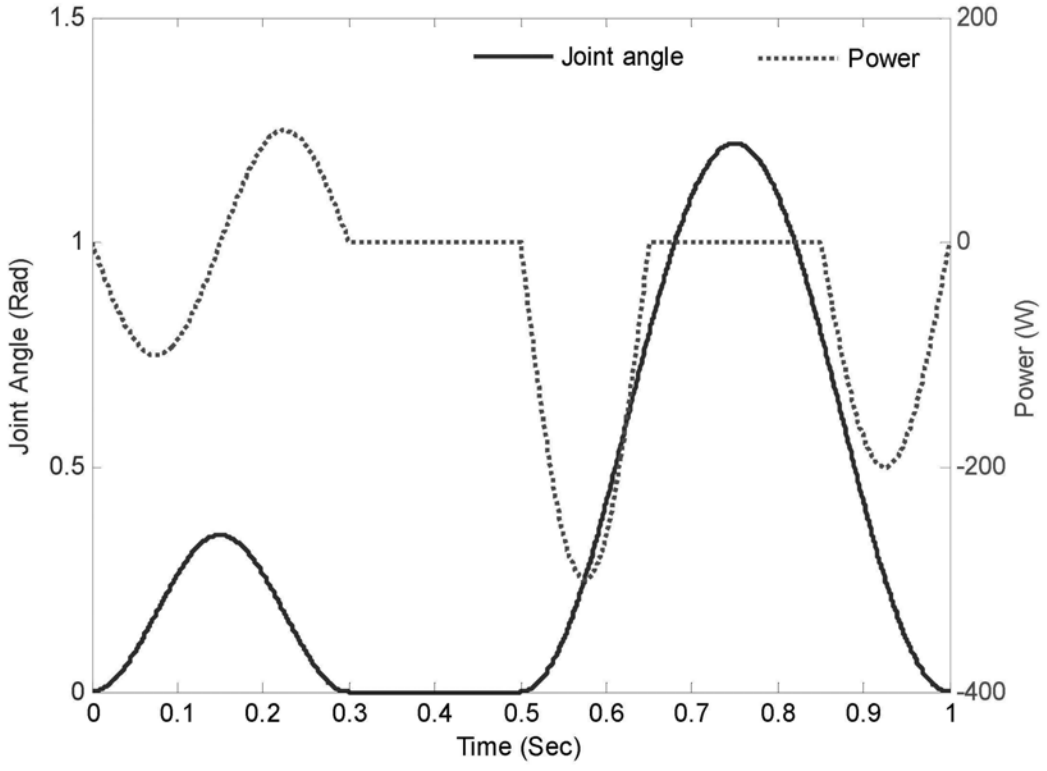

Figure 5.2-7 Knee joint angle and Knee power during normal walking

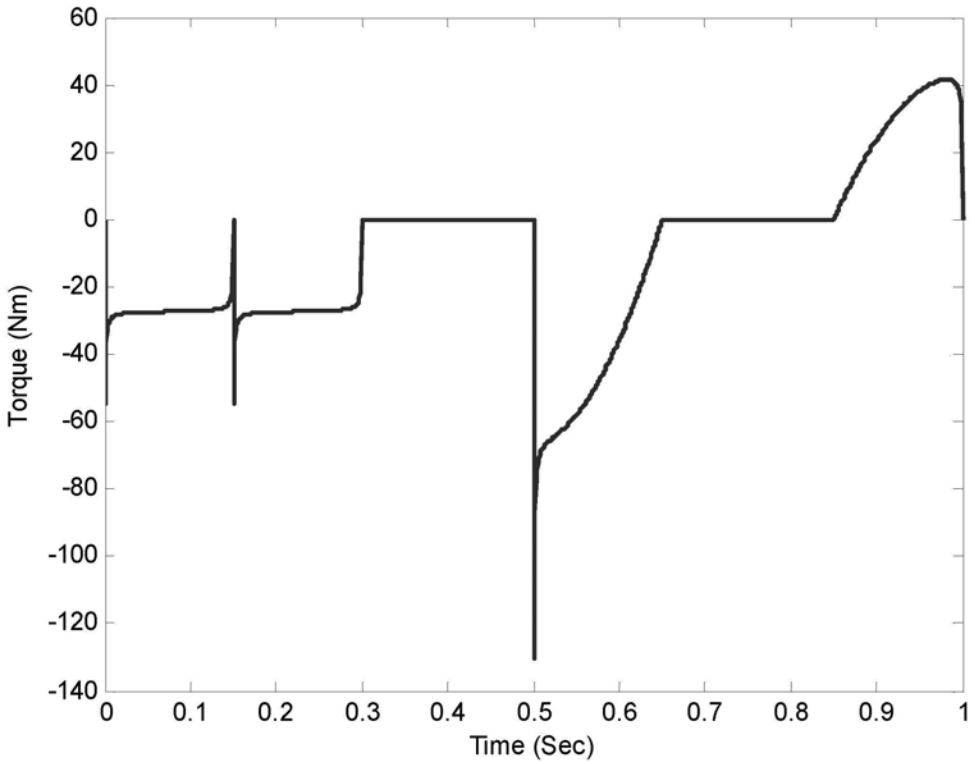

Figure 5.2-8 Torque of knee joint during normal walking

As seen in figure 5.2-7, only active power is required at the time interval 0.15~0.3 sec. At other time intervals only negative power or no power is required. Table 5.2-4 shows the working conditions of actuators for both knee braces at each time interval (Note: "off" means the actuator is turned off; "brake" means the MR actuator functions as brake; "clutch" means the MR actuator functions as clutch; "passive" means the motor works to provide passive torque; "active" means the motor works to provide active torque). It is noted that for the time interval 0.65~0.85 sec, though no power is required, but the knee brace without MR actuator should work to follow the motion of the leg due to large inertia of the motor. Figure 5.2-9 shows the experimental result of the motor current for the knee brace during free swing with speed 0.157 rad/sec. The average current of the motor current with swing speed 0.244 rad/sec, 0.333 rad/sec and 0.403 rad/sec is measured to be 0.25 A, 0.31 A and 0.41 A,

respectively. It can be seen that when the speed is fast, the motor current is large. The average swing speed is 4.2 rad/sec in figure 5.2-7 during the time interval 0.65-0.85 sec. So the current of DC motor would be larger than 0.41 A. Assume the motor current is 0.42 A, then the energy consumption during the follow state is about 10 W. While for the time interval 0.85~1 sec, both motor and MR actuator need to work since the MR actuator alone can only provide braking force during the bending process.

Table 5.2-4 Working conditions of actuators during normal walking

Time interval	Knee brace with MR actuator		Without MR actuator
	Motor	MR actuator	Motor
0-0.15 sec	off	brake	passive
0.15-0.3 sec	active	clutch	active
0.3-0.5 sec	off	off	off
0.5-0.65 sec	off	brake	passive
0.65-0.85 sec	off	off	follow
0.85-1 sec	passive	brake	passive

Assume the knee brace provide 50% of the torque during the walking and the maximum torque of the knee brace is 30 Nm. Based on the working conditions of the actuators shown in table 5.2-4, and the experimental results for bending and extending, the power consumption of the knee braces can be calculated as shown in table 5.2-5

Table 5.2-5 Power consumption during normal walking (Unit: W)

Time interval	Power with MR actuator		Power without MR actuator
	Motor	MR actuator	Motor
0-0.15 sec	0	4.8	10.57
0.15-0.3 sec	32.88	4.8	32.88
0.3-0.5 sec	0	0	0
0.5-0.65 sec	0	7.2	16.20
0.65-0.85 sec	0	0	10
0.85-1 sec	10.80	4.8	10.80
Total	9.79		12.57

From the results given in table 5.2-5, the power consumption of knee brace without MR actuator is 28.34% higher than that of knee brace with MR actuator.

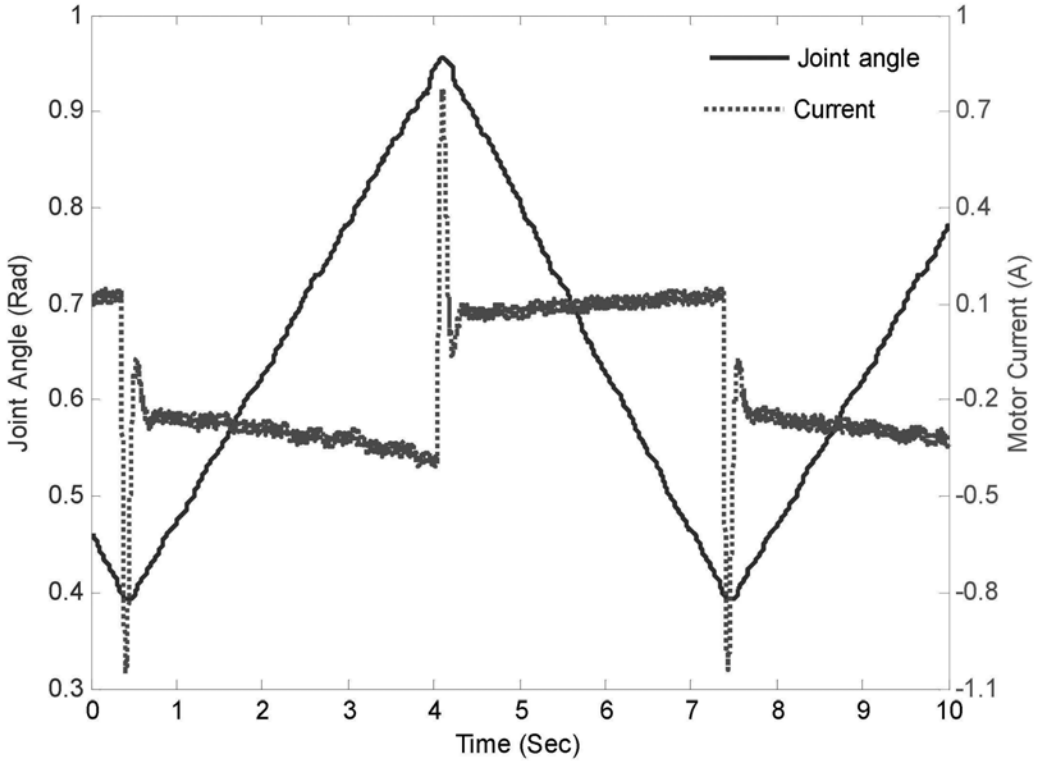

Figure 5.2-9 Motor current during free swing

5.3 Performance Comparison

For wearable assistance device, the characteristic of "low impedance" is very important. With low impedance, human body can do what he/she wants and does not have to be limited by the wearable device. The output inertia of the knee brace with DC motor is an important component of the total impedance of the device, because with gearbox, the inertia of motor is increased by the gear ratio, as shown in equation (5.5).

$$I_o = \eta^2 I_M \tag{5.5}$$

where I_o, I_M are the output inertia and motor inertia respectively, η is the gear ratio.

For the knee brace without MR actuator, the motor inertia is 0.134×10^{-4} kgm^2, the gear ratio is 468. The output inertia can be calculated as 2.9 kgm^2. It is equivalent to the inertia of lower leg with a mass of 46.4 kg bounded to the middle of the lower leg (suppose the length of the lower leg is 0.5 m). The torque caused by the inertia can be calculated as

$$\tau = I_o \alpha \tag{5.6}$$

where α is the angular acceleration.

The angular acceleration of the knee joint during normal walking can be shown in figure 5.3-1. The maximum angular acceleration is 96 rad/sec^2 (in both directions). So the maximum resistance torque caused by the inertia of motor is 278 Nm. So the knee joint can not move freely and the motor must work during knee motion, even no assistive torque is required.

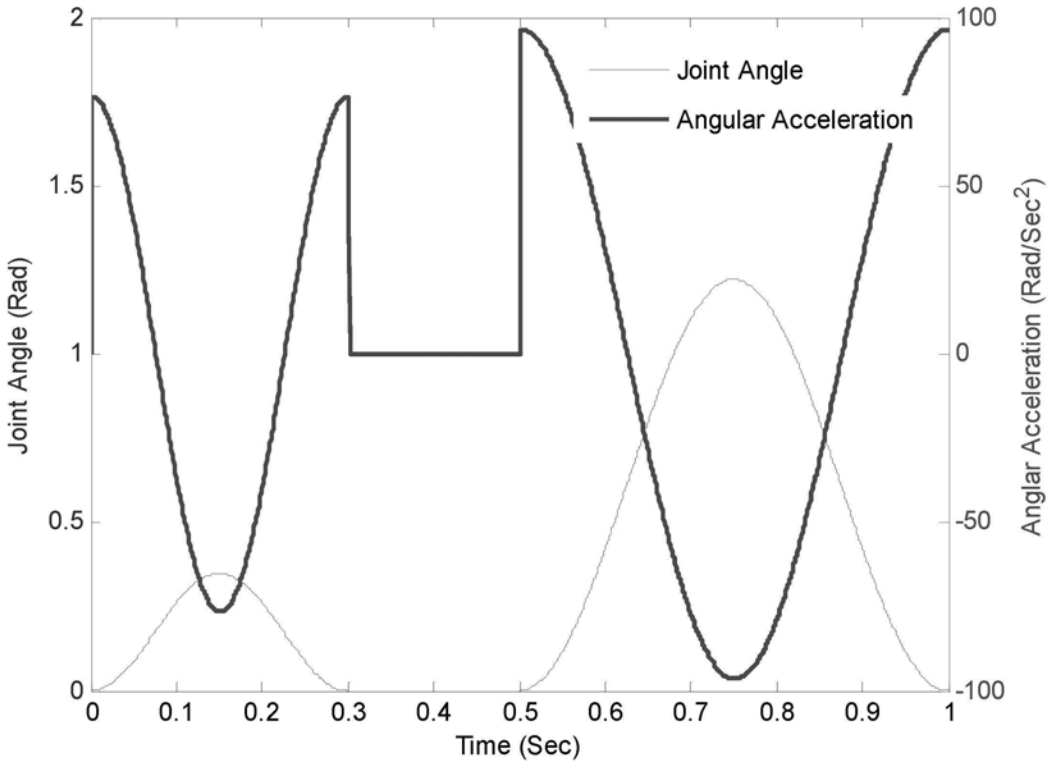

Figure 5.3-1 The angular acceleration of the knee joint during normal walking

For the knee brace with MR actuator, if the MR actuator is off, the joint can rotate freely and the inertia is mainly caused by the mass of the knee brace. The mass of the knee brace is about 1 kg and assume the mass centre is in the middle of the knee brace, the inertia of the knee brace can be calculated as about 0.06 kgm^2. If the MR actuator is on, and the yield torque of MR actuator is 29 Nm, the angular acceleration is larger than 10 kgm^2, the MR actuator is yielded and provides a constant resisting torque of 29 Nm, the inertia of the knee brace is still 0.06 Nm. If the angular acceleration is very small (smaller than 10 kgm^2), and the knee brace is in the extending direction, then the motor is forced to rotate by the knee brace, the inertia of the knee brace becomes the same as that of the knee brace without MR actuator. However, it will not limit the motion of the leg because once the angular acceleration is large or the force is large, the MR actuator is yield and the inertia is small again.

While applied to the leg, the assistive knee brace should have good force controllability. Once the knee brace produces force improperly, it may hurt human body or make the wearer to fall down. As seen in the torque tracking experimental results of MR actuator under control in Chapter Three, the MR actuator has excellent force controllability. DC motor has good position controllability but does not have good force controllability. Pratt et al. introduced elastic material in series with motor to turn the force control problem into position control issue (Pratt et al., 1995). The principle of this kind of actuator, which is called series elastic actuator (SEA), is shown in figure 5.3-2. By controlling the deformation (position) of the spring, the SEA can control the force output well. Also the elastic element can absorb shock and reduce the output inertia. However, when the frequency of force is high, the SEA can not provide assistive torque, and the lower the stiffness of the spring, the smaller the force bandwidth, as shown in figure 5.3-3. SEA does not have good force fidelity at both high force range and low force range, as shown in figure 5.3-4. For MR actuator, because the force output does not rely on the displacement, it does not have the force bandwidth problem. MR actuator has good force/torque fidelity at both high and low force/torque ranges, as shown in figure 5.3-5, which are the experimental results of the knee brace under adaptive control. The torques are measured by strain gauges.

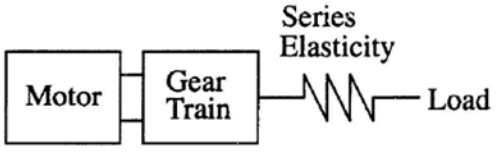

Figure 5.3-2 The principle of series elastic actuator

[Pratt et al., 1995]

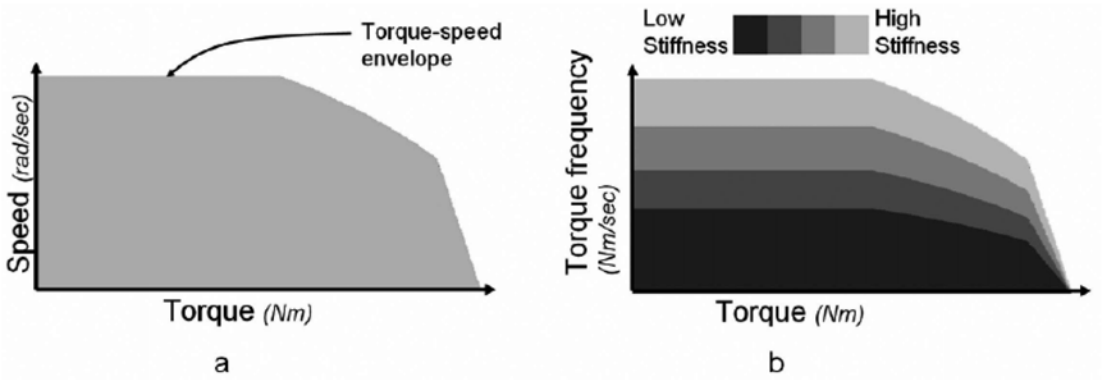

Figure 5.3-3 Force bandwidth of SEA

[Sensinger et al., 2006]

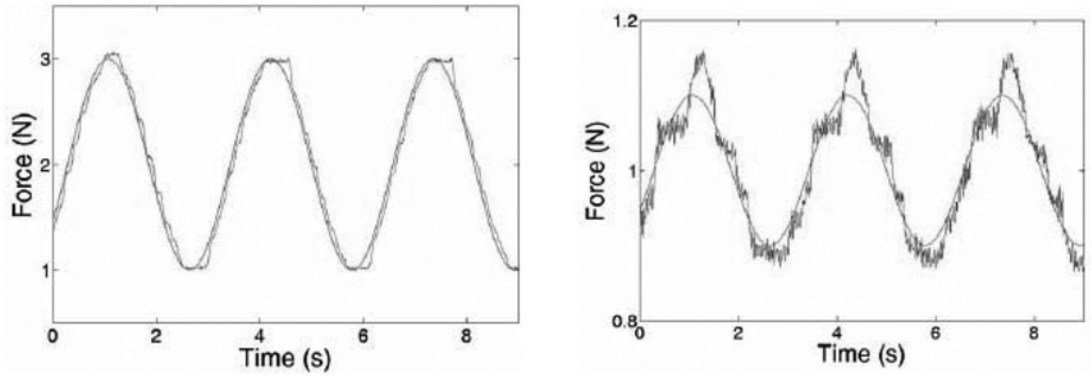

Figure 5.3-4 Force tracking at high range and low range of SEA

[Sensinger et al., 2006]

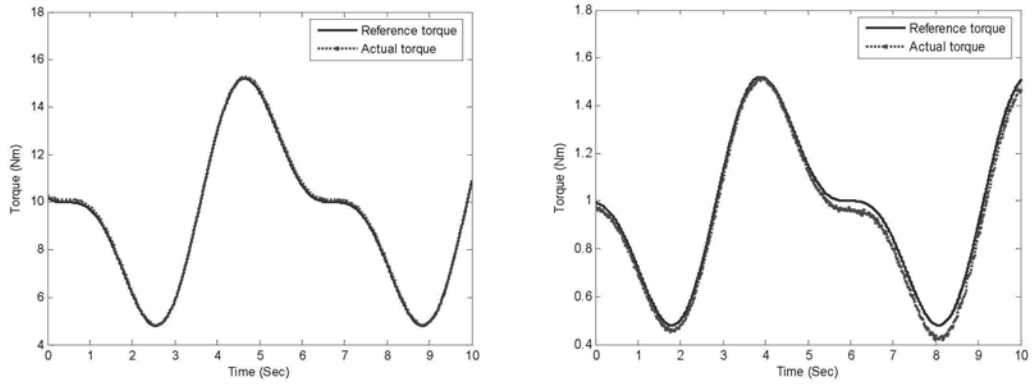

Figure 5.3-5 Torque tracking at high range and low range of MRA in knee brace

5.4 Safety Comparison

Safety is very important for devices that are directly used for human body. For the assistive knee braces, mechanical constraints are adopted to prevent the knee braces from over bended or over extended. However, if the knee brace reaches the constraint but the system does not react in time or the controller is out of control, it would still be dangerous. For comparison, experiments are carried out for the knee brace with MR actuator and without MR actuator to hit the constraints without control.

The experimental condition for the knee brace with MR actuator is: the motor rotates at a constant speed of 0.333 rad/sec, a 1.3 A current is applied to the MR actuator, when the knee brace reaches the constraint, manually turn off the current of MR actuator. Figure 5.4-1 shows the experimental results.

The experimental condition for the knee brace without MR actuator is: apply a constant speed signal to the motor to drive the knee brace rotate at speed of 0.244 rad/sec (due to the large output inertia of motor, a relative smaller speed is used here). Once the knee brace reaches the constraint, manually turn off the motor current immediately. Figure 5.4-2 shows the experimental results.

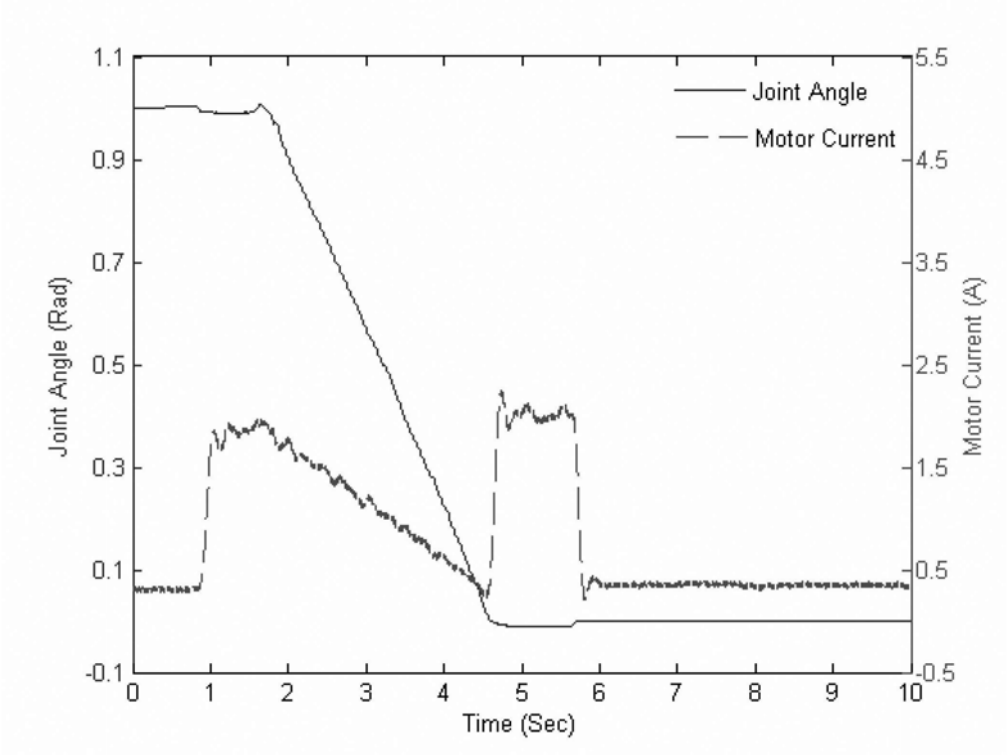

Figure 5.4-1 Safety testing for the knee brace with MR actuator

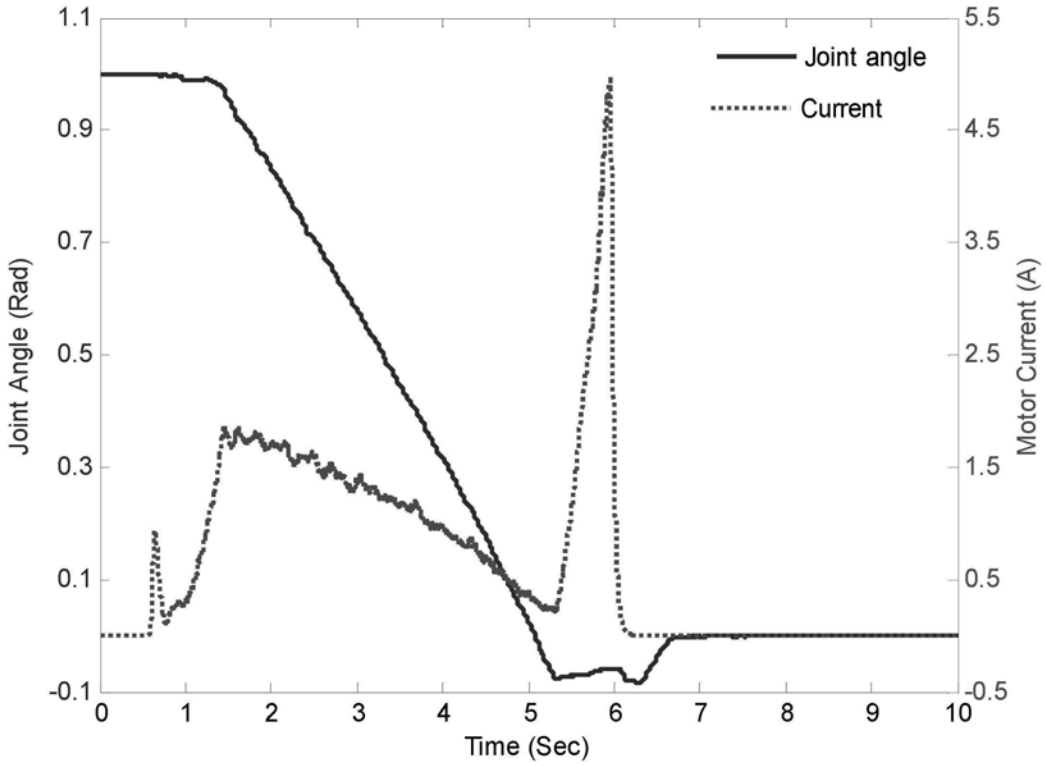

Figure 5.4-2 Safety testing for the knee brace without MR actuator

As seen from figure 5.4-1, once the MR actuator is turned on, the motor current increases immediately, shortly after that, the knee brace starts to extend, and the motor current begins to drop. Once the knee brace reaches the constraint, the knee brace can not rotate anymore, and the current of motor increases suddenly. Then the motor current is maintained at a relative high level until the MR actuator is turned off. Since the motor current is proportional to the torque of the knee brace, the variation of motor current is equivalent to the variation of the torque of the knee brace. When the knee brace reaches the constraint, the MR actuator works at yield state. The maximum torque of the knee brace is determined by the yield torque of MR actuator. So both the torque and the motor current will not become too large even the knee brace hits the constraint without control. Therefore, the knee brace with MR actuator is inherently safe.

On the other hand, observing figure 5.4-2, the knee brace without MR actuator starts to rotate shortly after the motor is turned on. Similar to that with MR actuator, the motor current drops as the joint angle becomes small. But when the knee brace reaches the constraint, the motor current increases to a very large value (about 5 A, which is the upper limit of the power source). As the torque is proportional to the motor current, the torque of the knee brace becomes very large too. And the motor is choked since the knee brace can not rotate. So the back EMF is zero and all the power is dissipated at the control electronics, which is 120 W here. The large power may burn the control electronics. And the large torque at this instant may damage the knee brace or hurt human body too. Figure 5.4-3 shows the photo of the mechanical constraint after the safety experiment. It can be seen that the surface of the knee brace is hurt. So the knee brace without MR actuator is not inherently safe.

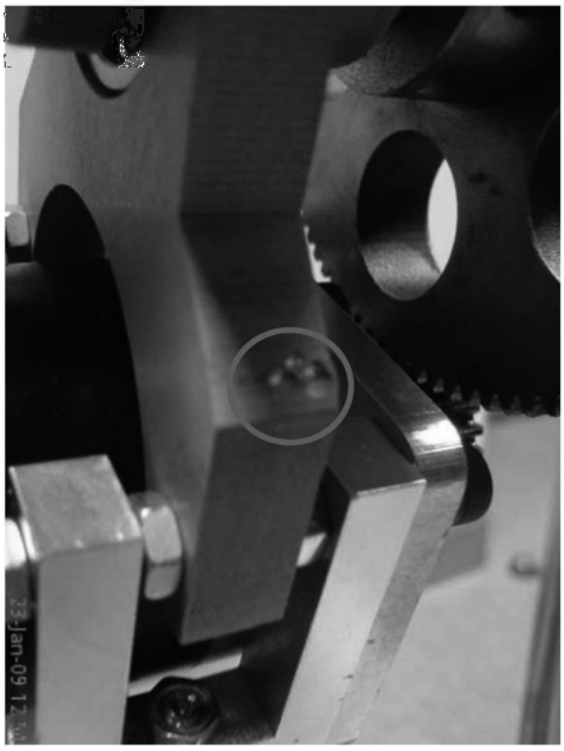

Figure 5.4-3 Photo of the knee brace without MR actuator after safety testing

If the knee brace is under control but the reaction time is not fast enough, the knee brace may also be dangerous in critical state. Figure 5.4-5 and figure 5.4-6 show both the knee braces under critical state (the knee brace has already hit the constraint but the motor still tries to drive the knee brace to extend), and the actuators are manually turned off. For the knee brace with MR actuator, the MR actuator is turned off; for the knee brace without MR actuator, the motor is turned off. Once the torque is released, the joint angle will increase slightly due to relief of stress. As seen from figure 5.4-4, the force of the knee brace is removed in milli-second when the MR actuator is turned off. But for the knee braces without MR actuator, the torque starts to relieve about 0.35 second after the motor is turned off, as shown in figure 5.4-5. This may be caused by the inertia of motor. So with MR actuator, the output of knee brace can be stopped quicker as compared with that without MR actuator.

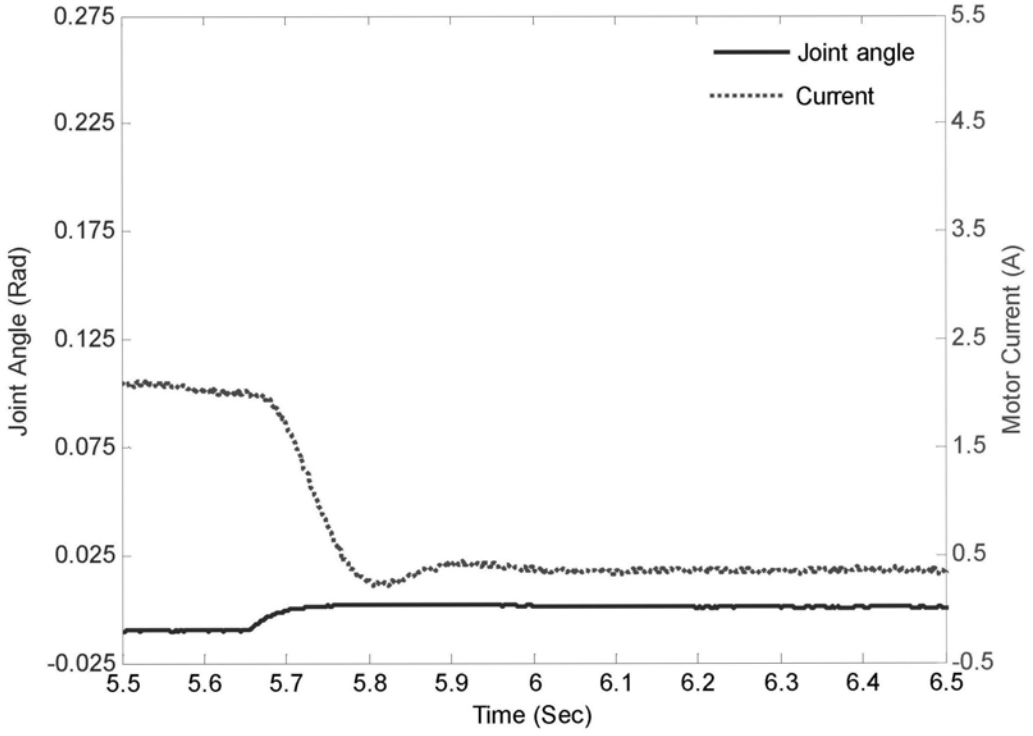

Figure 5.4-4 Torque relief of knee brace with MR actuator

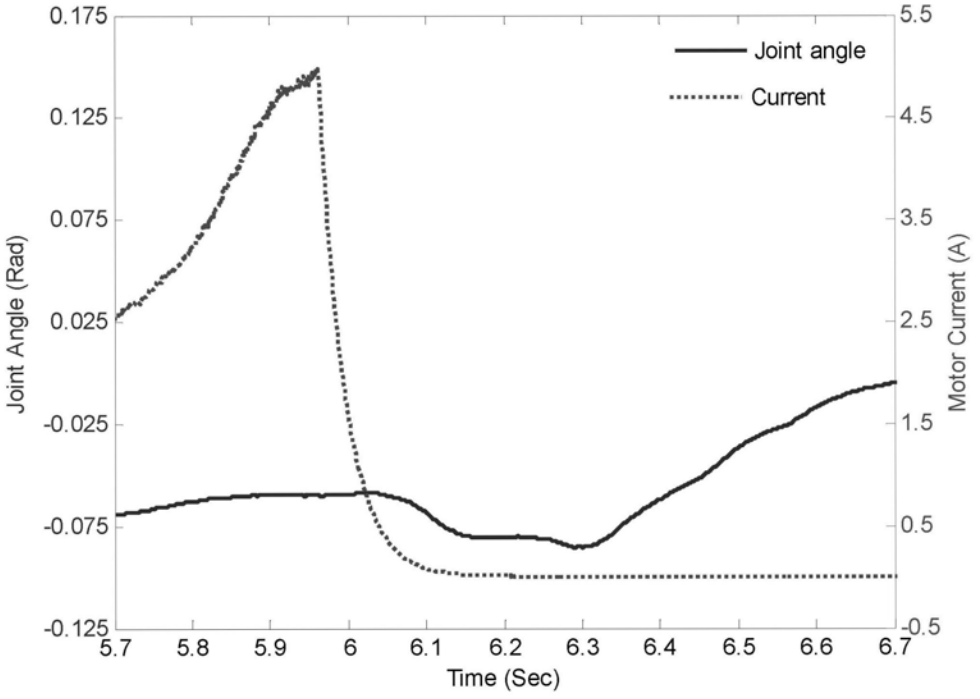

Figure 5.4-5 Torque relief of knee brace without MR actuator

5.5 Chapter Summary

The assistive knee brace with MR actuator is evaluated in three aspects in this chapter. An assistive knee brace without MR actuator is developed for comparison, where the DC motor provides both active and passive torque.

The power consumption studies show:

(1) For bending process, the knee brace without MR actuator does not consume much energy, but the knee brace with MR actuator saves more energy.

(2) For extending process, the knee brace with MR actuator consumes more power, it is due to the additional power consumption of MR actuator.

(3) For a cycle containing both bending and extending processes, the difference of mean power consumption for both knees is not significant. When the bending speed is slow and the extending speed is fast, the knee brace with MR actuator can be more energy efficient; while the bending speed is fast and the extending speed is slow, the knee brace without MR actuator may be more energy efficient.

(4) For normal walking, the knee brace with MR actuator is more energy efficient.

With MR actuator, the knee brace has much smaller inertia and better force controllability. Safety study shows that the knee brace with MR actuator is inherently safe: it produces neither too large force nor too large current even in extreme conditions. In case of emergency, the output of the knee brace with MR actuator can be stopped quickly.

CHAPTER SIX

CONCLUSION AND FUTURE WORK

6.1 Conclusion

In this research, the MR actuator for assistive knee braces is studied. The MR actuator that can function as a brake or a clutch is designed and fabricated. The assistive knee brace with both MR actuator and DC motor is developed and tested. The assistive knee brace with MR actuator is evaluated as compared to that without MR actuator.

The contributions of this thesis include:

1. Principle and detailed design of an MR actuator that has the functions of controllable brake and clutch are given;
2. Characteristics and torque tracking ability of the developed MR actuator under different controls are studied;
3. The assistive knee brace that uses both MR actuator and DC motor, together with force/position sensors is developed;
4. The assistive knee brace evaluation apparatus is developed and the corresponding motion analysis is performed;
5. Performances of the assistive knee brace under control are studied;
6. The assistive knee brace with MR actuator is evaluated in terms of power consumption, performance and safety as compared to the knee brace without MR actuator.

Experimental results show that the developed MR actuator can produce enough assistive torque, and the power consumption is low as compared to DC motor. On the

other hand, the response time is also acceptable for application to human body. With adaptive control, the MR actuator has good torque tracking ability, and the torque output can adapt to the environment and parameter variations. It is promising that the MR actuator could be used in the assistive knee brace where torque controllability and power consumption are important.

The assistive knee brace that uses both MR actuator and DC motor is developed. Strain gauges and potentiometer are used to measure the force and position information. A testing apparatus that mimic the motion of human body is designed for testing and evaluating the assistive knee brace. Simulation results show that when the motion of the knee brace is slow, the dynamic force can be neglected. IP-based state control and adaptive control are proposed for the motion control of the knee brace in the testing apparatus. Experimental results show that the knee brace can work well as proposed: when passive torque is required, only the MR actuator works to provide controllable torque; while active torque is needed, both the MR actuator and DC motor work so that the torque produced by motor is transferred to the knee brace through the MR actuator. The assistive knee brace is capable of providing a torque of about 30 Nm in both extending and bending phases.

Evaluation of the knee brace with MR actuator shows that the MR actuator is beneficial to assistive knee brace as compared to that without MR actuator. Study on power consumption shows that the knee brace with MR actuator consumes 28.34 % less power during normal walking cycle as compared to that without MR actuator. In addition, the knee brace with MR actuator has better force controllability and low inertia as compared to that without MR actuator. This makes the knee brace with MR

actuator promising where good torque controllability and lower impedance are desired for assistive knee braces. Moreover, the knee brace with MR actuator is inherently safe and the force/torque output can be stopped quickly in case of emergency. It makes the knee brace with MR actuator more suitable to patients with weakened muscle strength.

6.2 Future Work

Till now the knee brace still has not yet been applied to human body. Since the ultimate goal is to provide assistance force/torque for human leg, the next step is to test the knee brace in human leg. In this research, the knee brace is not applied to human body and the trajectory of the motion is specified. While applied to human leg, the knee brace should provide proper assistance torque as human body required. So how to detect the motion intention of human body in time and how to provide proper assistance torque quickly and efficiently will be the future research issues.

The total mass of current knee brace is larger than 3 kg, which is too heavy for practical application. The weight should be reduced. This goal can be achieved by using some other materials such as carbon materials, Ti-alloy, Fe-Co alloy, etc. The response time of the MR actuator can be further improved by reducing the eddy current of the MR actuator [Takesue et al., 2003].

The MR actuator can function as clutch or brake, this shifting function is achieved by a pair of one-way bearings. But the current knee brace can only provide active torque in the extending phase. It would be better if other shifting mechanism can be implemented without the limitations.

BIBLIOGRAPHY

Ahmadkhanlou F., Zite J. and Washington G., "A Magnetorheological Fluid-based Controllable Active Knee Brace," *Proceedings of SPIE on Industrial and Commercial Applications of Smart Structures Technologies*, Vol. 6527, pp. 65270O-1 – 65270O-10, 2007

An J. and Kwon D. S., "Five-bar Linkage Haptic Device with DC Motors and MR Brakes," *Journal of Intelligent Material Systems and Structures*, Vol. 20, pp. 97-107, 2009

Andrews A. W. and Bohannon R. W., "Short-term Recovery of Limb Muscle Strength After Acute Stroke," *Archives of Physical Medicine and Rehabilitation*, Vol. 84 (1), pp. 125-130, 2003

Bay L., West K., Sommer-Larsen P., Skaarup S. and Benslimane M., "A Conducting Polymer Artificial Muscle with 12% Linear Strain," *Advanced Materials*, Vol. 15 (4), pp. 310-313, 2003

Bhat N. and Kim W. J., "Precision Force and Position Control of an Ionic Polymer Metal Composite," *Proceedings of the Institution of Mechanical Engineers, Part I: Journal of Systems and Control Engineering*, Vol. 218 (6), pp. 421-432, 2004

Carlson J. D. and Chrzan M. J., "Magnetorheological Fluid Dampers," *U.S. Patent*, No. 5277281, 1994

Carlson J. D., "Portable Controllable Fluid Rehabilitation Devices," *U.S. Patent*, No. 5711746, 1998

Carlson J. D., and Jolly M. R., "MR Fluid, Foam and Elastomer Devices," *Mechatronics*, Vol. 10 (4-5), pp. 555-569, 2000

Carlson J. D., Matthis W. and Toscano J. R., "Smart Prosthetics Based on Magnetorheological Fluids," *Proceedings of SPIE on Smart Structures and Materials*, Vol. 4332, pp. 308-316, 2001

Choi H. J., Cho M. S., Kim J. W., Kim C. A. and Jhon M. S., "A Yield Stress Scaling Function for Electroheological Fluids," *Applied Physics Letters*, Vol. 78 (24), pp. 3806-3808, 2001

Damiano D. L., Martellotta T. L., Sullivan D. J., Granata K. P. and Abel M. F., "Muscle Force Production and Functional Performance in Spastic Cerebral Palsy: Relationship of Cocontraction," *Archives of Physical Medicine and Rehabilitation*, Vol. 81 (7), pp. 895-900, 2000

Deffenbaugh B., Herr H., Pratt G. and Wittig M., "Electronically Controlled Prosthetic Knee," *U. S. Patent*, No.6764520, 2004

Dodd K. J., Taylor N. F. and Damiano D. L., "A Systematic Review of the Effectiveness of Strength-training Programs for People with Cerebral Palsy," *Archives*

of Physical Medicine and Rehabilitation, Vol. 83 (8), pp. 1157-1164, 2002

Dong S. F., Lu K. Q., Sun J. Q. and Rudolph K., "A Prototype Rehabilitation Device with Variable Resistance and Joint Motion Control," *Medical Engineering & Physics*, Vol. 28 (4), pp. 348-355, 2006

Dong S. F., Lu K. Q., Sun J. Q. and Rudolph K., "Adaptive Force Regulation of Muscle Strengthening Rehabilitation Device with Magnetorheological fluids," *IEEE Transactions on Neural Systems and Rehabilitation Engineering*, Vol. 14 (1), pp. 55-63, 2006

Ferris D. P. Czerniecki J. M. and Hannaford B., "An Ankle-foot Orthosis Powered by Artificial Pneumatic Muscles," *Journal of Applied Biomechanics*, Vol. 21, pp. 189-197, 2005

Fisher N. M., Gresham G. E., Abrams M., Hicks J., Horrigan D. and Pendergast D. R., "Quantitative Effects of Physical Therapy on Muscular and Functional Performance in Subjects with Osteoarthritis of the Knees," *Archives of Physical Medicine and Rehabilitation*, Vol. 74, pp. 840-847, 1993

Halsey T. C., "Electrorheological Fluids," *Science*, Vol. 258 (5083), pp. 761-766, 1992

Herr H. and Wilkenfeld A., "User-adaptive Control of a Magnetorheological Prosthetic Knee," *Industrial Robot,* Vol. 30 (1), pp. 42-55, 2003

Herr H. and Kornbluh R., "New Horizons for Orthotic and Prosthetic Technology: Artificial Muscle for Ambulation," *Proceedings of SPIE on Smart Structures and Materials,* Vol. 5385 (1), pp. 1-9, 2004

Hiamtup P., Sirivat A. and Jamieson A. M., "Electrorheological Properties of Polyaniline Suspensions: Field-induced Liquid to Solid Transition and Residual Gel Structure," *Journal of Colloid and Interface Science*, Vol. 295 (1), pp. 270-278, 2006

Inoue K., "Rubbertuators and Applications for Robots," *The 4th International Symposium on Robotics Research*, pp. 57-63, 1988

Ivlev A. V., Morfill G. E., Thomas H. M., Rath C., Joyce G., Huber P., Kompaneets R., Fortov V. E., Lipaev A. M., Molotkov V. I., Reiter T., Turin M. and Vinogradov P., "First Observation of Electroheological Plasmas," *Physical Review Letters*, Vol. 100 (9), pp.095003 (4), 2008

Johnson D. C., Repperger D. W. and Thompson G., "Development of a Mobility Assist for the Paralyzed, Amputee and Spastic Person," *Proc. of the 1996 fifteenth Southern Biomedical Engineering* pp. 67-70 1996

Johnson M. J., Van der Loos H. F. M., Burgar C. G. Shor P. and Leifer L. J., "Experimental Results Using Force-feedback Cueing in Robot-assisted Stroke Therapy," *IEEE Transactions on Neural Systems and Rehabilitation Engineering* Vol.13 (3), 2005

Jung K., Nam J., Lee Y. and Choi H., "Micro Inchworm Robot Actuated by Artificial Muscle Actuator Based on Nonprestrained Dielectric Elastomer," *Proceedings of SPIE on Smart Structures and Materials,* Vol.5385 (357), 2004

Kavlicoglu B., Gordaninejad F., Evrensel C., Fuchs A. and Korol G., "A Semi-Active, High-Torque, Magnetorheological Fluid Limited Slip Differential Clutch," *Journal of Vibration and Acoustics,* Vol. 128 (5), pp. 604-610, 2006

Kawamoto H. and Sankai Y., "Comfortable Power Assist Control Method for Walking Aid by HAL-3," *IEEE International Conference on Systems, Man and Cybernetics,* Vol. 4, pp. 6, 2002

Kawamoto H., Lee S., Kanbe S. and Sankai Y., "Power Assist Method for HAL-3 Using EMG-based Feedback Controller," *IEEE International Conference on Systems, Man and Cybernetics,* Vol. 2, pp. 1648-1653, 2003

Kordonski W. I. and Golini D., "Fundamentals of Magnetorheological Fluid Utilization in High Precision Finishing," *Journal of Intelligent Material Systems and Structures,* Vol. 10 (9), pp. 683-689, 1999

Kornbluh R., Pelrine R., Eckerle J. and Joseph J., "Electrostrictive Polymer Artificial Muscle Actuators," *Proceedings of the IEEE Conference on Robotics & Automation,* Vol. 3, pp. 2147-2154, 1998

Kyoungchul K., Joonbum B. and Tomizuka M., "Control of Rotary Series Elastic Actuator for Ideal Force-mode Actuation in Human-robot Interaction Applications," *IEEE/ASME Transactions on Mechatronics,* Vol. 14 (1), pp. 105-118, 2009

Lau Y. K. and Liao W. H., "Design and Analysis of a Magnetorheological Damper for Train Suspension," *Proceedings of the Institution of Mechanical Engineers, Part F: Journal of Rail and Rapid Transit,* Vol. 219 (4), pp. 261-276, 2005

Lauria M., Legault M. A., Lavoie M. A. and Michaud F., "Differential Elastic Actuator for Robotic Interaction Tasks," *IEEE International Conference on Robotics and Automation,* pp. 3606-3611, 2008

Lee M. J., Jung S. H., Lee S., Mun M. S. and Moon I., "Control of IPMC-based Artificial Muscle for Myoelectric Hand Prosthesis," *IEEE International Conference on Biomedical Robotics and Biomechatronics,* pp. 1172-1177, 2006

Lee S. and Sankai Y., "Power Assist Control for Leg with HAL-3 Based on Virtual Torque and Impedance Adjustment," *IEEE International Conference on Systems, Man and Cybernetics,* Vol. 4, pp. 6, 2002

Lee S. and Sankai Y., "The Natural Frequency-based Power Assist Control for Lower Body with HAL-3," *IEEE International Conference on Systems, Man and Cybernetics,* Vol. 2, pp. 1642-1647, 2003

Li C.Q., Tokuda M., Furusho J., Koyanagi K., and Hashimoto Y., "Research and

Development of the Intelligently-controlled Prosthetic Ankle Joint," *IEEE International Conference on Mechatronics and Automation,* pp. 1114-1119, 2006

Liao W. H. and Wang D. H., "Semiactive Vibration Control of Train Suspension Systems via Magnetorheological Dampers," *Journal of Intelligent Material Systems and Structures*, Vol. 14 (3), pp. 161-172, 2003

Madden J. D. W., Vandesteeg N. A., Anquetil P. A., Madden P. G. A., Takshi A., Pytel R. Z., Lafontaine S. R., Wieringa P. A. and Hunter I. W., "Artificial Muscle Technology: Physical Principles and Naval Prospects," *IEEE Journal of Oceanic Engineering*, Vol. 29 (3), pp. 706-728, 2004

Neder J. A., Nery L. E., Shinzato G. T., Andrade M. S., Peres C. and Silva A. C., "Reference Values for Concentric Knee Isokinetic Strength and Power in Nonathletic Men and Women from 20 to 80 Years Old," *Journal of Orthopaedic & Sports Physical Therapy*, Vol. 29 (2), pp. 116-126, 1999

Nikitczuk J., Weinberg B. and Mavroidis C., "Rehabilitative Knee Orthosis Driven by Electro-Rheological Fluid based Actuators," *Proceedings of IEEE International Conference on Robotics and Automation*, pp. 2283-2289, 2005

Nikitczuk J., Das A., Vyas H., Weinberg B. and Mavroidis C., "Adaptive Torque Control of Electro-Rheological Fluid Brakes Used in Active Knee Rehabilitation Devices," *Proceedings of IEEE International Conference on Robotics and Automation*, pp. 393-399, 2006

Oh H. U., "Characteristics of a Magnetorheological Fluid Isolator Obtained by Permanent Magnet Arrangements," *Smart Materials and Structures*, Vol. 13, pp. 29-35, 2004

Otero T. F. and Sansinena J. M., "Artificial Muscles Based on Conducting Polymers," *Bioelectrochemistry and Bioenergetics*, Vol. 38 (2), pp. 411-414, 1995

Paluska S. A. and Mckeag D. B., "Knee Braces: Current Evidence and Clinical Recommendations for Their Use," *American Family Physician*, Vol. 61 (2), pp. 411-418, 2000

Parthasarathy M. and Klingenberg D. J., "Electrorheology: Mechanisms and Models," *Materials Science and Engineering*, Vol. 17 (2), pp. 57-103, 1996

Pelrine R., Kornbluh R., Pei Q., Stanford S., Oh S., Eckerle J., Full R., Rosenthal M. and Meijer K., "Dielectric Elastomer Artificial Muscle Actuators: Toward Biomimetic Motion," *Proceedings of SPIE on Smart Structures and Materials*, Vol. 4695, pp. 126-137, 2002

Piercarlo S. P., Marco A. C., Raffaele S., Roberto C., Fabio P., Augusto Z., Fabiola A. and Bianca C., "Osteoarthritis: An Overview of the Disease and its Treatment Strategies," *Seminars in Arthritis and Rheumatism*, Vol. 35 (1, supplement 1), pp. 1-10, 2005

Pratt G. A. and Williamson M. M., "Series Elastic Actuators," *Proc. of the IEEE International Conference on Intelligent Robots and Systems*, Vol. 1, pp. 399-406, 1995

Pratt G. A., Willisson P., Bolton C. and Hofman A., "Late Motor Processing in Low-impedance Robots: Impedance Control of Series-elastic Actuators," *Proc. of the American Control Conference*, Vol. 4, pp. 3245-3251, 2004

Pratt J. E., Krupp B. T., Morse C. J. and Collins S. H., "The RoboKnee: An Exoskeleton for Enhancing Strength and Endurance During Walking," *Proc. of the IEEE International Conference on Robotics & Automation*, pp. 2430-2435, 2004

Reed M. R. and Book W. J., "Modeling and Control of an Improved Dissipative Passive Haptic Display," *Proceedings of the IEEE International Conference on Robotics & Automation*, Vol. 1, pp. 311-318, 2004

Robison D. W., Pratt J. E., Paluska D. J. and Pratt G. A., "Series Elastic Actuator Development for a Biomimetic Walking Robot," *Proceedings of the IEEE International Conference on Advanced Intelligent Mechatronics*, pp. 561-568, 1999

Sensinger J.W. and Weir R. F., "Design and Analysis of a Non-backdrivable Series Elastic Actuator," *Proceedings of the IEEE International Conference on Rehabilitation Robotics*, pp. 390-393, 2005

Sensinger J.W. and Weir R. F., "Improvements to Series Elastic Actuators,"

Proceedings of the IEEE International Conference on Mechatronic and Embedded Systems and Applications, pp. 1-7, 2006

Shimada K., Akagami Y., Kamiyama S., Fujita Y., Miyazaki T. and Shibayama A., "New Microscopic Polishing with Magnetic Compound Fluid (MCF)," *Journal of Intelligent Material Systems and Structures*, Vol. 13, pp. 9-15, 2002

Shtarkman E. M., "Fluid Responsive to a Magnetic Field," *U.S. Patent*, No. 4992190, 1991

Shtarkman E. M., "Fluid Responsive to a Magnetic Field," *U.S. Patent*, No. 5167850, 1992

Swanson D. K. and Book W. J., "Path-following Control for Dissipative Passive Haptic Displays," *International Symposium on Haptic Interfaces for Virtual Environment and Teleoperator Systems*, pp. 101-108, 2003

Takesue N., Furusho J. and Sakaguchi M., "Improvement of Response Properties of MR-fluid Actuator by Torque Feedback Control," *Proceedings of IEEE International Conference on Robotics & Automation*, pp. 3825-3830, 2001

Takesue N., Furusho J. and Kiyota Y., "Analytic and Experimental Study on Fast Response MR-fluid Actuator," *Proceedings of IEEE International Conference on Robotics & Automation*, pp. 202-207, 2003

Teixeira-Salmela L. F., Olney S. J., Nadeau S. and Brouwer B., "Muscle Strengthening and Physical Conditioning to Reduce Impairment and Disability in Chronic Stroke Survivors," *Archives of Physical Medicine and Rehabilitation*, Vol. 80, pp. 1211-1218, 1999

Tondu B. and Lopez P., "Modeling and Control of McKibben Artificial Muscle Robot Actuators," *IEEE Control System Magazine*, Vol. 20 (2), pp. 15-38, 2000

Vallery H., Ekkelenkamp R. Van der Kooij H. and Buss M., "Passive and Accurate Torque Control of Series Elastic Actuators," *IEEE International Conference on Intelligent Robots and Systems*, pp. 3534-3538, 2007

Weinberg B., Nikitczuk J., Patel S., Patritti B., Mavroidis C., Bonato P. and Canavan P., "Design, Control and Human Testing of an Active Knee Rehabilitation Orthotic Device," *Proceedings of IEEE International Conference on Robotics and Automation*, pp. 4126-4133, 2007

Weiss K. D., Carlson J. D. and Nixon D. A., "Viscoelastic Properties of Magneto- and Electro-Rheological Fluids," *Journal of Intelligent Material Systems and Structures*, Vol. 5 (11), pp. 772-775, 1994

Wen W. J., Huang X. X., Yang S. H., Lu K. Q. and Sheng P., "The Giant Electrorheological Effect in Suspensions of Nanoparticles," *Nature Materials*, Vol. 2, pp. 727-730, 2003

Winslow W. M., "Induced Fibration of Suspensions," *Journal of Applied Physics*, Vol. 20 (12), pp.1137-1140, 1949

Wyeth G., "Demonstrating the Safety and Performance of a Velocity Sourced Series Elastic Actuator," *IEEE International Conference on Robotics and Automation*, pp. 3642-3647, 2008

Yoo J. H. and Wereley N. M., "Design of a High-efficiency Magnetorheological Valve," *Journal of Intelligent Material Systems and Structures*, Vol. 13, pp. 679-685, 2002

Yoo J. H. and Wereley N. M., "Performance of a Magnetorheological Hydraulic Power Actuation System," *Journal of Intelligent Material Systems and Structures*, Vol. 15, pp. 847-658, 2004

Zite J., Ahmadkhanlou F., Neelakantan V. and Washington G., "A Magnetorheological Fluid Based Orthopedic Active Knee Brace," *Proceedings of SPIE on Smart Structures and Materials*, Vol. 6171, pp. 148-156, 2006

APPENDIX

A. MR Fluid Datasheet

LORD TECHNICAL DATA

MRF-132DG Magneto-Rheological Fluid

Description

LORD MRF-132DG fluid is a hydrocarbon-based magneto-rheological (MR) fluid formulated for general use in controllable, energy-dissipating applications such as shocks, dampers and brakes.

MRF-132DG fluid is a suspension of micron-sized, magnetizable particles in a carrier fluid. When exposed to a magnetic field, the rheology of MRF-132DG fluid reversibly and instantaneously changes from a free-flowing liquid to a semi-solid with controllable yield strength. Altering the strength of the applied magnetic field precisely and proportionally controls the consistency or yield strength of the fluid.

MRF-132DG fluid can be used in *valve mode* (fluid flowing through an orifice) or in *shear mode* (fluid shearing between two surfaces). In the absence of a magnetic field, MRF-132DG fluid flows freely or allows free movement. Upon application of a magnetic field, the fluid's particles align with the direction of the field in chain-like fashion, thereby restricting the fluid's movement within the gap in proportion to the strength of the magnetic field.

Features and Benefits

Fast Response Time – responds instantly and reversibly to changes in a magnetic field.

Dynamic Yield Strength – provides high yield strength in the presence of a magnetic field and very low yield strength in the absence of a magnetic field; allows for a wide range of controllability.

Temperature Resistant – performs consistently throughout a broad temperature range, meeting the requirements of demanding applications such as automotive shock absorbers.

Hard Settling Resistant – provides high resistance to hard settling; easily redispersed.

Non-Abrasive – formulated to not abrade the devices in which the MR fluid is used.

Application

For more information on MR technology, refer to the MR Design Guides located on www.lord.com/mr.

Mixing – Under common flow conditions, no separation is observed between particles and the carrier fluid. However, a degree of separation may eventually occur under static conditions. If needed, use a paint shaker to redisperse the particles into a homogeneous state prior to use.

Storage

Keep container tightly closed when not in use.

Typical Properties*

Appearance	Dark Gray Liquid
Viscosity, Pa-s @ 40°C (104°F) Calculated as slope 800-1200 sec^{-1}	0.092 ± 0.015
Density	
g/cm^3	2.98-3.18
(lb/gal)	(24.7-26.5)
Solids Content by Weight, %	80.98
Flash Point, °C (°F)	>150 (>302)
Operating Temperature, °C (°F)	-40 to +130 (-40 to +266)

*Data is typical and not to be used for specification purposes.

LORD
AskUsHow™

Cautionary Information

Before using this or any LORD product, refer to the Material Safety Data Sheet (MSDS) and label for safe use and handling instructions.

For industrial/commercial use only. Not to be used in household applications. Not for consumer use.

Shear Stress as a function of Shear Rate with no Magentic Field applied at 40°C (104°F)

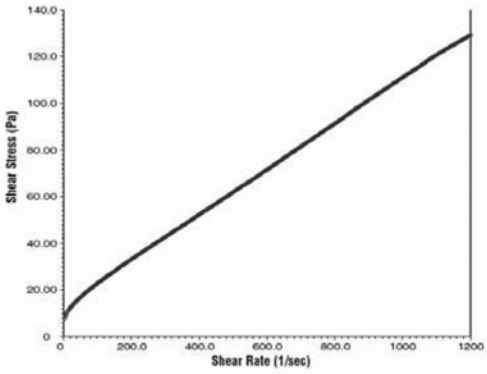

Yield Stress vs. Magnetic Field Strength

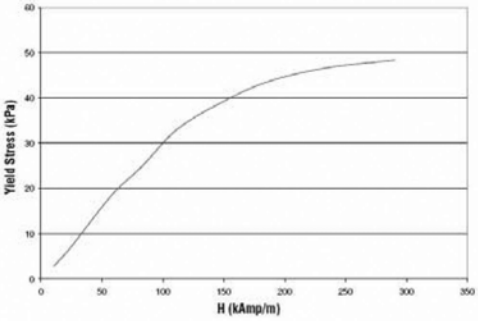

Typical Magnetic Properties

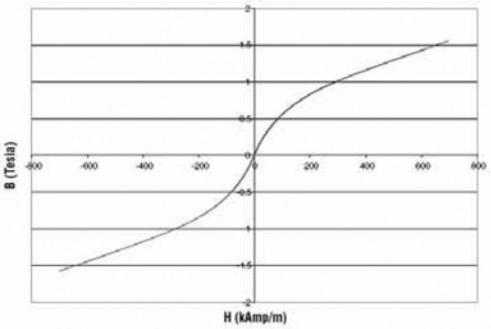

Values stated in this technical data sheet represent typical values as not all tests are run on each lot of material produced. For formalized product specifications for specific product end uses, contact the Customer Support Center.

Information provided herein is based upon tests believed to be reliable. In as much as LORD Corporation has no control over the manner in which others may use this information, it does not guarantee the results to be obtained. In addition, LORD Corporation does not guarantee the performance of the product or the results obtained from the use of the product or this information where the product has been repackaged by any third party, including but not limited to any product end-user. Nor does the company make any express or implied warranty of merchantability or fitness for a particular purpose concerning the effects or results of such use.

"Ask Us How" is a trademark of LORD Corporation or one of its subsidiaries.

LORD provides valuable expertise in adhesives and coatings, vibration and motion control, and magnetically responsive technologies. Our people work in collaboration with our customers to help them increase the value of their products. Innovative and responsive in an ever-changing marketplace, we are focused on providing solutions for our customers worldwide . . . Ask Us How.

LORD Corporation
World Headquarters
111 Lord Drive
Cary, NC 27511-7923
USA

Customer Support Center (in United States & Canada)
+1 877 ASK LORD (275 5673)

www.lord.com

LORD Ask Us How™

[http://www.lord.com]

B. DC Motor Datasheet

maxon DC motor

RE 40 ∅40 mm, Graphite Brushes, 150 Watt

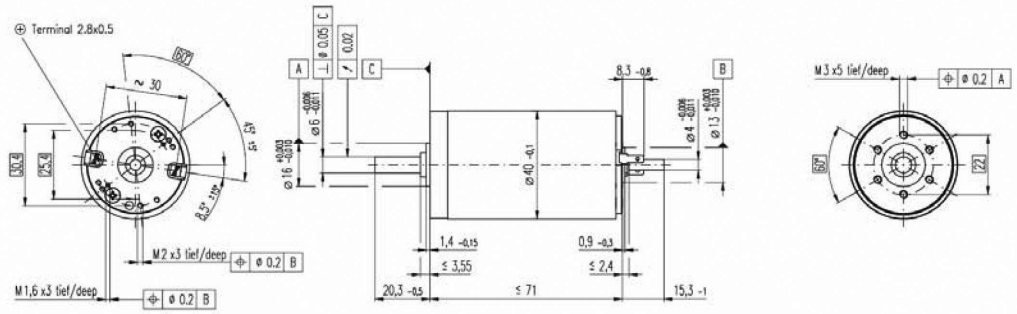

M 1:2

Stock program
Standard program
Special program (on request)

Order Number	148866	148867	148877	218008	218009	218010	218011	218012	218013	218014	218015
Motor Data											
Values at nominal voltage											
1 Nominal voltage V	12.0	24.0	48.0	48.0	48.0	48.0	48.0	48.0	48.0	48.0	48.0
2 No load speed rpm	6920	7580	7580	6420	5560	3330	2690	2130	1710	1420	987
3 No load current mA	241	137	68.6	53.7	43.7	21.9	16.7	12.5	9.67	7.77	5.16
4 Nominal speed rpm	6370	6930	7000	5810	4920	2700	2050	1500	1080	774	339
5 Nominal torque (max. continuous torque) mNm	94.9	170	184	183	177	187	187	189	189	188	188
6 Nominal current (max. continuous current) A	6.00	5.77	3.12	2.62	2.20	1.38	1.12	0.898	0.721	0.593	0.413
7 Stall torque mNm	1680	2280	2500	1990	1580	995	796	641	512	415	289
8 Starting current A	102	75.7	41.4	28.0	19.2	7.26	4.68	3.00	1.92	1.29	0.627
9 Max. efficiency %	88	91	92	91	91	89	88	87	86	85	83
Characteristics											
10 Terminal resistance Ω	0.117	0.317	1.16	1.72	2.50	6.61	10.2	16.0	24.9	37.1	76.6
11 Terminal inductance mH	0.0245	0.0823	0.329	0.460	0.612	1.70	2.62	4.14	6.40	9.31	19.2
12 Torque constant mNm / A	16.4	30.2	60.3	71.3	82.2	137	170	214	266	321	461
13 Speed constant rpm / V	581	317	158	134	116	69.7	56.2	44.7	35.9	29.8	20.7
14 Speed / torque gradient rpm / mNm	4.15	3.33	3.04	3.23	3.53	3.36	3.39	3.35	3.37	3.44	3.45
15 Mechanical time constant ms	6.03	4.81	4.39	4.36	4.35	4.31	4.31	4.31	4.31	4.32	4.33
16 Rotor inertia gcm²	139	138	138	129	118	123	121	123	122	120	120

Specifications

Thermal data

17	Thermal resistance housing-ambient	4.65 K / W
18	Thermal resistance winding-housing	1.93 K / W
19	Thermal time constant winding	41.6 s
20	Thermal time constant motor	1120 s
21	Ambient temperature	-30 ... +100°C
22	Max. permissible winding temperature	+155°C

Mechanical data (ball bearings)

23	Max. permissible speed	12000 rpm
24	Axial play	0.05 - 0.15 mm
25	Radial play	0.025 mm
26	Max. axial load (dynamic)	5.6 N
27	Max. force for press fits (static)	110 N
	(static, shaft supported)	1200 N
28	Max. radial loading, 5 mm from flange	28 N

Other specifications

29	Number of pole pairs	1
30	Number of commutator segments	13
31	Weight of motor	480 g

Values listed in the table are nominal.
Explanation of the figures on page 49.

Option
Preloaded ball bearings

Operating Range Comments

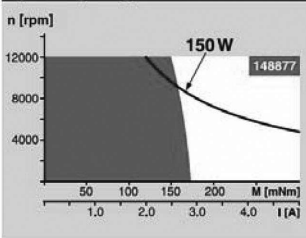

Continuous operation
In observation of above listed thermal resistance (lines 17 and 18) the maximum permissible winding temperature will be reached during continuous operation at 25°C ambient.
= Thermal limit.

Short term operation
The motor may be briefly overloaded (recurring).

Assigned power rating

maxon Modular System Overview on page 16 - 21

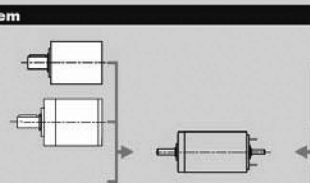

Planetary Gearhead
∅42 mm
3 - 15 Nm
Page 244

Planetary Gearhead
∅52 mm
4 - 30 Nm
Page 247

Recommended Electronics:

ADS 50/5	Page 276
ADS 50/10	277
ADS_E 50/5	277
ADS_E 50/10	277
EPOS 24/5	294
EPOS2 50/5	295
EPOS 70/10	295
EPOS P 24/5	297
Notes	18

Encoder MR
256 - 1024 CPT,
3 channels
Page 259

Encoder HED_ 5540
500 CPT,
3 channels
Page 262 / 264

Brake AB 28
∅45 mm
24 VDC, 0.4 Nm
Page 308

Industrial Version
Encoder HEDL 9140
Page 267
Brake AB 28
Page 309

May 2008 edition / subject to change

[http://www.maxonmotor.com]